

University of Windsor

Scholarship at UWindor

Electronic Theses and Dissertations

Theses, Dissertations, and Major Papers

4-13-2017

Flexural Strengthening of RC beams using Fiber Reinforced Cementitious Matrix, FRCM

Abdulla Jabr
University of Windsor

Follow this and additional works at: <https://scholar.uwindsor.ca/etd>

Recommended Citation

Jabr, Abdulla, "Flexural Strengthening of RC beams using Fiber Reinforced Cementitious Matrix, FRCM" (2017). *Electronic Theses and Dissertations*. 5942.
<https://scholar.uwindsor.ca/etd/5942>

This online database contains the full-text of PhD dissertations and Masters' theses of University of Windsor students from 1954 forward. These documents are made available for personal study and research purposes only, in accordance with the Canadian Copyright Act and the Creative Commons license—CC BY-NC-ND (Attribution, Non-Commercial, No Derivative Works). Under this license, works must always be attributed to the copyright holder (original author), cannot be used for any commercial purposes, and may not be altered. Any other use would require the permission of the copyright holder. Students may inquire about withdrawing their dissertation and/or thesis from this database. For additional inquiries, please contact the repository administrator via email (scholarship@uwindsor.ca) or by telephone at 519-253-3000ext. 3208.

**Flexural Strengthening of RC beams using Fiber
Reinforced Cementitious Matrix, FRCM**

By

Abdulla Jabr

A Thesis
Submitted to the Faculty of Graduate Studies
through the Department of **Civil and Environmental Engineering**
in Partial Fulfillment of the Requirements for
the Degree of **Master of Applied Science**
at the University of Windsor

Windsor, Ontario, Canada

2017

© Abdulla Jabr 2017

**Flexural Strengthening of RC beams using Fiber
Reinforced Cementitious Matrix, FRCM**

By

Abdulla Jabr

APPROVED BY:

N. Zamani, Outside Dept. Reader

Department of Mechanical, Automotive & Materials Engineering

S. Cheng, Dept. Reader

Department of Civil and Environmental Engineering

F. Ghrib, Principal Advisor

Department of Civil and Environmental Engineering

A. El Ragaby, Co-Advisor

Department of Civil and Environmental Engineering

January 17, 2017

DECLARATION OF ORIGINALITY

I hereby certify that I am the sole author of this thesis and that no part of this thesis has been published or submitted for publication.

I certify that, to the best of my knowledge, my thesis does not infringe upon anyone's copyright nor violate any proprietary rights and that any ideas, techniques, quotations, or any other material from the work of other people included in my thesis, published or otherwise, are fully acknowledged in accordance with the standard referencing practices. Furthermore, to the extent that I have included copyrighted material that surpasses the bounds of fair dealing within the meaning of the Canada Copyright Act, I certify that I have obtained a written permission from the copyright owner(s) to include such material(s) in my thesis and have included copies of such copyright clearances to my appendix.

I declare that this is a true copy of my thesis, including any final revisions, as approved by my thesis committee and the Graduate Studies office, and that this thesis has not been submitted for a higher degree to any other University or Institution.

ABSTRACT

The use of externally bonded Fiber reinforced polymer (FRP) sheets has been successfully used in the repair and strengthening of both the shear and flexural capacities of reinforced concrete (RC) beams, slabs and columns since the 90's. However, the externally bonded FRP reinforcements still presents many disadvantages, such as poor performance in elevated temperature and fire resistance, lack of permeability, and strength degradation when exposed to ultraviolet radiation. To remedy such drawbacks, fiber/Fabric Reinforced Cementitious Matrix (FRCM) has been recently introduced. The FRCM system consists of fiber mesh or grid embedded in a cementitious bonding material. The present research investigates the flexure strengthening of reinforced concrete (RC) beams with FRCM. The experimental testing included sixteen large scale concrete beams, 150 mm x 250 mm x 2400 mm, internally reinforced with steel bars, and strengthened in flexure with FRCM. The investigated parameters were the effect of axial stiffness, internal steel reinforcement, and the concrete strength. Two steel reinforcement ratios of 0.18 and 0.36 of the balanced reinforcement ratio as well as three FRCM systems using, Glass, Carbon and PBO (Polyparaphenylene benzobisoxazole) fibers were investigated. Test results are presented in terms of load-deflection, load- strain and load-crack width relationships. The test results indicated that the PBO-FRCM significantly increased the ultimate capacity of the strengthened RC beams compared to the glass and carbon FRCM.

ACKNOWLEDGEMENTS

I would like to thank my supervisors, Dr. Amr Elragaby and Dr. Faouzi Ghrib for giving me the opportunity to be part of their team and for their endless support since I started my Masters research journey. A special recognition for their guidance, encouragement, expertise, and immense knowledge that they have provided me throughout the years.

I would also like to express my sincere gratitude to Dr. Nadar Zamani and Dr. Shaohong Cheng for accepting to be members of my Master's committee.

I would also like to thank Matthew St. Louis and all the technical staff of the Structural Laboratory of the Department of Civil and Environmental Engineering at the University of Windsor.

I would also like to thank all the graduate students at the Department of Civil and Environmental Engineering for their advices, discussions and help.

I would like to thank my beloved parents Mohammed and Zainab for everything they have done for me, and for all the love and belief. Their ultimate support, encouragement, and trust brought me to where I am now. I cannot thank them enough for all they have done for me. Also, I would like to thank my brother Salem for his love and constant support throughout the years in good and bad times, I would like to thank him for being a supportive brother and my best friend.

Lastly, I would like to thank my wife Heba for her patience and support throughout the times. I am glad to have an understanding wife who sacrificed a lot so that I could succeed.

TABLE OF CONTENTS

DECLARATION OF ORIGINALITY.....	iii
ABSTRACT	iv
ACKNOWLEDGEMENTS	v
LIST OF TABLES.....	ix
LIST OF FIGURES	x
LIST OF SYMBOLS.....	xv
LIST OF ABBREVIATIONS	xvii
CHAPTER 1	
INTRODUCTION.....	1
1.1 General.....	1
1.2 Research Objectives	6
1.3 Scope.....	7
1.4 Thesis Outline.....	7
CHAPTER 2	
LITERATURE REVIEW	9
2.1 Mechanical Properties	9
2.2 Durability	12
2.3 Behaviour of FRCM Strengthened RC Beams	13
2.3.1 Typical Load-Deflection Behaviour	14

2.3.2	Bond Performance	15
2.3.3	Flexural Strengthening	19
2.4	Summary of experimental testing findings on flexural strengthening of RC beams using FRCM.....	24
2.5	Theoretical Analysis	25
 CHAPTER 3		
EXPERIMENTAL PROGRAM		31
3.1	Phase 1: Tensile Characterization of G-FRCM.....	31
3.1.1	Coupons specimen preparation.....	31
3.1.2	Materials Properties	33
3.1.3	Test Set-up and Instrumentations.....	35
3.2	Phase 2: Flexural strengthening of RC Beams	37
3.2.1	Specimen Preparation	42
3.2.2	FRCM Application	48
3.2.3	Test Set-up	51
3.2.4	Instrumentation.....	52
 CHAPTER 4		
TEST RESULTS AND DISCUSSION.....		55
4.1	Phase I: Test Results and Analysis.....	55
4.1.1	Tensile test results on Glass-FRCM	55
4.1.2	Tensile test results on PBO-FRCM.....	57
4.1.3	Tensile test results on C-FRCM.....	57
4.1.4	Mechanical Properties of the FRCM systems	59
4.2	Phase 2: Test Results and Analysis.....	61

4.2.1	Effect of FRCM Axial Stiffness	62
4.2.2	Effect of the internal steel reinforcement ratio	84
4.2.3	Effect of Concrete Compressive Strength	96
4.2.4	Effect of Mortar type	103
 CHAPTER 5		
CONCLUSION		108
5.1	Overview	108
5.2	Conclusions	108
5.3	Recommendation for Future Work	110
REFERENCES.....		111
VITA AUCTORIS		117

LIST OF TABLES

Table 3.1 Details of the fibers used in the FRCM systems	34
Table 3.2 Details of group I test specimens- effect of fabric type on the FRCM axial stiffness	38
Table 3.3 Details of group II specimens-effect of number of layers on FRCM axial stiffness	39
Table 3.4 Details of group III test specimens-effect of having same FRCM axial stiffness	40
Table 3.5 Details of group IV specimens - effect of reinforcement ratio	40
Table 3.6 Details of group V specimens- effect of concrete strength.....	41
Table 3.7 Details of group VI specimens- effect of the FRCM matrix type	41
Table 3.8 Test Matrix.....	42
Table 4.1 Mechanical Properties of the tested FRCM systems – 2-Layers coupons	60
Table 4.2 Test results summary on the effect of the FRCM material type	64
Table 4.3 Effect of number of layers on the axial stiffness results summary.....	75
Table 4.4 Test results summary for the effect of the FRCM system type	80
Table 4.5 Effect of steel reinforcement ratio test results	86
Table 4.6 Effect of concrete compressive strength test results.....	97
Table 4.7 Effect of mortar type (summary of results)	104
Table 4.8 Test results for all specimens.....	107

LIST OF FIGURES

Figure 1.1 Deteriorated Slab (Hoffman Architects,2014)	1
Figure 1.2 Steel plate bonding (adapted from chemosystems)	2
Figure 1.3 Carbon fiber sheets (adapted from exclutec)	3
Figure 1.4 Application of externally bonded FRP sheets (adapted from Media Buildings)	4
Figure 1.5 Stress-strain relationship of FRP composites materials (Newhook and Svecova, 2007)	4
Figure 1.6 Types of fiber grids: (a)PBO grid; (b) Carbon grid; (c) Glass grid	5
Figure 1.7 Application of FRCM (adapted from Ruredil)	6
Figure 2.1 Clevis grip.....	9
Figure 2.2 Clamping grip	10
Figure 2.3 Stress-strain curves with clevis grip obtained by Arbeloda et al, 2015	11
Figure 2.4 FRCM Stress-Strain behavior diagram (Reprinted with permission, STRUCTURE magazine, September 2014)	12
Figure 2.5 Typical load-deflection behavior of FRCM strengthened beam.....	15
Figure 2.6 Failure modes: (a) Type I; (b) Type II; (c) Type III (D’Ambrisi et al. (2011)	16
Figure 2.7 Failure modes illustration: (a) Type I; (b) Type II; (c) Type III.....	17
Figure 2.8 Single-lap shear test set-up (adopted from D’Antino et al, 2014)	18
Figure 2.9 Different strengthening schemes studied by D’Ambrisi and Focacci (2011) .	20
Figure 2.10 Load-deflection behavior for slab type elements: (a) control; (b) strengthened (adapted from Loreto et al, 2013)	23
Figure 2.11 Flexural strength analysis for a typical rectangular section: (a) Geometry of	

the section; (b) Axial strain distribution; (c) Internal forces	27
Figure 3.1 Details of test specimen preparation: (a) plan view of test specimen; (b) test specimen during construction	32
Figure 3.2 Cutting FRCM panel using wet-diamond saw.....	33
Figure 3.3 Types of fiber grids or meshes: (a) Glass grid; (b) PBO grid; (c) Carbon grid	34
Figure 3.4 Test Preparation: (a) clevis grips; (b) initial test set-up; coupons after gluing steel	36
Figure 3.5 Final Test set-up.....	36
Figure 3.6 Test specimen details	37
Figure 3.7 Formwork for fabrication of RC beams.....	43
Figure 3.8 Fabrication of steel-cages for RC beams.....	43
Figure 3.9 Fabrication and Casting of second batch of RC beams: (a) wooden formwork before casting; (b) steel cages inserted inside formwork; (c) formwork after casting; (d) another photo for formwork after casting; (e) covering the specimens after casting; (f) curing process; (g) specimens after curing	47
Figure 3.10 FRCM application for the first set of beams: (a) specimen after roughening; (b) specimen after putting the bottom fiber in place; (c) initial mortar layer applied; (d) first FRCM layer fully covered; (e) u-wrap strips put in place; (f) u-wrap strips totally covered with mortar	49
Figure 3.11 Irregular pattern of concrete surface after removal of plastic strip.....	50
Figure 3.12 FRCM strengthening application procedure; (a) initial mortar layer applied; (b) FRCM mesh partially embedded inside mortar; (c) FRCM mesh embedded totally	

inside mortar; (d) U-wrapped FRCM strips embedded inside mortar; (e) FRCM mesh covered with mortar; (f) finishing after application of second FRCM layer	51
Figure 3.13 Beam test specimen set-up.....	52
Figure 3.14 Instrumentation set-up	53
Figure 3.15 Instrumentations details: (a) two Deflection LVDTs; (b) LVDT for measuring first crack; (c) steel strain gauge at the bottom face of the steel reinforcement at midspan; (d) top PI-gauge to measure concrete compression at midspan; (e) top two PI-gauges; (f) bottom two PI-gauges to measure concrete tension;.....	54
Figure 4.1 Stress-strain behavior of the G-FRCM coupons.....	56
Figure 4.2 Failure of G-FRCM coupons	56
Figure 4.3 Stress-strain behavior for PBO-FRCM coupons	57
Figure 4.4 Carbon-FRCM stress-strain behavior	58
Figure 4.5 C-FRCM and PBO-FRCM coupon failures	58
Figure 4.6 Comparison of the stress-strain behavior of glass, carbon, and PBO-FRCM	60
Figure 4.7 Typical load-deflection flexural behaviour of a RC beam.....	62
Figure 4.8 PBO-FRCM strengthened beams failure mode: (a) partial detachment of bottom side FRCM; (b) another view of FRCM partial detachment; (c) slippage of fibers close to support; (d) detachment of FRCM u-wrap strip; (e) closer photo of FRCM u-wrap strip detachment	66
Figure 4.9 Carbon-FRCM strengthened beams failure mode: (a) detachment of FRCM; (b) slippage of FRCM; (c) increased slippage of fibers; (d) closer view of FRCM detachment	67
Figure 4.10 Load-deflection relationship for group I beams	69

Figure 4.11 Load-deflection relationship for group II beams	69
Figure 4.12 Load-critical crack width relationship for group I beams	70
Figure 4.13 Load-critical crack width relationship for group II beams	71
Figure 4.14 Load-concrete-FRCM strain relationship for group I.....	72
Figure 4.15 Load-concrete-FRCM strain relationship for group II	72
Figure 4.16 Load-deflection relationship for group I beams	76
Figure 4.17 Load-deflection relationship for group II beams	77
Figure 4.18 Load-critical-crack width relationship for group I beams	77
Figure 4.19 Load-critical-crack width relationship for group II beams.....	78
Figure 4.20 Glass-FRCM Strengthened beam, A4-G-4L, failure mode	81
Figure 4.21 Load-deflection relationship for group I beams	82
Figure 4.22 Load-critical crack width relationship for group I beams.	83
Figure 4.23 Load-concrete-FRCM strain relationship for group I beams	83
Figure 4.24 Percentage increase in load capacity on the effect of steel reinforcement ratio	87
Figure 4.25 Load-deflection relationship for group I beams	89
Figure 4.26 Load-deflection relationship for group II beams	90
Figure 4.27 Load-deflection at midspan relationship for group III beams	90
Figure 4.28 Load-critical crack width relationship for group I beams	91
Figure 4.29 Load-critical crack width relationship for group II beams	92
Figure 4.30 Load-critical crack width relationship for group III beams.....	92
Figure 4.31 Load-concrete-FRCM strain relationship for group I beams	94
Figure 4.32 Load-concrete-FRCM strain relationship for group II beams	94

Figure 4.33 Load-concrete-FRCM strain relationship for group III beams	95
Figure 4.34 Load-deflection relationship for group I beams	98
Figure 4.35 Load-deflection relationship for group II beams	98
Figure 4.36 Load-critical crack width relationship for group I beams	100
Figure 4.37 Load-critical crack width relationship for group II beams	101
Figure 4.38 Load vs concrete-FRCM strain relationship for group I beams.	102
Figure 4.39 Load-deflection relationship for A2-C*-2L and A2-C-2L.....	105

LIST OF SYMBOLS

Symbol	Description
A_f	area of the fabric reinforcement per unit width, mm ² /mm
A_s	cross-sectional area of the longitudinal internal tension steel reinforcement, mm ²
A_s'	area of the internal steel reinforcement in compression, mm ²
b	width of the rectangular cross section, mm
C	compression force provided by the concrete, kN
c_u	distance from the extreme compression to the neutral axis of the cross section, mm
d	effective depth of the beam cross section, mm
d'	distance from the centroid of the compressive steel reinforcement to the top of the cross section, mm
E_c	modulus of elasticity of concrete, MPa
E_f	modulus of elasticity of the cracked FRCM specimen, GPa
E_s	modulus of elasticity of steel reinforcement
$E_s A_{steel}$	axial stiffness of the internal tension steel reinforcement, kN
$E_f A_{frcm}$	axial stiffness of the FRCM, kN
f'_c	concrete compressive strength, MPa
f_{fe}	effective tensile stress level in the FRCM at failure, MPa
f_{fu}	ultimate tensile strength of FRCM, MPa
f_r	modulus of rupture of concrete, MPa
f_y	yield strength of the steel reinforcement, MPa
h	height of the rectangular cross-section, mm
h	height of the rectangular cross-section, mm
l	length of the beam, mm
N	number of FRCM layers

n	modular ratio of elasticity, $\frac{E_s}{E_c}$
T_f	tensile force provided by the FRCM, kN
T_s	tensile force provided by the steel reinforcement, kN
α_1	multiplier of f'_c to determine intensity of the equivalent block stress for concrete
β_1	ratio of depth of equivalent rectangular stress block factor of concrete
ϵ_c	compressive strain in the concrete, mm/mm
ϵ_{fe}	effective tensile strain in the FRCM at failure, mm/mm
ϵ_{fd}	design tensile strain in FRCM, mm/mm
ϵ_{fu}	ultimate tensile strain of FRCM, mm/mm
ϵ'_c	compressive strain of the unconfined concrete which corresponds to f'_c , mm/mm
ϕ_m	strength reduction factor for flexure

LIST OF ABBREVIATIONS

Abbreviation	Description
AC	Acceptance Criteria
ACI	American Concrete Institute
ASTM	American Standards for Testing and Materials
BOP	Bend-Over Point
COV	Coefficient of Variance
FRP	Fiber Reinforced Polymer
FRCM	Fabric/Fiber Reinforced Cementitious Matrix
C-FRCM	Carbon Fabric Reinforced Cementitious Matrix
G-FRCM	Glass Fabric Reinforced Cementitious Matrix
HSC	High Strength Concrete
PBO	Polyparaphenylene benzobisoxazole
PBO-FRCM	Polyparaphenylene benzobisoxazole Fabric Reinforced Cementitious Matrix
PCS	Post-cracking stiffness
PDI	Pseudo-ductility index
PYS	Post-yielding stiffness
LSR	Low Steel Reinforcement
LVDT	Linear Variable Differential Transducer
MSR	Moderate Steel Reinforcement
NSC	Normal Strength Concrete
RC	Reinforced Concrete
TRM	Textile Reinforced Mortar

CHAPTER 1

INTRODUCTION

1.1 General

Deterioration of concrete structures is a very common problem that Civil Engineers, all over the world, are facing. There are many factors that contribute in concrete structures deterioration. According to the Cement Organization, the major cause of concrete deterioration is the corrosion of the internal steel reinforcement as shown in Figure 1.1[Hoffmann Architects, 2014]. Reinforcement corrosion in the presence of cracking is due to exposure to harsh environments; as well as aggressive chemicals.



Figure 1.1 Deteriorated slab (Hoffman Architects,2014)

In many countries around the world, structures suffer from aging and exposing to harsh environments without proper maintenance or rehabilitation. For example, in Canada, more than 40% of the bridges were built 50 years ago and in need of significant rehabilitation (Bisby, 2004). In the US, it is estimated that about 87,450 bridges are structurally deficient and require rehabilitation (FHWA, 2002). Deteriorated structures may be demolished in

case of severe damage, however in many cases and under moderate damage, rehabilitation can be a very economical solution. The rehabilitation of deteriorated structures is one of the most critical issues facing today's Civil Engineers. Not only some structures need repair, but they may necessitate to be modified or redesigned according to the current needs. For example, some structures were built to carry loads that are significantly smaller than the current code requirements. Therefore, engineers need to design and evaluate strengthening methods to respond to those needs. Therefore, structural rehabilitation (strengthening or repair) is considered one of the most important aspects and challenges facing the construction industry now-a-days. There are many common rehabilitation techniques such as section enlargement, crack injection, external posttensioning, and externally bonded steel plates, as shown in Figure 1.2.



Figure 1.2 Steel plate bonding (adapted from [chemosystems](http://chemosystems.com))

Over the past two decades, externally-bonded fiber-reinforced polymer (FRP) sheets attracted wide attention, and was adopted in the rehabilitation of RC slabs, beams and columns due to its ease of application and significant enhancement of the strength. Externally bonded fiber reinforced polymer (FRP) sheets made of fiber net (as shown in Figure 1.3) embedded in epoxy matrix has been successfully used in the repair and

strengthening of the shear and flexural capacities of reinforced concrete (RC) beams, slabs and columns since the 1990's (Mahoney, 2013).



Figure 1.3 Carbon fiber sheets (adapted from [exclutec](#))

Today, fiber-reinforced composites are widely used as strengthening system of existing reinforced concrete structures as shown in Figure 1.4. FRP composites are well-known for their high tensile strength, resistance to corrosion, and light weight. FRP possess a linear-elastic stress-strain relationship up to failure as shown in Figure 1.5. The ultimate strain of the fibers limits the ultimate tensile strain of the FRP. The tensile strength of the FRP depends mainly on the fiber type, and the density of the fiber. It is fundamental to recall that FRP systems are characterized by a sudden brittle type of failure which is not a preferred type of failure. The epoxy agents gives the system some of its properties in terms of bonding and protection to environment. However, it is also responsible for many disadvantages, such as its lack of permeability, as it traps moisture, thereby threatening bonding integrity of RC (D'Ambrisi and Focacci, 2011). In addition, low temperature conditions affect the bond integrity as well (Tumialan and De Luca, Structure Mag.). Moreover, at elevated temperature, the polymer resin decomposes which significantly

reduces the strength of the FRP system (Bisby et al, 2011). Also, the epoxy showed considerable degradation due to ultraviolet radiation when exposed to light and is also considered a toxic hazard to the installer. Due to the mentioned drawbacks of FRP, its use is limited for outdoor applications in dry conditions only.



Figure 1.4 Application of externally bonded FRP sheets (adapted from [Media Buildings](#))

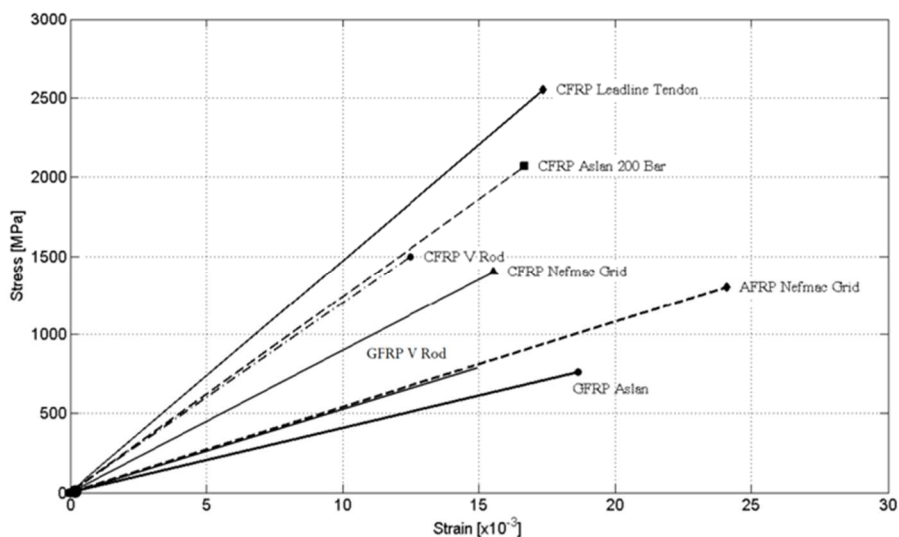


Figure 1.5 Stress-strain relationship of FRP composites materials (Newhook and Svecova, 2007)

Most of the mentioned durability drawbacks of FRP are due to the inherent properties of the polymer adhesive. Consequently, the focus has shifted to develop inorganic, cement-based, bonding matrix to be used in the composites systems. These cement-based composites were later called FRCM (Fiber Reinforced Cementitious Matrix). In FRCM, a structural reinforcing mesh, fabric or textile with open structure, is used instead of fiber sheets, as shown in Figure 1.6. The strands of the FRCM reinforcing mesh are typically made of fibers that are individually coated or bonded together by a polymeric resin that does not fully impregnate the fibers. Therefore, the term “dry fibers” is used to define an FRCM mesh (ACI-549-4R-13). Many types of FRCM are currently available depending on the type of fibers used, which include Glass, Carbon and polyparaphenylene benzobisoxazole (PBO). PBO fibers are a new generation of fiber that possesses a very high-strength and high modulus of elasticity that is superior to that of Carbon.

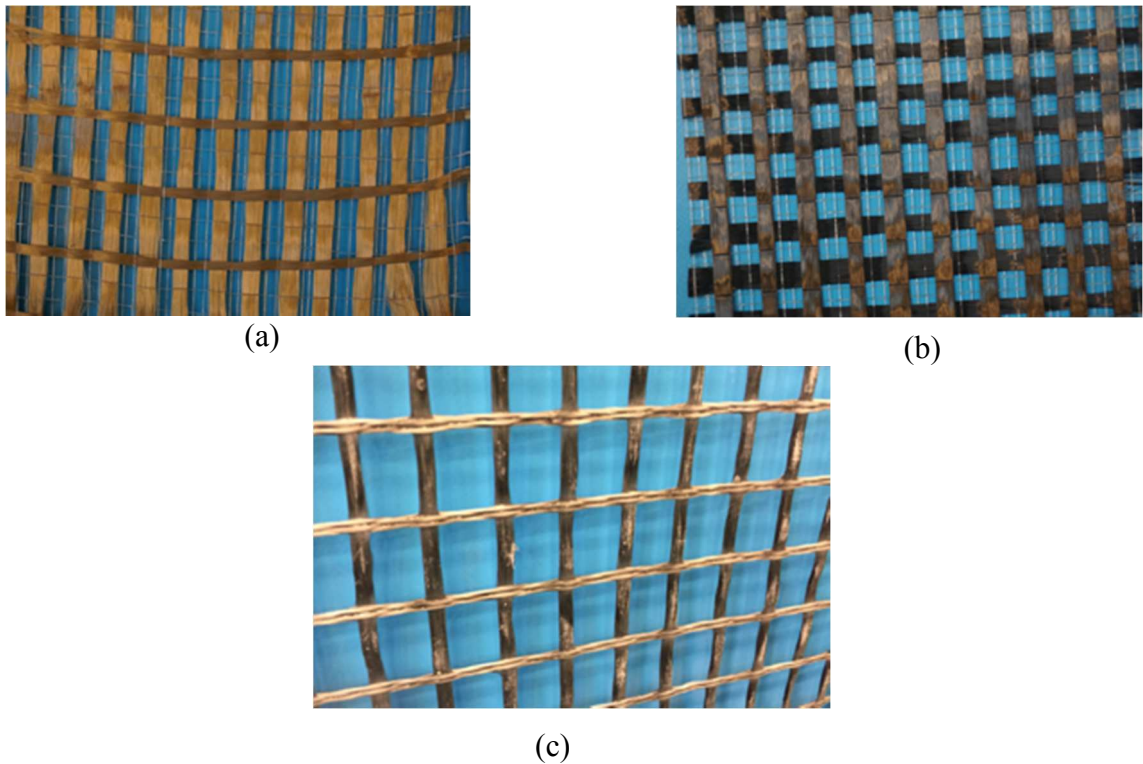


Figure 1.6 Types of fiber grids: (a)PBO grid; (b) Carbon grid; (c) Glass grid

With each type of fibers, unlike the FRP, certain cement mortar (shown in Figure 1.7) has to be used, and due to the presence of cementitious bonding material, the FRCM system, is less affected by temperature fluctuations and possesses porous properties that allow moisture to diffuse through RC structures where FRCM is applied (Tumialan and De Luca,2014). In comparison to FRP, FRCM is inherently incombustible (D'Ambrisi and Focacci,2011), hence, making it a much safer and a convenient alternative. Moreover, research has shown that FRCM can be applied to concrete structures in low temperature conditions and onto wet surfaces (Bisby et al, 2011). There are other common terms used in the literature to describe FRCM such as TRM (textile reinforced mortar) and TRC (textile reinforced concrete). TRC and TRM are terms commonly used in Europe.



Figure 1.7 Application of FRCM (adapted from [Ruredil](#))

1.2 Research Objectives

The objectives of this research is to study and investigate the use of FRCM in

strengthening reinforced concrete beams in flexure. The research focuses on filling the gaps that have not yet been investigated in the literature. The study included the following objectives:

- Compare the effectiveness of Glass, PBO and Carbon-FRCM systems in the flexural strengthening of reinforced concrete (RC) beams.
- Investigate the effect of steel reinforcement ratio and FRCM strengthening ratio on the efficiency of the FRCM systems to strengthen RC-beams.
- Investigate the effect of concrete strength on the efficiency of FRCM strengthening.

1.3 Scope

To fulfil the objectives of this research, two main phases are conducted. The first phase includes tensile characterization of the three FRCM systems, Glass, Carbon and PBO, through uniaxial tensile testing of FRCM coupons. This phase includes testing over 30 coupons of the three FRCM systems. The second phase includes testing 16 large scale reinforced concrete beams under four-point bending loading scheme. The 16 RC beams include three control specimens and 13 specimens strengthened with different configurations of FRCM. The investigated parameters included the internal steel reinforcement ratio, the concrete strength, the FRCM system type, the FRCM axial stiffness, the cementitious matrix or bonding material type, and the number of FRCM layers. Also, a brief comparison between the theoretical and experimental results is conducted.

1.4 Thesis Outline

The thesis includes the following five chapters:

Chapter 1:

This chapter includes the introduction, research objectives, scope, and thesis outline

Chapter 2:

This chapter discussed and summarized the literature review. The literature review is organized into five sections. The first section reviews previous research on the mechanical properties of the FRCM material itself. The second section discusses research on the durability of the FRCM system compared to FRP. The third part summarizes previous research on the flexural strengthening of RC beams using FRCM. The last section explains the available analytical models to predict the ultimate capacity of RC beam strengthened in flexure.

Chapter 3:

This chapter presents the full description of the two phases of the experimental program and details of the material properties, preparation of the test specimen, the test-matrix, the test set-up, and instrumentation.

Chapter 4:

This chapter introduces and discusses the test results in terms of comparisons of the load-deflection behaviour, load-critical crack width behaviour, load-concrete and FRCM strain behaviour, failure modes, post-cracking and post-yielding flexural stiffness, and the Pseudo-Ductility Index.

Chapter 5:

This chapter concludes and summarizes the results and findings of this research. Also, some recommendations are listed in this chapter.

CHAPTER 2

LITERATURE REVIEW

2.1 Mechanical Properties

To study the performance of FRCM systems, it is very important to study its mechanical properties under tensile stresses. In the last decade, several research were conducted to evaluate the tensile performance of FRCM composites. A very important and comprehensive research was performed by Arboleda et al (2015) for the characterization of the tensile behavior of FRCM composites. The tensile loading was applied under two different boundary conditions, clevis and clamping grips. The clevis grip assembly, as shown in Figure 2.1, consisted of two steel plates glued to the ends of the coupons. The steel plates were pinned to a transversal pin on the extended part of the plates, and this whole system was connected to a clevis joint, which was pinned to a shackle.

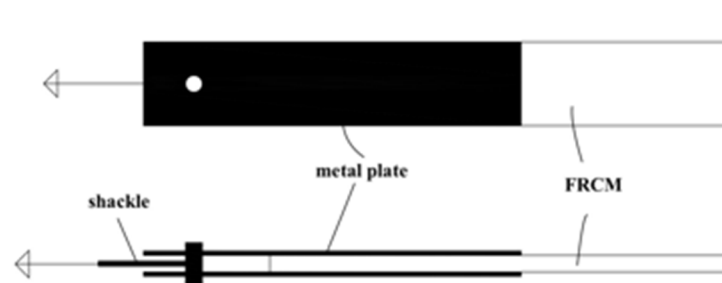


Figure 2.1 Clevis grip

The clamping grip, shown in Figure 2.2, was obtained by gluing GFRP (Glass Fiber Reinforced Polymer) tabs at the ends of the FRCM coupons, and then pressing (clamping) the two ends in the testing machine grips. It was noticed that using the clamping grip, the coupons were allowed to reach their ultimate strength by limiting slippage failure. When

the clevis grip is used, the failure mode is dominated by the slipping of the fabrics from the mortar. The clevis grip presents a more realistic failure behavior that is expected to occur in the field.

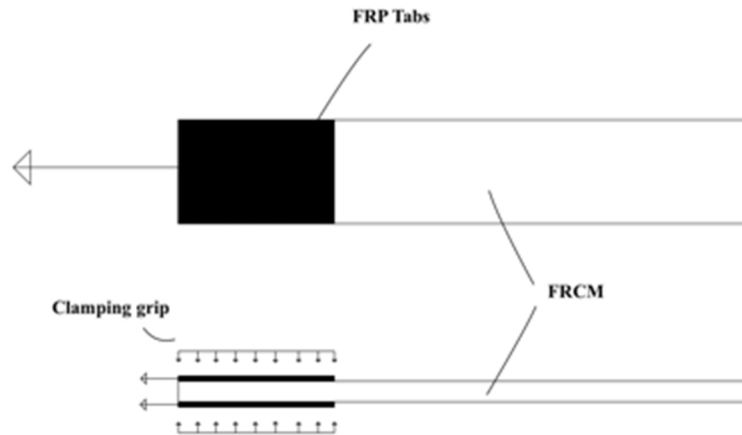


Figure 2.2 Clamping grip

In both tests, the tensile stress of the coupon was determined by dividing the tensile load by the fabric's nominal cross-sectional area. Five different FRCM systems were used. The first three systems composed of dry fibers only of PBO, Carbon, and Glass. The other two systems composed of Glass and Carbon fabric having a protective coating over the dry fibers.

The typical stress-strain diagram of FRCM materials tested using clevis grips is shown in Figure 2.3. The stress-strain behavior of FRCM can be modeled as three main linear phases as shown in Figure 2.4. The first phase represents the linear uncracked state where the cement mortar resists the load. Then, as the load increases, the mortar starts to crack and the stress transfers from the mortar to the fabric and that is represented by the multicracking process of the matrix. The point or stage at which the first crack takes place is called transition point and also called bend-over point (Mobasher 2012). The transition point represents the beginning of the multicracking process. Then the specimen goes

through a multicracking process in which the mortars cracks till all the stresses are transferred from the mortar to the fabric. At this point, the fabric is the only carrying component of the load till it fails either by rupturing of fibers or by slipping of fiber within the matrix. From the reported observations, the stress-strain behavior can be modeled as bi-linear relationship for the purpose of analysis and design. Unlike FRCM, the typical tensile stress-strain behavior of FRP has only a single perfect linear-elastic phase in which the fibers are loaded until failure. Comparing both stress-strain behaviors, it can be concluded that the tri-linear behavior of the FRCM due to the multi-cracking process in the matrix as well as the gradual failure due to the slippage of fibers resulted in a ductile response, like the post yielding behavior of mild steel. The post-cracking and post-failure ductile behaviors make the FRCM preferable strengthening and repair materials compared to FRP.

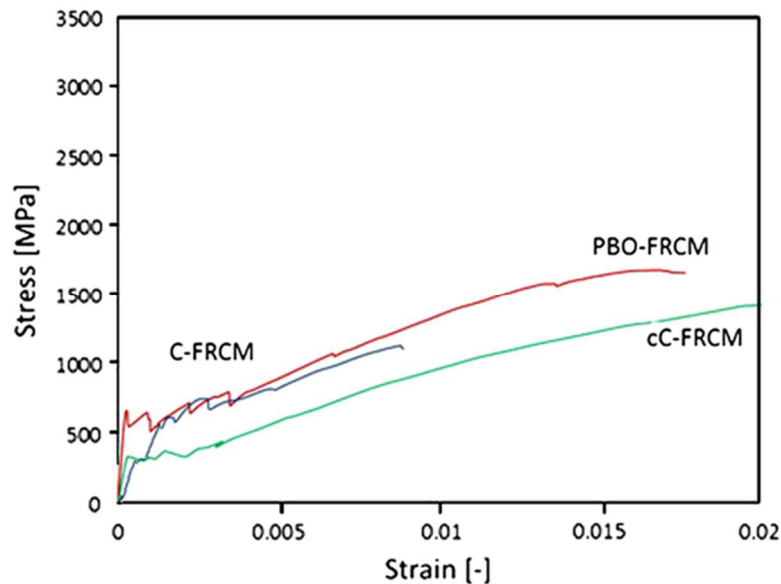


Figure 2.3 Stress-strain curves with clevis grip obtained by Arbeloda et al, 2015

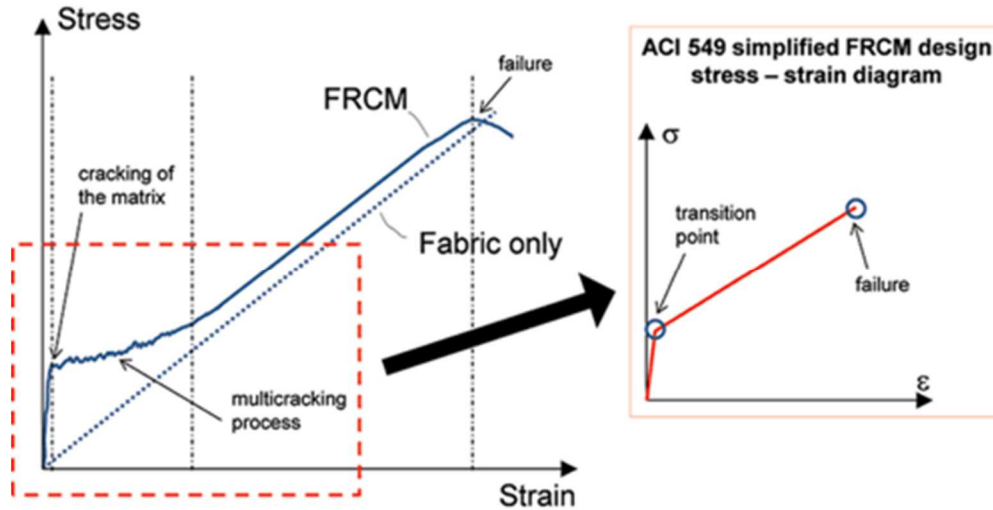


Figure 2.4 FRCM stress-Strain behavior diagram (Reprinted with permission, STRUCTURE magazine, September 2014)

2.2 Durability

One of the most important reasons that makes FRCM preferable over FRP systems is its superior durable properties. As mentioned earlier, the FRCM system, unlike the FRP, is less affected by temperature fluctuations and it also possesses porous properties that allow moisture to diffuse through RC structures. Bisby et al (2010) carried out a research to compare the flexural performance of beams strengthened with FRP & FRCM at elevated temperature. In total, 3 sets of beams were tested, each set consisting of 12 beams. Each set has 3 control beams, 6 beams strengthened with FRP system and 3 beams strengthened with PBO-FRCM. The first set of beams were tested in room temperature (about 20°C), whereas the second and third sets were tested in 50°C and 80°C respectively. The beams tested in elevated temperature were heated for about 6 hours till the desired temperature was reached.

For the first set of beams tested at room temperature, the strengthened beams showed

a better performance and a significant increase in ultimate load capacity. The control beams had a flexural failure whereas the strengthened beams failed in shear due to the presence of the FRP/FRCM systems which strengthened the beams in flexure.

The second set of beams, were tested at 50°C, showed reductions in ultimate strengths of the beams compared with the ones tested at room temperature. For the beams strengthened with FRP, the reductions ranged between 10% and 52%. However, the beams strengthened with FRCM systems showed a reduction of 6%. Some of the beams strengthened with FRP had a flexure/debonding failure due to the breaking down or decomposition of the epoxy that bonds the FRP to the concrete surface. This type of failure was not noticed in the beams strengthened with FRCM due to the usage of cement based matrix as bonding agent which is less affected by the temperature fluctuations.

The last set of beams, tested at elevated temperature(80°C), showed significant reduction in the strengths of the beams. The beams strengthened with FRP experienced a reduction in ultimate load capacity that ranged between 64% and 74%. At this temperature, all of the beams strengthened with FRP had a flexure/debonding failure. However, the beams strengthened with FRCM showed a better performance, as the reduction in ultimate load reached only 28%. The reduction might be due to the decrease in concrete strength with the increase in temperature. Those beams did not experience any debonding of the FRCM system which shows that the FRCM has superior characteristics in elevated temperature compared to FRP.

2.3 Behaviour of FRCM Strengthened RC Beams

The use of FRCM is gaining a wide attention in the last ten years. Many research have been conducted to assess the performance of FRCM as a strengthening technique for

various concrete and masonry structural members. It can be used to strengthen columns, slabs, and beams. This section only discusses the use of FRCM as a method of strengthening reinforced concrete beams.

2.3.1 Typical Load-Deflection Behaviour

According to the current literature, the load-deflection behavior of a typical reinforced concrete beam strengthened with FRCM can be modeled as tri-linear relationship representing the un-cracked section, post cracking and post-yielding stages as shown in Figure 2.5. The first stage is at which the reinforced concrete takes the load until cracking. This stage is independent of the internal steel reinforcement and the FRCM. As the load increases, more flexural cracks start to develop and propagate within the critical bending moment area (post cracking), and the beam seems to be resisting loading in a linear-elastic behavior, with reduced flexure stiffness till the internal steel reinforcement yields. The slope in the second phase is lower than that of the first phase. The effect of FRCM can be noticed in phase II, as the yield point(load) usually increases compared to non-strengthened beams. Also, the strengthened beam is always expected to have a higher post-cracking stiffness compared to unstrengthened beam. After yielding of the internal steel reinforcement, the load capacity of the beam is very close to its ultimate. The effect of the FRCM is noted again, in this phase, as the ultimate capacity is expected to be higher than the control. Also, the post-yielding stiffness is expected to be higher.

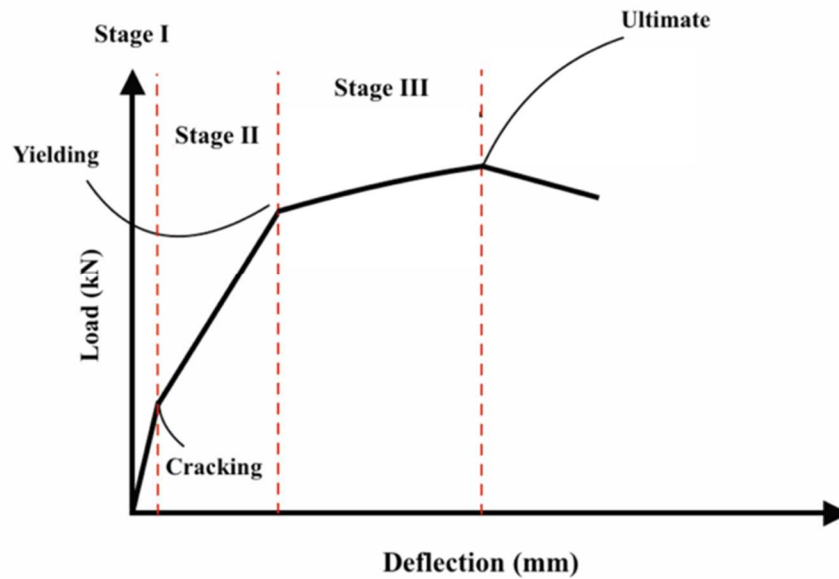


Figure 2.5 Typical load-deflection behavior of FRCM strengthened beam

2.3.2 Bond Performance

D'Ambrisi et al. (2013) concluded that the effectiveness of the FRCM in increasing the ultimate capacity depends on the bond properties of the fiber/matrix and the matrix/concrete interfaces. The bond performances FRCM materials was found to depend on the fibers/matrix coupling, therefore different types of fibers and mortars will have totally different behavior with the same concrete substrate. According to D'Ambrisi et al. (2011), the typical observed failure modes of FRCM strengthened concrete beams under flexure loads can be classified into three main categories, namely i) type 1: slippage of fibers from the matrix, ii) type 2: detaching of the FRCM matrix from the concrete substrate and/or iii) type 3: delamination at the fiber net layer within the FRCM matrix, as shown in Figure 2.6.

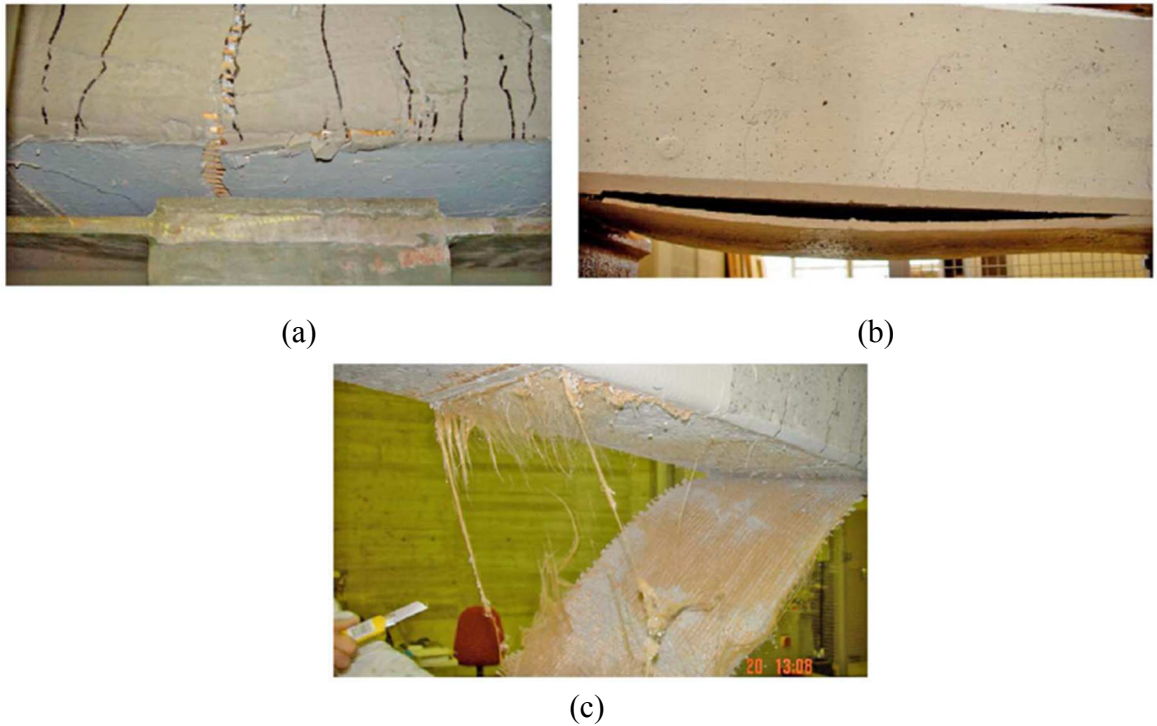
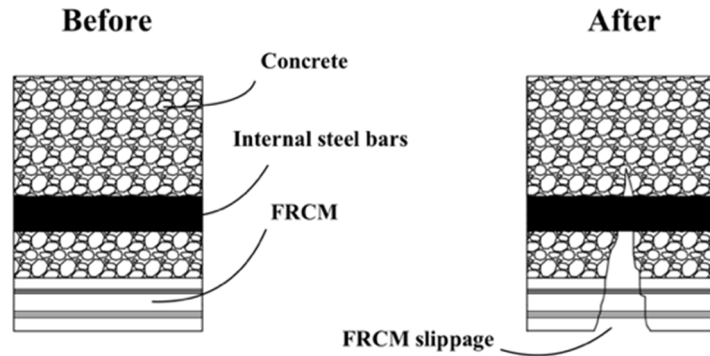
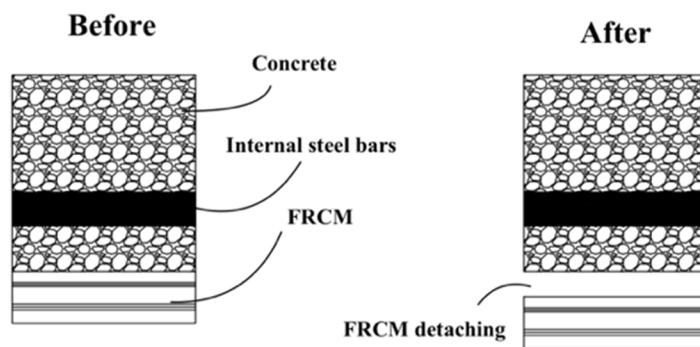


Figure 2.6 Failure modes: (a) Type I; (b) Type II; (c) Type III (D'Ambrisi et al. (2011))

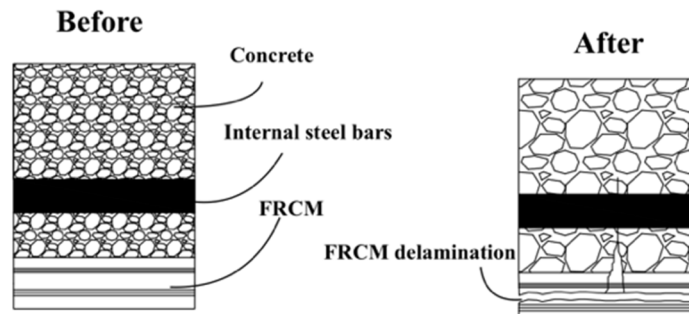
Type I, slippage of fibers, usually occur due to development of wide crack through the matrix. Type II, detaching of FRCM from the concrete substrate, is usually due to poor bonding between the FRCM matrix and the concrete substrate. This type of failure is usually classified as premature failure. Type III, delamination of the fiber within the FRCM matrix, is usually due to high normal and shear stresses that are associated with the increased number of FRCM layers. Figure 2.7 shows an illustration of the three types of failure modes. Failure of the strengthened RC beams is usually triggered by one or a combination of the previous bond failure modes of FRCM.



(a)



(b)



(c)

Figure 2.7 Failure modes illustration: (a) Type I; (b) Type II; (c) Type III

It was found that PBO-FRCM always has a better bond performance than the Carbon FRCM. The failure mode of Carbon FRCM is mainly by delamination and/or detachment. For PBO-FRCM materials, D'Antino et al (2014) also concluded that, prior to failure, a considerable fibers/matrix slip occurs and at failure without detachment of cement based

matrix from the concrete substrate. D'Ambrisi et al. (2012) found that the fibers net density and the number of fibers net layers control the bond behavior and characteristics of FRCM since the delamination occurs at the fibers/matrix interface. It is worth to be mentioned that all the available investigations in the current literature on the bond performance of FRCM and concrete were carried out using single or double shear tests (direct shear) on concrete blocks with only PBO FRCM strips as shown in Figure 2.8.

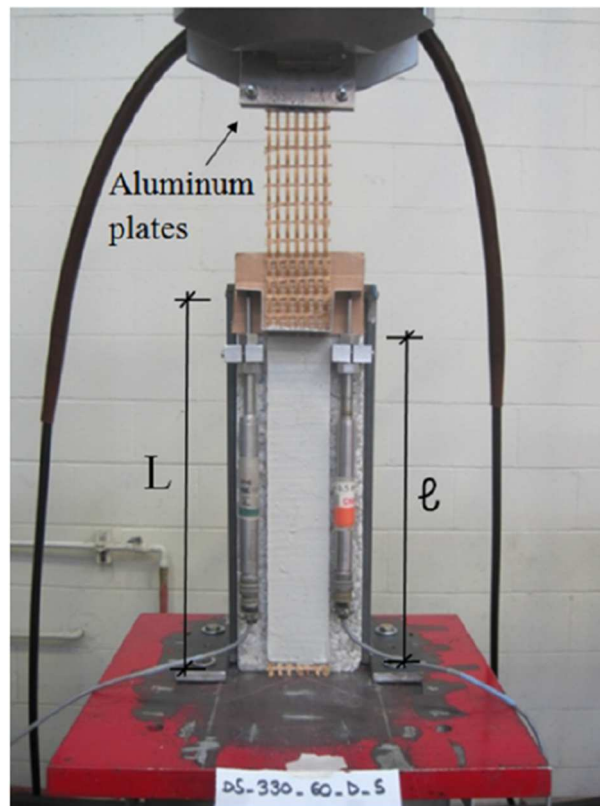


Figure 2.8 Single-lap shear test set-up (adopted from D'Antino et al, 2014)

Several research studies, were carried out to identify the load-slip behavior between fiber/bonding-material, and FRCM/concrete-substrate to predict the ultimate strain at which the beam fails. D'Ambrisi et al (2012) carried out an experimental test to assess the bond-slip behavior of PBO-FRCM and concrete. It was reported that the FRCM strain at failure (or debonding) decreases as the number of layer increases. This is validated due to

the nature of the failure modes as it shifts from excessive slippage to delamination as number of layers increases from 1 to 4 (Loreto et al, 2014). Ombres (2015) suggested a non-linear bond-slip model based on experimental data for beams strengthened with PBO-FRCM. This bond-slip model was only based on very limited data. This model has to be verified and calibrated through using more data. Jung et al (2015) also proposed a bond-strength model which was a modification of the well-known model proposed by Teng et al. (2003) that was used for externally bonded reinforcement (EBR). The modification was done based on the database of experimental data of four studies. Although studies were carried out to understand the bond-slip behavior and to use it towards predicting the ultimate load capacity of RC beams strengthening, most of the studies focused on the PBO-FRCM system only to be assessed. Also, all the previously mentioned models are not validated by independent research.

2.3.3 Flexural Strengthening

D'Ambrisi and Focacci (2011) experimentally investigated the effectiveness of FRCM for the flexural strengthening of RC beams having reinforcement ratio of 0.11 of the balanced reinforcement ratio, ρ_b . Two FRCM material, Carbon fiber nets and PBO fiber nets were tested. The axial stiffness of the Carbon and PBO-FRCM are 1600 kN and 2560 kN, respectively. Four main parameters were inspected:

- 1) Strengthening material (PBO and Carbon-FRCM)
- 2) Net type (PBO fiber thickness in the transverse direction)
- 3) Different matrices (bonding material, M50 vs M750)
- 4) Strengthening scheme (different U-wrapping configurations as shown in Figure 2.9)

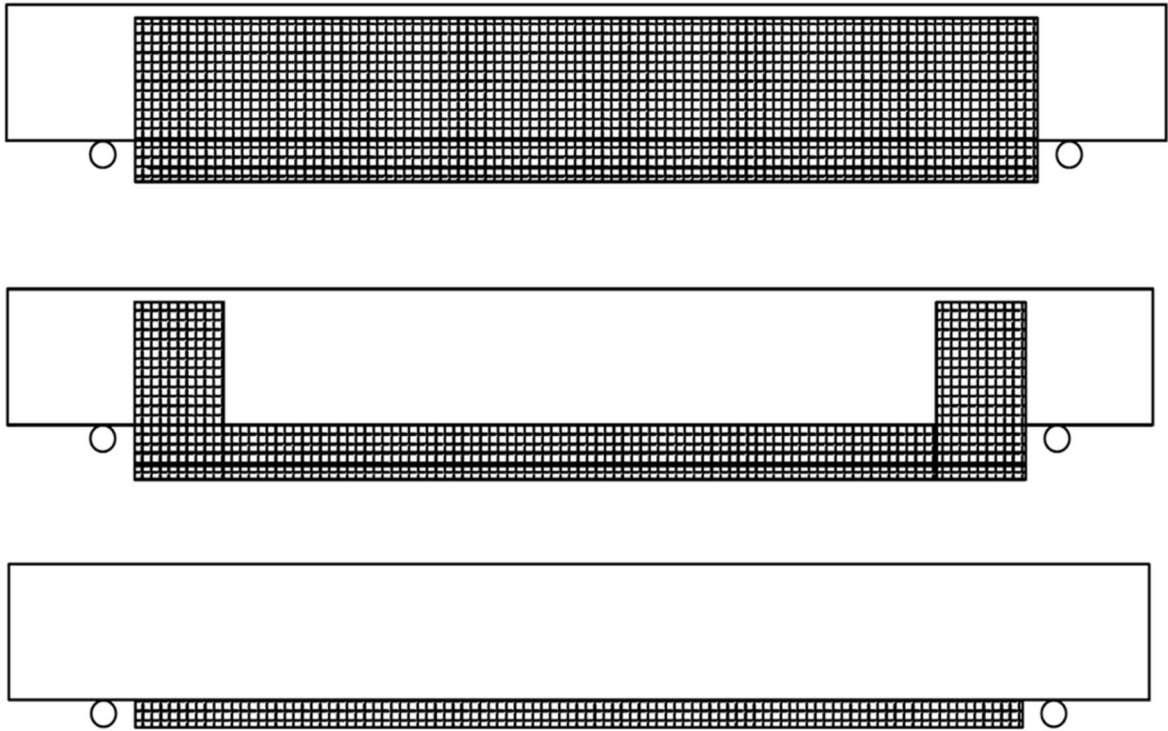


Figure 2.9 Different strengthening schemes studied by D'Ambrisi and Focacci (2011)

The experimental results showed clearly that FRCM materials are very effective for strengthening RC beams in flexure. Also, results showed that beams strengthened with PBO-FRCM materials performed better than Carbon FRCM materials. The beams strengthened with PBO-FRCM showed about 30% increase in the load capacity, compared to only 15% for the ones strengthened with Carbon FRCM. This is consistent with the axial stiffness of each material. It was concluded that the debonding or detaching of FRCM and concrete depend mainly on the number of FRCM layers and the fiber type. The fiber net type is very important in determining the effectiveness of the system as in this test two different PBO fiber nets were used. The main difference between the net type is the effective fiber thickness in the transverse direction, where the first net had a 0.022 mm fiber thickness and the second one had about 0.011 mm fiber thickness. It was observed

that the thicker fiber, which had higher axial stiffness, performed better and obtained higher increase in the ultimate load of the RC beams. The effectiveness of FRCM materials depends mainly on the matrix (bonding material) used. The beam strengthened with PBO-FRCM having Matrix M750 showed better bond than M25. The increase in the ultimate was about 37% for beams strengthened with PBO using matrix M750, whereas the beams having M25 showed about 30% increase. The strengthening scheme plays a very important role in the performance of the FRCM. It was reported that continuous FRCM U-wrapping scheme (Figure 2.9) seems to show the highest improvement in the ultimate load, followed by the FRCM U-wrap strips at the ends (Figure 2.9) and bottom FRCM reinforcement only (Figure 2.9) that showed increase of 15% and 8%, respectively.

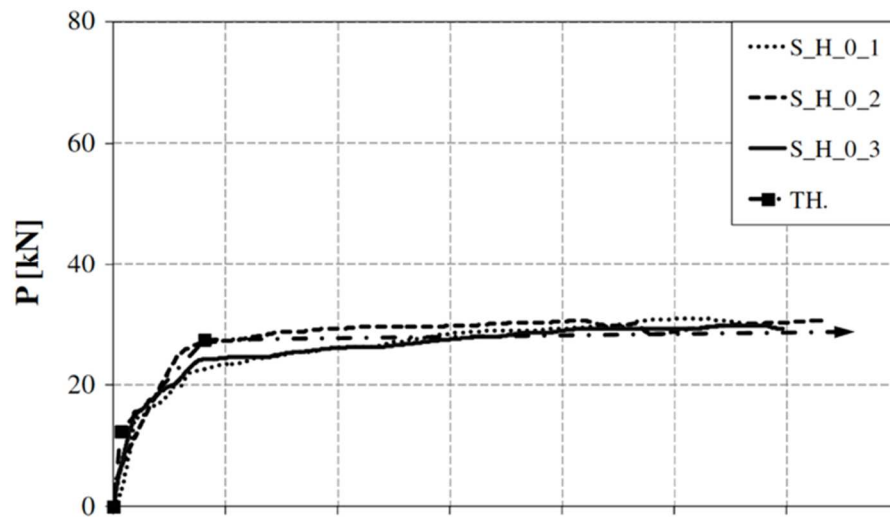
Loreto et al (2013) studied the performance of RC-Slab-Type element externally bonded with PBO-FRCM. The experimental considered the effect of the following parameters:

- 1) Concrete Strength (29 and 42 MPa)
- 2) Number of layers (one and four).

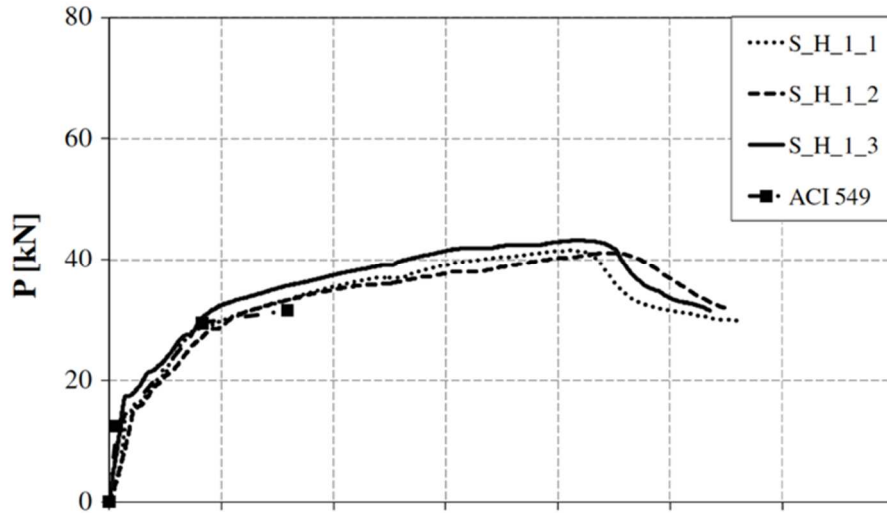
The axial stiffness of the PBO-FRCM system used is 1952 kN and 7807 kN for 1 and 4 layers, respectively. The authors found that the performance of PBO-FRCM demonstrates a very promising composite material for strengthening of Slab-Type RC in flexure. The strength increase of the tested beams was in a range of 35% to 112%. The percentage increase of the strength is consistent with the increase of the axial stiffness of the applied FRCM. The observed failure modes were slippage of the fabric within the matrix and delamination of the FRCM from the concrete substrate. Crushing of concrete followed those failures.

In comparison with the control beam, the beams strengthened with one layer FRCM had a similar crack pattern to that of the control beam, and due to this crack pattern, the crack developed into the FRCM, which made the slippage of the fabric visible. Whereas, for the beams strengthened with four layer FRCM, the FRCM system helped in reducing the crack's width, and in which the cracks were not developed into FRCM exposed surface. This caused the FRCM to delaminate rather than to slip. In either cases, did the FRCM reach its ultimate tensile strength and therefore no rupture of fibers was observed.

As for the load-deflection relationship, it was noticed that the contribution of the FRCM started after the yielding steel, and a steeper load-deflection slope compared with the control beam represented this contribution as shown in Figure 2.10.



(a)



(b)

Figure 2.10 Load-deflection behavior for slab type elements: (a) control; (b) strengthened (adapted from Loreto et al, 2013)

Babaeidarabad et al (2014) performed an experimental study to investigate the effectiveness of PBO-FRCM to externally strengthen RC beams in flexure. The test parameters for this experiment are:

- 1) Number layers (one and four layers)
- 2) Compressive strength of concrete (29.1 MPa and 42.9 MPa).

Each test was replicated three times. The axial stiffness of the PBO-FRCM system used was 973 kN and 3892 kN for 1 and 4, layers respectively. The FRCM system was bonded on the bottom (tension) side only. Experimental results show that FRCM improved the flexural capacity of RC beams. It was noticed that all the control beams failed by crushing of concrete. The increase in strength for low-strength concrete is higher than that of high-strength concrete. For low-strength concrete, the flexural capacity increased 32% (1-layer) and 92% (4-layers). For high-strength concrete, flexural capacity increased by 13% (1-layer) and 73% (4-layers).

2.4 Summary of experimental testing findings on flexural strengthening of RC beams using FRCM

During the last five years, extensive experimental studies were carried out on the flexural behavior of RC beams strengthened with various FRCM systems. The test results and findings of these research studies can be summarized as follows:

- ✓ The FRCM flexural strengthening of RC beams showed a significant increase in the ultimate capacity of up to 92%.
- ✓ The increase in the ultimate capacity proportion directly with the increase of the axial stiffness of the FRCM fiber net (which depends on the fabric type and number of FRCM layers).
- ✓ The PBO-FRCM materials performed better in enhancing the ultimate load capacity than Carbon-FRCM materials, which is consistent with the axial stiffness of each material.
- ✓ It was concluded that three main bond failure types accosted with FRCM, slippage of fibers, detachment of FRCM from concrete and delamination within the FRCM mortar and fabric, control the strengthening effectiveness.
- ✓ The bond properties of FRCM depend mainly on the cement mortar matrix and fiber arrangements.
- ✓ The increase in ultimate strength of strengthened beams having low-strength concrete is higher than that of high-strength concrete.

However, there is still gaps in the current literature that need to be addressed in order to reach a complete understanding of the effect of FRCM as strengthening and repairing

systems. By examining the main test parameters that were covered in the current literature, it was found that:

- Two types of fibers, PBO and Carbon-FRCM, were investigated for the flexural strengthening.
- A very low steel reinforcement ratio (less than $0.195\rho_b$) was used in all the strengthened RC beams in all the previous research .
- In terms of number of FRCM layers, previous researchers focused more on investigating the effect of extreme number of layers, i.e. 1-layers vs 4-layers.
- No comparison was carried out between the three FRCM systems; Glass, Carbon and PBO.

Therefore, the present research focuses on filling the gaps that have not been investigated in the literature. The following objectives are set:

- Compare the performance of glass, PBO and carbon FRCM system in the flexure strengthening of reinforced concrete (RC) beams.
- Investigating the effect of steel reinforcement ratio on the efficiency of the FRCM systems to strengthen RC-beams.
- Investigating the effect of concrete strength on the efficiency of carbon and PBO-FRCM systems.

2.5 Theoretical Analysis

The theoretical analysis adopted by the ACI guideline (ACI 549.4R-13) is by using the tensile characteristics obtained from coupon testing rather than a bond-slip or bond-strength models. As mentioned earlier in this chapter, the AC434 and the ACI 549.4R-13 guidelines require the coupon testing to be conducted using clevis grips boundary condition

to allow for slippage of fibers from the matrix. Thus, the ultimate strains/stresses calculated as per ACI 549.4R-13 takes into consideration the slippage of fibers. The contribution of FRCM to enhance the ultimate capacity as per ACI 549.4R-13 is based on the following assumptions:

- Plane sections remain plane after loading.
- Full bond between the FRCM system and the concrete substrate is assumed to remain effective.
- The maximum compressive strain in concrete is 0.003.
- FRCM has a bilinear behavior to failure where only the second linear part of the curve is used in analysis and design.

The assumptions proposed by the ACI are typical for any section analysis for externally bonded reinforcement applications. The only assumption that is questionable is that the bond between the FRCM system and concrete remains effective. This assumption is valid unless premature debonding occurs which limits the contribution of the FRCM. If debonding occurs at a later stage close to failure, the assumption does not have a significant affect on the contribution of the FRCM.

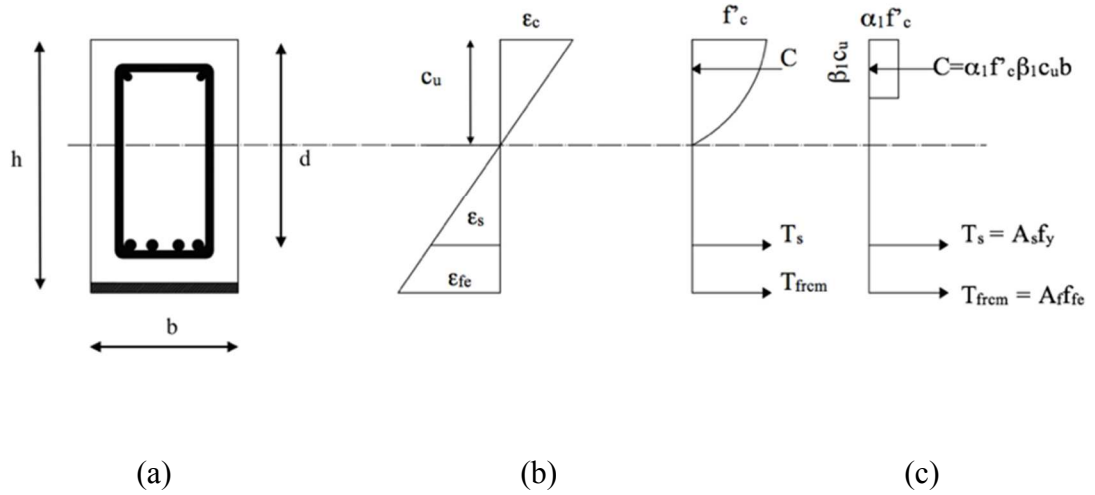


Figure 2.11 Flexural strength analysis for a typical rectangular section: (a) Geometry of the section; (b) Axial strain distribution; (c) Internal forces

As per the ACI-549, the effective tensile strain in the FRCM system at failure, ϵ_{fe} , is limited to ϵ_{fd} , the design strain of the FRCM system, in equation (2)

$$\epsilon_{fe} = \epsilon_{fd} \leq 0.012 \quad (2)$$

It has to be noted that the ACI-549 defines the design strain of the FRCM system, ϵ_{fd} , as the average strain of the FRCM at failure minus one standard deviation. The effective tensile stress of the FRCM at failure, f_{fe} , is then calculated in terms of E_f , the cracked elastic modulus of the FRCM system, and ϵ_{fe} effective tensile strain according to equation (3)

$$f_{fe} = E_f \epsilon_{fe} \quad (3)$$

Then, using strain compatibility, the compressive strain in concrete can be written in terms of the effective tensile strain in the FRCM according to equation (4)

$$\epsilon_c = \frac{\epsilon_{fe} \times c_u}{h - c_u} \quad (4)$$

where

“ ϵ_c ” is the concrete compressive strain

“ c_u ” is the neutral axis depth initial trial

“h” is the height of the concrete member (beam).

Also, using strain compatibility, the steel tensile strain can be written in terms of the effective tensile strain in the FRCM according to equation (5)

$$\varepsilon_s = \frac{d-C_u}{h-C_u} \varepsilon_{fe} \quad (5)$$

where

“d” is the effective depth of the concrete cross-section

Then, steel, assumed to be perfectly elastic plastic material, the stress is calculated as the lower of the yield stress or the stress at the time of failure as per equation (6)

$$f_s = \begin{cases} E_s \varepsilon_s & \text{if } E_s \varepsilon_s \leq f_y \\ f_y & \end{cases} \quad (6)$$

where

“f_y” is the steel yield stress

“E_s” is the modulus of elasticity of steel

The concrete stress block factors can then be calculated as per the ACI 318, according to equations (7)-(9),

$$\varepsilon'_c = \frac{1.7 f'_c}{E_c} \quad (7)$$

$$\beta_1 = \frac{4\varepsilon'_c - \varepsilon_c}{6\varepsilon'_c - 2\varepsilon_c} \quad (8)$$

$$\alpha_1 = \frac{3\varepsilon'_c \varepsilon_c - (\varepsilon_c)^2}{3\beta_1 (\varepsilon'_c)^2} \quad (9)$$

Then, the internal force equilibrium (eq 10) should be satisfied by the calculation of a new value for the neutral axis depth is done to equation (11)

$$T_s + T_{frcm} = C \quad (10)$$

where

$$T_s = A_s f_s \quad (10a)$$

$$T_{\text{frcm}} = nA_f b f_{fe} \quad (10b)$$

$$C = \alpha_1 f'_c \beta_1 b c_u \quad (10c)$$

substituting eq. (10a, 10b, and 10c) into eq. (10) and rearranging

$$c_u = \frac{A_s f_s + nA_f b f_{fe}}{\alpha_1 f'_c \beta_1 b} \quad (11)$$

where

“ A_s ” is the internal steel reinforcement area

“ n ” is the number of FRCM layers

“ A_f ” is the area of FRCM layer per unit width

If the new value of the neutral axis, calculated from equation (10), is close to the initial guessed value, then this iteration is valid. If it is not close, then another iteration has to be carried out until convergence (the two values of the neutral axis depth are very close). Finally, the nominal moment resistant M_n is calculated by taking the moment contribution of the steel reinforcement M_s and the FRCM M_{frcm} according to the equations (12), (13) and (14)

$$M_s = A_s f_s \left(d - \frac{\beta_1 c_u}{2} \right) \quad (12)$$

$$M_{\text{frcm}} = nA_f b f_{fe} \left(h - \frac{\beta_1 c_u}{2} \right) \quad (13)$$

$$M_n = \phi_m (M_s + M_f) \quad (14)$$

The strength reduction factor ϕ_m is given by eq. 16, which is defined in the ACI 562 and ACI-318 as

$$\phi_m = \begin{cases} 0.9 & \text{for } \varepsilon_t \geq 0.005 \\ 0.65 + \frac{0.25(\varepsilon_t - \varepsilon_{sy})}{0.005 - \varepsilon_{sy}} & \text{for } \varepsilon_{sy} < \varepsilon_t < 0.005 \\ 0.65 & \text{for } \varepsilon_t < \varepsilon_{sy} \end{cases} \quad (15)$$

where

“ ϵ_t ” is the net tensile strain at the extreme tension steel reinforcement

“ ϵ_{sy} ” is the steel yield strain

It should be noted that when predicting the maximum load capacity, ϕ_m , the strength reduction factor, is taken as 1.0. However, for design purposes, the reduction factor is taken according to equation 16. The philosophy behind using the strength factor is to compensate element with low ductility with a higher reserve of strength (Babaeidarabad et al, 2014). The ACI design provisions limits the total force that is contributed by the FRCM. The increase in flexural strength contributed by the FRCM should not exceed 50% of the existing flexural capacity of the structure prior to FRCM application (clause 11.1.1).

CHAPTER 3

EXPERIMENTAL PROGRAM

The experimental program consists of two main phases. The first phase includes the characterization of the mechanical properties of glass, carbon and PBO-FRCM through tensile testing on 30 coupon specimens. The second phase consists of constructing and testing of 16 large-scale RC beams, to assess the flexural strengthening using FRCM.

3.1 Phase 1: Tensile Characterization of G-FRCM

The purpose of the first phase is to assess the mechanical properties of the glass, PBO, and carbon-FRCM. At the time at which this research phase was carried out, no previous research was conducted to measure or characterize the mechanical properties of glass-FRCM. However by the end of 2015, Arboleda et al (2015) published the results of a study on the mechanical properties of glass, PBO and carbon FRCM systems. The coupon test was carried out according to Annex A of AC434 (ICC Evaluation Service, 2013).

3.1.1 Coupons specimen preparation

Three sets of specimens were prepared from the Glass, Carbon and PBO-FRCM. Each set consisted of at least five, two layers coupons. All the coupons having dimensions of 410 mm long, 50 mm wide and 15 mm thick, were prepared from the FRCM panels as shown in Figure 3.1. The mortar or the cementitious matrix was mixed according to the specifications provided by the manufacturer. For the Glass-FRCM, a ratio of 3.5-3.78 liters of water was used per 22.7 kg mortar. For the Carbon-FRCM, a ratio of 6.5-7 liters of water was used per 25 kg of mortar. For the PBO-FRCM a ratio of 6 liters of water was used per 25 kg of mortar. The mixing was done using a heavy duty, low-speed drill with Propeller-type paddle. The panels were prepared first by laying 5 mm thick layer of mortar of, then

installing the fabric grid, followed by covering that fabric grid with another 5 mm of mortar. The same procedure is applied for the second layer of grid.



(a)

(b)

Figure 3.1 Details of test specimen preparation: (a) plan view of test specimen; (b) test specimen during construction

Moist curing was maintained for the first 24 hours as per the ACI 308R-01 recommendations for concrete curing. Panels were then left to cure for 28 days. After 28 days, the panels were cut using wet-diamond saw. It was very important to use a wet-diamond saw to prevent any cracking or damage to the coupons. After cutting, the coupons were left to dry.



Figure 3.2 Cutting FRCM panel using wet-diamond saw

3.1.2 Materials Properties

The Glass-FRCM specimens were fabricated using Sika Wrap-350 Glass Grid (Figure 3.3a) and Sika Monotop 623 Mortar. The Glass net used in this study is a balanced bi-directional glass fabric net having an alkali resistant coating. The spacing of the fabric tows is 18.2 mm x 14.2 mm (center to center). The fabric grid has an ultimate tensile stress of about 77 kN/m in the longitudinal direction and 76 kN/m in the transverse direction. The mortar used is a one-component, polymer-modified and early strength gaining, cementitious mortar. As provided by the manufacturer, the density of the mortar is 2030 kg/m³ (126 lb./ft³) as per ASTM C185. The mortar has a compressive strength of 18 MPa (after 24 hours), 30 MPa (after 7 days) and 40 MPa (after 28 days) as per ASTM C109.

The PBO-FRCM specimen was fabricated using Polyparaphenylene benzobisoxazole (PBO) fiber mesh (Figure 3.3b) with a stabilized inorganic matrix (M750) specially

designed to bond very well with the PBO fibers and the concrete substrate. The spacing of the fabric toss is 20 mm x 15 mm (center to center). The mesh had an ultimate tensile stress of about 265 kN/m in the longitudinal direction and 66.5 kN/m in the transverse direction. As provided by the manufacturer, the density of the matrix is 1800 kg/m³ (112.3 lb./ft³). It has a compressive strength of 30 MPa (at 28 days).

The Carbon-FRCM (Figure 3.3c) specimen was fabricated using bidirectional carbon fiber mesh and a stabilized inorganic matrix (M25) of pozzolanic nature. The fabric has a nominal spacing of 10 mm in both directions. As provided by the manufacturer, the density of the matrix is 1500 kg/m³ (93.6 lb./ft³). It has a compressive strength of 20 MPa (at 28 days).

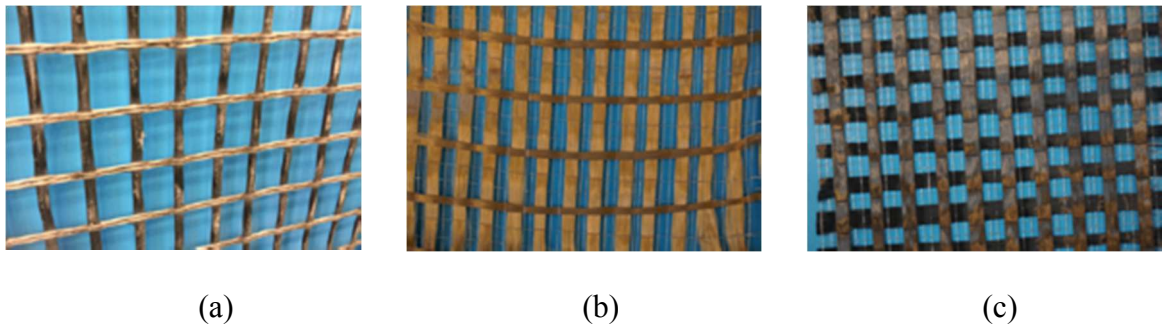


Figure 3.3 Types of fiber grids or meshes: (a) Glass grid; (b) PBO grid; (c) Carbon grid

Table 3.1 Details of the fibers used in the FRCM systems

Type of Fabric	Young's Modulus (GPa)	Ultimate tensile strength (MPa)	Ultimate tensile strain (mm/mm)	Density (g/cm ³)	Equivalent dry fabric thickness (mm)
Glass^a	80	2600	0.0345	2.6	0.023 ^b
PBO^a	270	5800	0.0215	1.56	0.046 ^b
Carbon^a	240	4800	0.018	1.82	0.047 ^c

^a Properties were provided by the manufacturer

^b Equivalent thickness in the wrap direction

^c Equivalent thickness in both directions

3.1.3 Test Set-up and Instrumentations

The coupons were tested according to Annex A of AC434 (ICC Evaluation Service 2013). Uniaxial tensile tests were carried out on the coupons using clevis grip to allow the slippage of fabrics to control the failure. Four steel tabs with clevis openings were glued covering 100 mm on the upper and bottom sides of the specimens as shown in Figure 3.4(c). The clevis grip consists of two shackles connected to each other and pinned to the steel tabs on the specimen and the testing fixture. Two 50 mm clip-on extensometer covering the top and bottom ends of the exposed surface were used. Since, the clip-on extensometer cannot cover the whole exposed surface of the coupon, it was then replaced with the MTS Video Extensometer as shown in Figure 3.5. The video extensometer was used to track four target points, two of them were located within the two ends of the exposed coupon, and the other two were located at the top and bottom steel plates. To use the video extensometer, special preparation procedures should be followed. Speckled paint was applied to the specimen surface to allow point-to-point strain measurement. The load was applied under displacement control, a loading rate of 0.2 mm/min, as recommended by AC434, was applied.



(a)



(b)



(c)

Figure 3.4 Test preparation: (a) clevis grips; (b) initial test set-up; (c) coupons after gluing steel

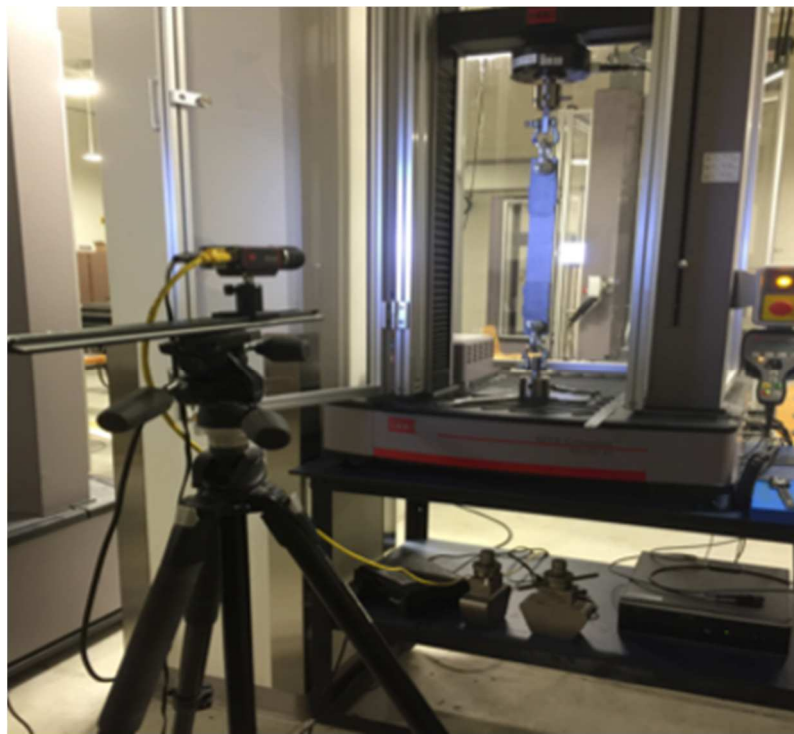


Figure 3.5 Final test set-up

3.2 Phase 2: Flexural strengthening of RC Beams

The second phase consists of constructing and testing of large-scale RC beams under flexure loads. A total of 16 beams, each is 150 mm wide x 250 mm deep x 2400 mm long, were constructed and tested. The RC beams were reinforced internally with steel bars and utilize different concrete strengths. Two different bottom longitudinal steel reinforcement were used, 2#10M, which results in a reinforcement ratio of 0.18 of the balanced reinforcement ratio, ρ_b and 4#10M with a reinforcement ratio of $0.36 \rho_b$. All beams were over-designed for shear and were reinforced with 8-mm stirrups spaced at 150 mm to prevent any shear failure. Two top longitudinal bars of 8 mm diameter were used as stirrups support. The details of the beam cross-section are shown in Figure 3.6.

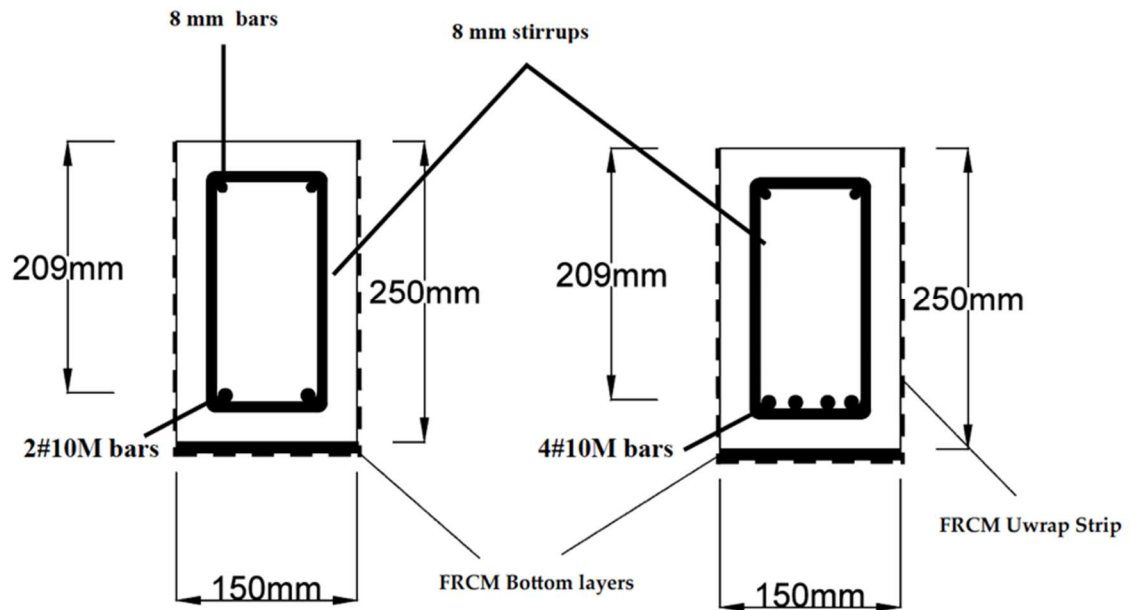


Figure 3.6 Test specimen details

The main investigated parameters are:

1. Axial Stiffness of the FRCM
2. Steel reinforcement ratio ($0.18 \rho_b$ and $0.36 \rho_b$)
3. Concrete Strength (30 and 50 MPa)
4. Bonding material (M25 Vs M750 mortar)

The test matrix was designed to include 16 large scale RC beam specimens which were divided into several groups, each group investigates and compares the effect of one parameter. A focus is placed on the effect of the FRCM axial stiffness, $E_f A_f$. The axial stiffness of the FRCM strengthening depends on the fabric type and the number of fabric layers. To study the effect of axial stiffness using different fabric types, seven beams, Group I, were constructed, tested. Three different FRCM fabric types, Glass, Carbon, and PBO, were considered. Group I test specimens were constructed using 30 MPa concrete and were strengthened using two layers of FRCM. Table 3.2 shows the details of Group I test specimens.

Table 3.2 Details of group I test specimens- effect of fabric type on the FRCM axial stiffness

	Specimen ID	Reinforcement	Reinforcement ratio	FRCM material	EA_{frcm} (kN)	$\frac{EA_{frcm}}{EA_{steel}}$
1	A2-0	2#10M	0.18 ρ_b	Control	-	-
2	A2-C-2L			Carbon	1233	4.3
3	A2-P-2L			PBO	1710	3.1
4	A4-0	4#10M	0.36 ρ_b	Control	-	-
5	A4-P-2L			PBO	1710	2.1
6	A4-C-2L			Carbon	1233	1.5
7	A4-G-2L			Glass	850	1.1

The beam designation used in the table is as follows:

1. The first character refers to the concrete strength, The letter A stands for 30 MPa compressive concrete strength, and letter B stands for 50 MPa concrete strength.
2. The second character is the number of bottom longitudinal reinforcing steel bars
3. The third character is the FRCM fabric type which is specified as 0 (control), P (PBO), C (Carbon), and G (Glass).
4. The fourth character is for the number of FRCM layers followed by letter “L”

Accordingly, A4-P-2L stands for the test specimen with 4#10M internal reinforcing steel bars which is externally strengthened with two layers PBO-FRCM system.

To study the effect of axial stiffness using different number of layers, six beams, group II, were tested. Group II test specimens were constructed using 30 MPa concrete and were strengthened using only Carbon FRCM. Table 3.3 shows the details of Group II test specimens.

Table 3.3 Details of group II specimens-effect of number of layers on FRCM axial stiffness

	Specimen ID	Reinforcement	Reinforcement ratio	EA_{frcm} (kN)	$\frac{EA_{frcm}}{EA_{steel}}$	No. of layers
1	A2-0	2#10M	0.18 ρ_b	-	-	-
2	A2-C-2L	2#10M	0.18 ρ_b	1233	3.1	2
3	A2-C-3L	2#10M	0.18 ρ_b	1710	4.6	3
4	A4-0	4#10M	0.36 ρ_b	-	-	-
5	A4-C-2L	4#10M	0.36 ρ_b	1233	1.5	2
6	A4-C-3L	4#10M	0.36 ρ_b	1710	2.3	3

To further study the effect of axial stiffness and the effect of strengthening systems, six beams, including four beams having constant axial stiffness, Group III, were tested. Group III test specimens were constructed using 30 MPa concrete and were strengthened

with different FRCM systems and different number of layers, but with the same overall axial stiffness. Table 3.4 shows the details of group III test specimens.

Table 3.4 Details of group III test specimens-effect of having same FRCM axial stiffness

	Specimen ID	Reinforcement	Reinforcement ratio	EA_{frcm}	$\frac{EA_{frcm}}{EA_{steel}}$	No. of layers
1	A2-0	2#10M	0.18 ρ_b	-	-	-
2	A2-P-2L	2#10M	0.18 ρ_b	1710	4.3	2
3	A2-G-4L	2#10M	0.18 ρ_b	1700	4.2	4
4	A4-0	4#10M	0.36 ρ_b	-	-	-
5	A4-P-2L _{avg} ¹	4#10M	0.36 ρ_b	1710	2.1	2
6	A4-C-3L	4#10M	0.36 ρ_b	1850	2.3	3

¹A4-P-2L_{avg} is the average results of the two specimens, A4-P-2L and A2-P*-2L

The second investigated parameter is the effect of the internal steel reinforcement ratio. To study its effect on the performance of FRCM strengthened beams, eight beams, group IV, were tested, including two control beams. Group III test specimens were constructed using 30 MPa concrete and were strengthened with two layers of PBO or Carbon FRCM. Table 3.5 shows the details of group IV test specimens.

Table 3.5 Details of group IV specimens - effect of reinforcement ratio

	Specimen ID	Reinforcement Ratio	$\frac{EA_{frcm}}{EA_{steel}}$	FRCM Material	No. of Layers
1	A2-0	0.18 ρ_b	-	Control	-
2	A2-P-2L	0.18 ρ_b	4.3	PBO	2
3	A4-P-2L _{avg} ¹	0.36 ρ_b	2.1	PBO	2
4	A2-C-2L	0.18 ρ_b	3.1	Carbon	2
5	A4-C-2L	0.36 ρ_b	1.5	Carbon	2
6	A2-C-3L	0.18 ρ_b	4.6	Carbon	3
7	A4-C-3L	0.36 ρ_b	2.3	Carbon	3
8	A4-0	0.36 ρ_b	-	Control	-

¹A4-P-2L_{avg} is the average results of the two duplicate specimens, A4-P-2L and A2-P*-2L

The third investigated parameter is the effect of concrete strength. To study the effect of concrete strength, six beams, group V, were tested and two concrete strengths were studied. The strengths studied represents low and high strength normal concrete. All the specimens were constructed using 2#10M, having steel reinforcement ratio of $0.18\rho_b$. This comparison shows how the concrete strength affects the performance of FRCM for PBO and Carbon-FRCM. Table 3.6 shows the details of group V test specimens.

Table 3.6 Details of group V specimens- effect of concrete strength

	Specimen ID	Reinforcement Ratio	Target f'_c (MPa)	$\frac{EA_{frcm}}{EA_{steel}}$	FRCM Material
1	A2-0	$0.18 \rho_b$	30	-	Control
2	A2-P-2L	$0.18 \rho_b$	30	4.3	PBO
3	B2-P-2L	$0.18 \rho_b$	50	4.3	PBO
4	A2-C-3L	$0.18 \rho_b$	30	4.6	Carbon
5	B2-C-3L	$0.18 \rho_b$	50	4.6	Carbon
6	B2-0	$0.18 \rho_b$	50	-	Control

The fourth investigated parameter is the matrix type. A brief comparison was made to study the effect of the bonding material on the carbon mesh. Three beams, group VI, were tested, and two mortars were used, M25 and M750. Table 3.7 shows the comparison table for this criteria. Table 3.8 presents the details of the 16 test specimens in this study.

Table 3.7 Details of group VI specimens- effect of the FRCM matrix type

	Specimen ID	Reinforcement Ratio	FRCM matrix type	Target concrete strength (MPa)	$\frac{EA_{frcm}}{EA_{steel}}$
1	A2-0	$0.18 \rho_b$	Control	30	-
2	A2-C-2L	$0.18 \rho_b$	M25	30	3.1
3	A2-C*-2L	$0.18 \rho_b$	M750	30	3.1

Table 3.8 Test Matrix

	Specimen ID	Reinforcement	Reinforcement ratio	Target f'_c (MPa)	FRCM material	No. of Layers
1	A2-0	2#10M	0.18 ρ_b	30	Control	-
2	A4-0	4#10M	0.36 ρ_b	30	Control	-
3	B2-0	2#10M	0.18 ρ_b	50	Control	-
4	A2-C-2L	2#10M	0.18 ρ_b	30	Carbon	2
5	A2-C-3L	2#10M	0.18 ρ_b	30	Carbon	3
6	A2-C*-2L ¹	2#10M	0.18 ρ_b	30	Carbon	2
7	A4-C-2L	4#10M	0.36 ρ_b	30	Carbon	2
8	A4-C-3L	4#10M	0.36 ρ_b	30	Carbon	3
9	B2-C-3L	2#10M	0.18 ρ_b	50	Carbon	3
10	A2-P-2L	2#10M	0.18 ρ_b	30	PBO	2
11	A4-P-2L	4#10M	0.36 ρ_b	30	PBO	2
12	A4-P**-2L ²	4#10M	0.36 ρ_b	30	PBO	2
13	B2-P-2L	2#10M	0.18 ρ_b	50	PBO	2
14	A2-G-4L	2#10M	0.18 ρ_b	30	Glass	4
15	A4-G-2L	4#10M	0.36 ρ_b	30	Glass	2
16	A4-G-2L	4#10M	0.36 ρ_b	30	Glass	2

¹A2-C*-2L is carbon-FRCM specimen with M750 mortar

²A2-P**-2L is duplicate PBO-FRCM specimen

3.2.1 Specimen Preparation

The specimens were fabricated and casted in the Structural Lab at the University of Windsor. Special custom-made wood formwork was made. The formwork consisted of double-sided ply-wood sheets supported by 4x4 wood strips at the bottom and 2x4 wood studs on the sides. In order to have the plywood sheets in place for the exact dimension of the beam, strips of 2x4 are attached to the top of the formwork to prevent any movement of the sheets during casting. The strips are removed after casting. The steel-cages inside the beams are also built and fabricated in the Structural lab as shown in Figures 3.7 and

3.8.



Figure 3.7 Formwork for fabrication of RC beams



Figure 3.8 Fabrication of steel-cages for RC beams.

Casting was done in three batches. The first two batches were for the 30 MPa concrete strength specimens and the third batch was for the 50 MPa specimens. For the first batch the steel-cages were put in place, upright. However, for the second and third batch, the

steel-cage were placed upside down. Therefore, the specimens were casted inverted, so that we can control the roughness of the surface on which the FRCM are placed. Also, for the second and third batches, a plastic texture strip was placed in the locations at which the FRCM U-wrapped strips are placed so that it ensures that the surface has controlled level of irregularity rather than having a very smooth surface at which the mortar are bonded to. The specimens are moist cured for three days and then left to cure for more than 28 days in total. Figure 3.9 shows the casting procedure. The average compressive strength was measured by testing three cylinders with a nominal diameter of 101.6 mm (4 in) for each beam. All beam specimens were tested after 28-days and the compressive strength on the testing day was between 32 and 35 MPa with an average of 33 MPa for normal strength concrete and 48.7 MPa for high strength concrete (3rd patch). The reinforcing bars has a yield strength, f_y , of about 500 MPa and modulus of elasticity, E , of 200 GPa.



(a)



(b)



(c)



(d)



(e)



(f)



(g)

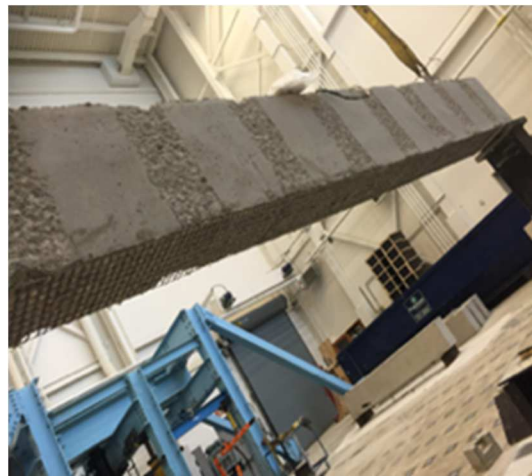
Figure 3.9 Fabrication and casting of second batch of RC beams: (a) wooden formwork before casting; (b) steel cages inserted inside formwork; (c) formwork after casting; (d) another photo for formwork after casting; (e) covering the specimens after casting; (f) curing process; (g) specimens after curing

3.2.2 FRCM Application

For the first batch of RC beams, the bottom surface at which the FRCM will be applied was smooth. The typical and most ideal method of roughening or preparing the surface for FRCM application is by the use of dry-sand blasting, which will expose the concrete aggregate for a better bonding between the FRCM matrix and the concrete substrate. However, since this equipment was not available, a hammer and chisel was used. After roughening, the surface was dampened with clean water, but without having any standing water at the surface. The FRCM mesh was held in place in the bottom of the beam by gluing few points to the surface. Then, the mortar was applied, followed by a layer of the mesh. This procedure was repeated for the additional layers. Figure 3.10 shows the application procedure for the first batch of beams.



(a)



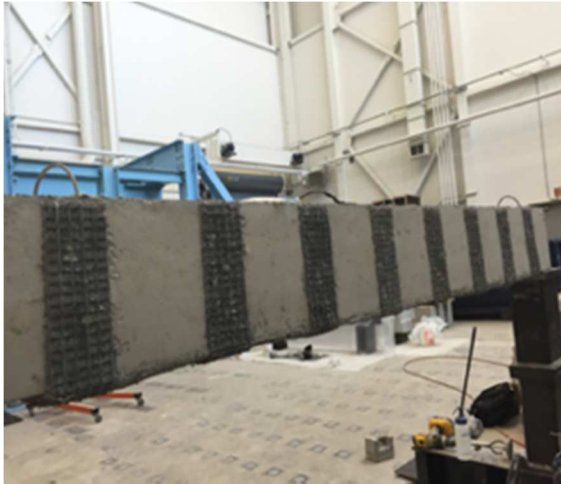
(b)



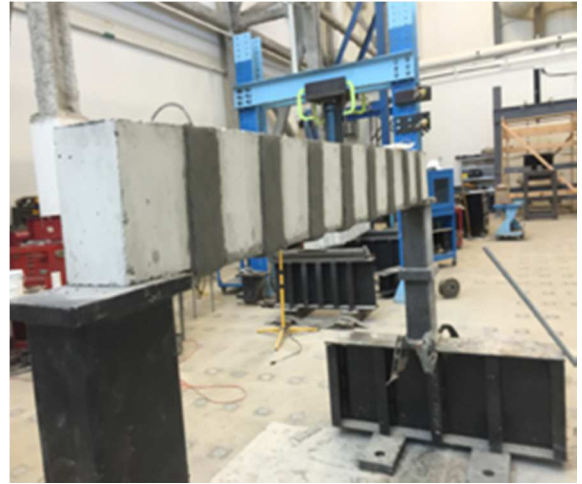
(c)



(d)



(e)



(f)

Figure 3.10 FRCM application for the first set of beams: (a) specimen after roughening; (b) specimen after putting the bottom fiber in place; (c) initial mortar layer applied; (d) first FRCM layer fully covered; (e) u-wrap strips put in place; (f) u-wrap strips totally covered with mortar

For the second and third batch of beams, the steel-cage was placed inverted, so that when casting the actual bottom of the beam is on top and the roughness of the beam can be controlled. After pouring the concrete on the formwork, the top surface of the beam is only leveled, but not finished so that the surface is rough. Also, as mentioned earlier, a plastic was glued on the sides of the formwork at the location at which the u-wraps will be placed. This plastic is removed immediately after the removal of the formwork. It gives the surface

an irregular pattern as in Figure 3.11, so when the mortar is placed it can have a better bonding.



Figure 3.11 Irregular pattern of concrete surface after removal of plastic strip

In order to apply the FRCM, the surface of the beam was dampened by wet water, but without having any standing water at the surface. An initial layer of mortar was applied, approximately 3-mm thick. Then, the first FRCM mesh was laid down, embedded in the mortar and totally covered by another layer of mortar. This procedure was repeated for each layer of both the main bottom FRCM strengthening and the U-wraps. Figure 3.12 shows illustrations for the different steps. The applied strengthening was then wet-cured for 3 days.



(a)



(b)



(c)



(d)



(e)



(f)

Figure 3.12 FRCM strengthening application procedure; (a) initial mortar layer applied; (b) FRCM mesh partially embedded inside mortar; (c) FRCM mesh embedded totally inside mortar; (d) u-wrapped FRCM strips embedded inside mortar; (e) FRCM mesh covered with mortar; (f) finishing after application of second FRCM layer

3.2.3 Test Set-up

The test specimens were simply supported on a roller and pin supports over a span of 2200 mm. Two concentrated loads, spaced at 500 mm, were applied at mid-span using a stiff spreader beam. The load was monotonically applied at a rate of 2 mm/minute using a 250 KN hydraulic actuator. Figure 3.13 shows the test and beam setup details.

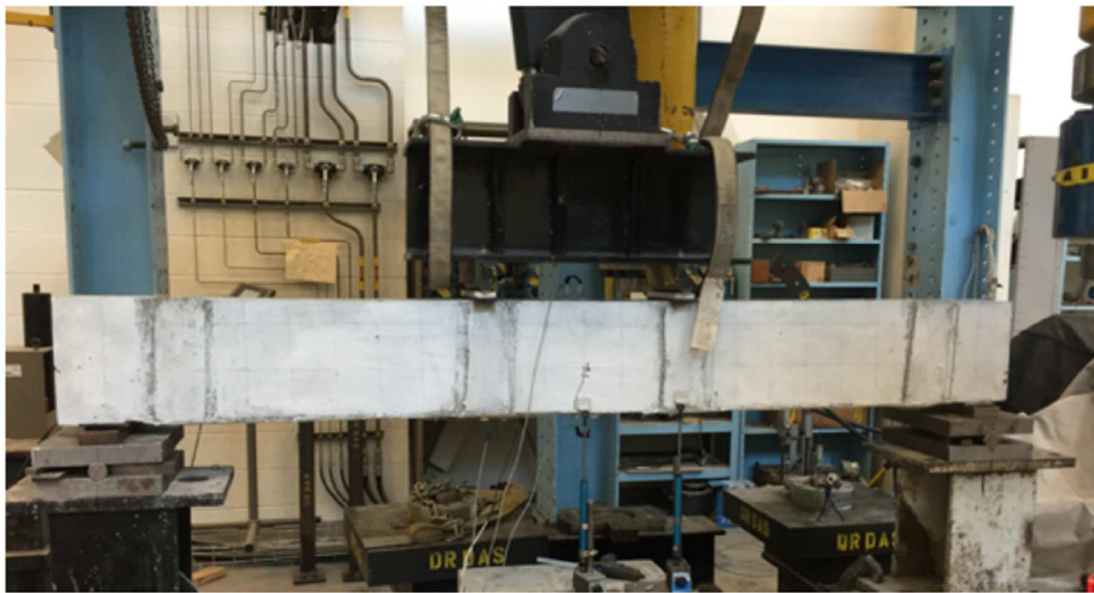
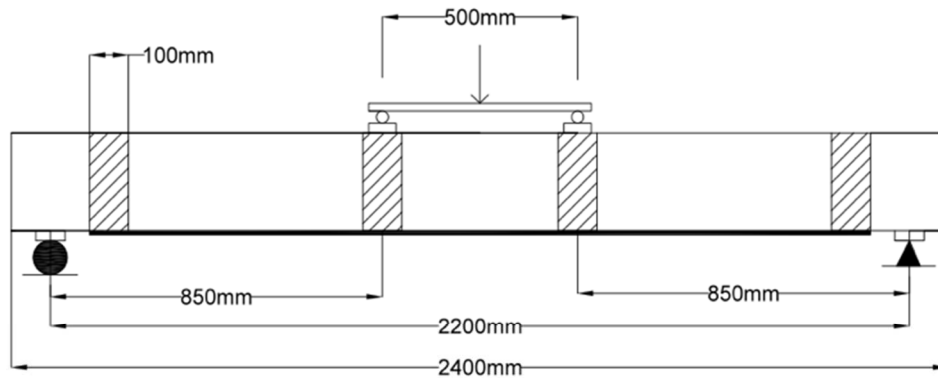


Figure 3.13 Beam test specimen set-up

3.2.4 Instrumentation

The four-point bending test gives the specimen a critical point at the midspan. At the midspan, it is expected that the maximum deflection and all the maximum strains will be detected. Also, the location under which the concentrated load will be applied is considered a second critical point. The instrumentation includes the following:

- I. Two Linear Variable Differential Transducers (LVDTs) were used to measure the deflection on the beam at the midspan and at location of load.

- II. A short-stroke LVDT was installed at the first crack developed around mid-span, region of maximum moment i.e. between the two concentrated loads.
- III. Two electric-foil strain gauges, 10 mm long, were installed on the bottom surface of the steel reinforcement before casting the concrete to measure the strain at midspan.
- IV. Four Pi-gauges were installed at the mid-span and load on the beam top surface and on the FRCM surface to measure the maximum compressive and tensile strain.

Figures 3.14, and 3.15 shows the instrumentation details of the set-up. It can be noticed from Figure 3.15(d) that there is a long electric-foil concrete strain beside the PI-gauge. This was used to verify the strains obtained by the PI-gauge.

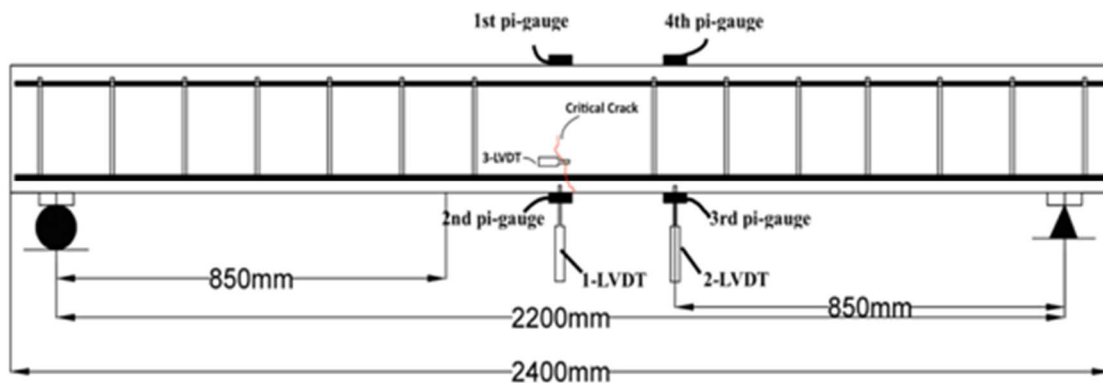
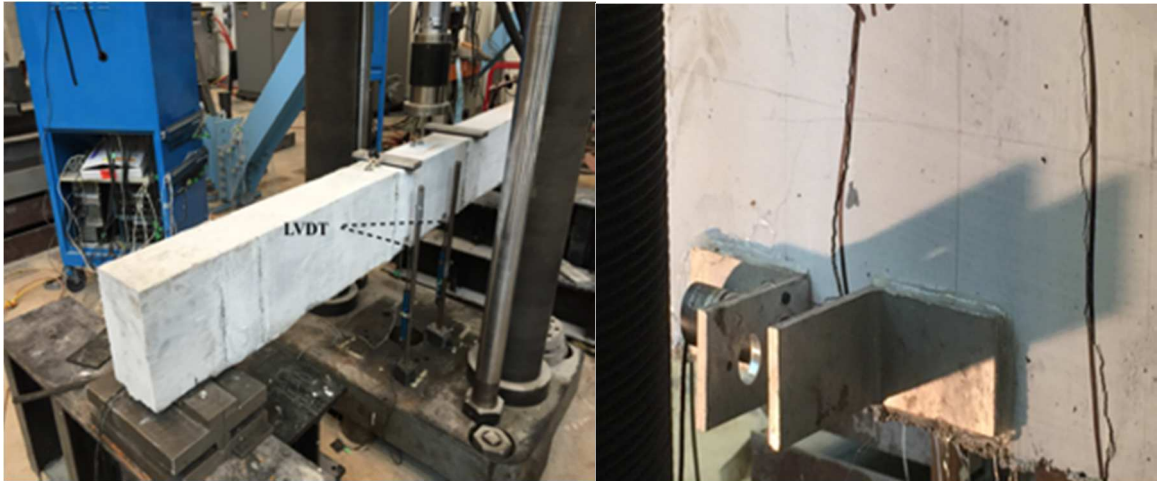


Figure 3.14 Instrumentation set-up

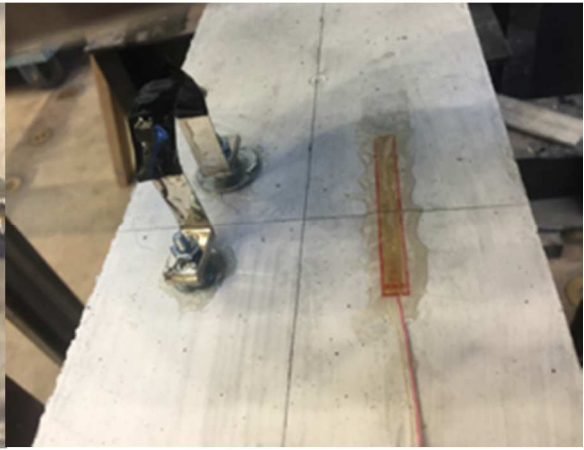


(a)

(b)



(c)



(d)



(e)



(f)

Figure 3.15 Instrumentations details: (a) two deflection LVDTs; (b) LVDT for measuring first crack; (c) steel strain gauge at the bottom face of the steel reinforcement at midspan; (d) top PI-gauge to measure concrete compression at midspan; (e) top two PI-gauges; (f) bottom two PI-gauges to measure concrete tension;

CHAPTER 4

TEST RESULTS AND DISCUSSION

This chapter is divided into two main sections to discuss the test results of phases I and II of the experimental program. Phase I includes the test results of the tensile characterization of the FRCM coupons and phase II includes the test results and analysis of the 16 large-scale reinforced concrete beams strengthened with different configurations of FRCM.

4.1 Phase I: Test Results and Analysis

In phase I, tensile characterization of glass, carbon and PBO-FRCM coupons were carried per the AC434 recommendations. Five coupons for each material were tested and data were recorded as described in Chapter 3, Section 3.1.

4.1.1 Tensile test results on Glass-FRCM

Figure 4.1 presents the typical recorded stress-strain behavior for a two-layer glass-FRCM coupon. The stress-strain behavior of the 2-layers coupons can be modeled as tri-linear behavior. The first stage, the stress varies between 0 and 300 MPa, represents the linear uncracked state of the FRCM. As the load increase, cracks started to develop in the mortar matrix and the load is transferred from the mortar to the fabric. This stage is called the multicracking process stage (second stage). This stage is recognized by significant reduction of the stiffness, with large increase in the strain with no or little increase in the stress. After the mortar is fully cracked, the load is resisted mainly by the fibers. This stage (stage three) is continuous up to failure. Most of the specimens failed due to slippage of fiber from the matrix, however, few of them failed by rupture of fibers as shown in Figure 4.2.

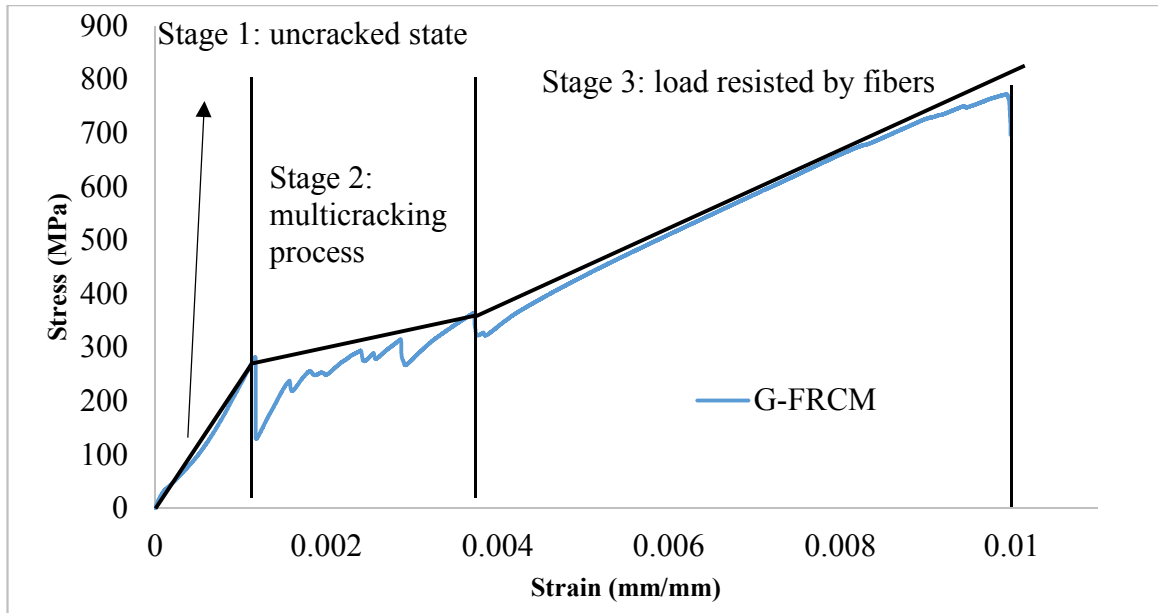


Figure 4.1 Stress-strain behavior of the G-FRCM coupons



Figure 4.2 Failure of G-FRCM coupons

4.1.2 Tensile test results on PBO-FRCM

Five PBO-FRCM coupon specimens were tested. Similar to the two-layered G-FRCM, the tested PBO-FRCM coupons showed typical trilinear behavior as illustrated in Figure 4.3. The uncracked stage of the PBO-FRCM coupons reached up to about 550 MPa. Contrary to the glass-FRCM coupons, none of the PBO-FRCM coupons reached the ultimate capacity of the fibers in which the fibers ruptures. The dominant failure mode was slippage of fibers as shown in Figure 4.5(a).

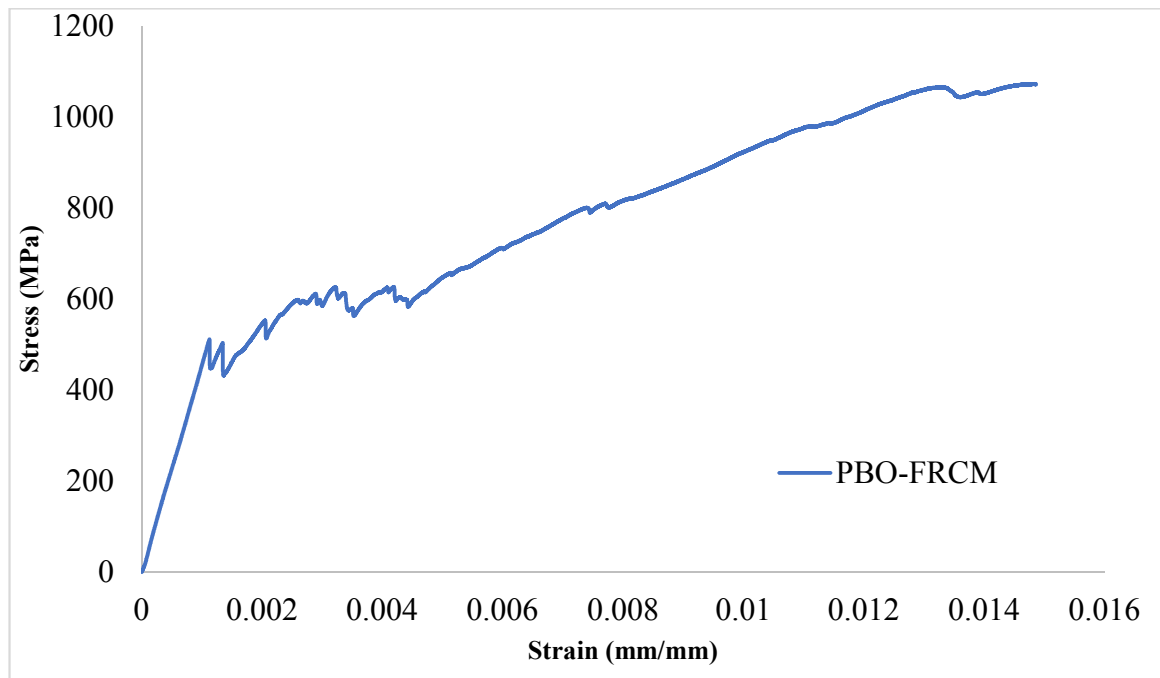


Figure 4.3 Stress-strain behavior for PBO-FRCM coupons

4.1.3 Tensile test results on C-FRCM

Carbon-FRCM coupons showed a similar performance to the PBO-FRCM in terms of stress-strain behavior and failure mode as shown in Figure 4.4. The uncracked stage of the carbon-FRCM coupons, the stress reaches 300 MPa. Contrary to the glass-FRCM, carbon-FRCM did not reach the ultimate capacity and no fiber rupturing was observed. The most dominant failure mode was also the slippage of fibers as shown in Figure 4.5(b).

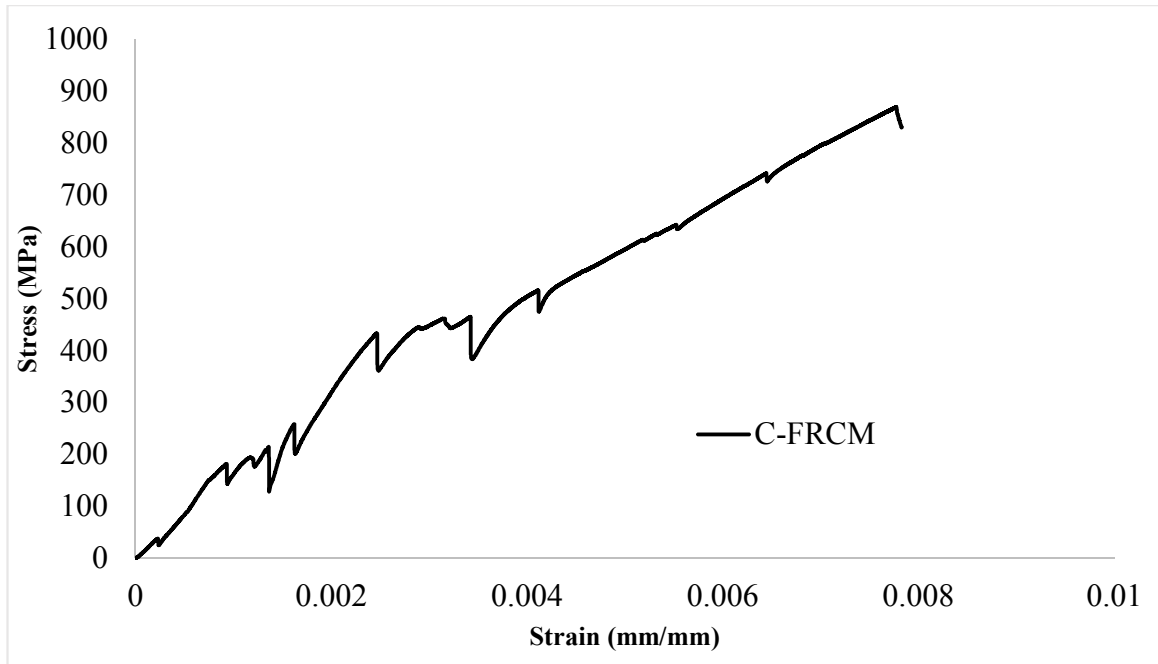


Figure 4.4 Carbon-FRCM stress-strain behavior



(a) PBO coupon front view and side view

(b) Carbon coupon front view

Figure 4.5 C-FRCM and PBO-FRCM coupon failures

4.1.4 Mechanical Properties of the FRCM systems

In order to characterize the tensile performance of the FRCM systems, the following characteristic parameters were calculated based on the net fabric area:

- Ultimate tensile strain, ϵ_{fu}
- Ultimate tensile stress, f_{fu}
- Modulus of Elasticity of the cracked specimen, E_f

The stress is computed by dividing the load induced by the cross-sectional area of the fabric as provided by the manufacturer. The modulus of elasticity of the cracked specimen is computed using the equation provided by the AC434 given below. This equation takes the cracked elastic modulus as 90% of the stress subtracted by 60% of the stress divided by the difference of the strains at 90% and 60% stresses, respectively. AC434 equation to compute the modulus of elasticity of the cracked specimen is given as:

$$E_f = \frac{\Delta f}{\Delta \epsilon} = \frac{0.9f_{fu} - 0.6f_{fu}}{\epsilon_{@0.9f_{fu}} - \epsilon_{@0.6f_{fu}}}$$

The summary of the test results is presented in table 4.1. The stress-strain behavior of all materials were typical and all consisted of the three stages shown in Figure 4.6. This behavior was also reported by several studies (Arboleda et al, 2015 and Loreto et al, 2013). It was observed that the transition point usually occurs at around 1000 microstrain, and the multicracking process between 1000 and 4000 microstrain for all the three coupons. Consistent with the three material's dry fiber properties, PBO-FRCM showed the highest cracked modulus of elasticity and ultimate tensile strength, followed by carbon-FRCM and glass-FRCM, respectively. PBO-FRCM showed about 38% and 90% higher cracked modulus of elasticity compared to Carbon and Glass, respectively. Similarly, PBO showed about 12.5% and 31.7% higher ultimate tensile strength compared to carbon and glass,

respectively. In conclusion, PBO showed the highest axial stiffness followed by carbon and glass. Also, it should be reported that the tensile characterization of FRCM coupons is very sensitive to the test set-up.

Table 4.1 Mechanical properties of the tested FRCM systems – 2-Layers coupons

FRCM Property	Symbol	Material	Mean	Standard Deviation	COV (%)
Modulus of Elasticity of the cracked specimen(GPa)	E_f	Glass	59.8	7.8	13
		Carbon	82.2	13.2	16.1
		PBO	113.8	25.8	22.6
Ultimate tensile strength(MPa)	f_{fu}	Glass	715	41	5.7
		Carbon	837	60.9	7.3
		PBO	942	86.4	9.2
Ultimate tensile strain(mm/mm)	ϵ_{fu}	Glass	0.00935	0.000632	6.7
		Carbon	0.00888	0.000695	7.9
		PBO	0.0111	0.00337	30.3
Fiber Area per unit width¹ mm²/mm	A_f	Glass		0.0473	
		Carbon		0.05	
		PBO		0.05	
Total fiber area in the coupon specimen mm²		Glass		4.73	
		Carbon		5	
		PBO		5	

¹ This value is provided by the manufacturer

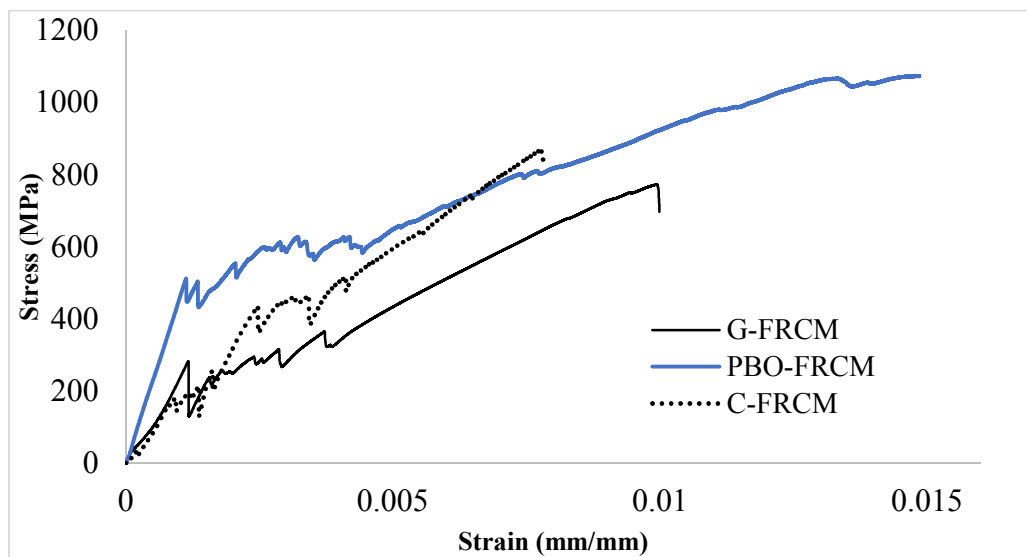


Figure 4.6 Comparison of the stress-strain behavior of Glass, Carbon, and PBO-FRCM

4.2 Phase 2: Test Results and Analysis

This section is divided into several subsections. Each subsection discusses the effect of an individual test parameter on the behavior of RC beams strengthened with FRCM. The parameters investigated are as following:

1. Axial stiffness of the FRCM system
2. Steel reinforcement ratio ($0.18 \rho_b$ and $0.36 \rho_b$)
3. Concrete strength (30 and 50 MPa)
4. Bonding material (M25 Vs M750 mortar)

In each subsection, the test results are presented in terms of comparisons of:

- ✓ Ultimate load capacity, post-cracking and post-yielding flexural stiffness and the Pseudo-Ductility Index
- ✓ Failure mode
- ✓ Load-deflection relationship at the midspan.
- ✓ Load-strain relationship at the midspan
- ✓ Load-crack width relationship

For each specimen, the load and deflection values at cracking, steel yielding and ultimate load (as shown in Figure 4.7) are presented. The post-cracking stiffness (PCS) of the beam, the gradient of the load-deflection curve in stage II, is calculated as the ratio of the difference in load to the difference in deflection between yielding and cracking points. Similarly, the post-yielding stiffness (PYS), the gradient of the load-deflection curve at stage III, is calculated as the ratio of the difference in load to the difference in deflection between ultimate and yielding. The Pseudo-ductility index (PDI) is a recommend parameter to reflect the enhancement in the ductility behavior of the FRCM strengthened

RC beams (Babaeidarabad et al, 2014). It is calculated as the ratio between the deflection values at failure and yielding. The deflection at failure can be taken at the load value 20% below the ultimate load in the descending part of load deflection curve (Babaeidarabad et al, 2014). Generally, the beam with higher pseudo-ductility ratio has higher tendency to redistribute the moment, increase its global deformation capacity and energy dissipation.

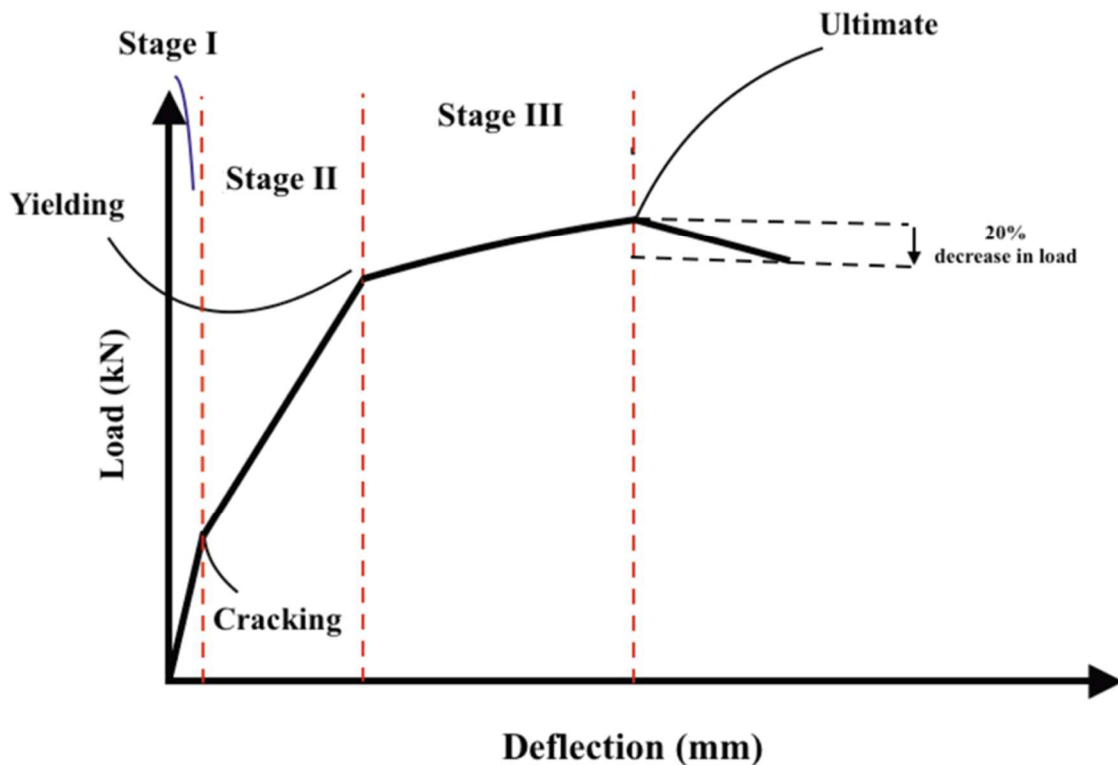


Figure 4.7 Typical load-deflection flexural behaviour of a RC beam

4.2.1 Effect of FRCM Axial Stiffness

There are two main factors that affects the FRCM axial stiffness of a beam. The first factor is the fabric type. As mentioned in section 4.1, PBO-FRCM has the highest axial stiffness followed by Carbon-FRCM and Glass-FRCM, respectively. Therefore, beams strengthened with a layer of PBO-FRCM has higher axial stiffness compared to the ones strengthened with Carbon or Glass. The second factor is the number of layers. Adding more

FRCM layers, increases the axial stiffness of a strengthened beam.

To investigate the effect of the FRCM axial stiffness, three scenarios were studied. The first scenario included the effect of FRCM fabric type on the axial stiffness. In this scenario, the comparison was based on the analysis of different FRCM fabric type with the same number of layers, and therefore having different axial stiffness. The second scenario included studying the effect of number of layers on the axial stiffness. In this scenario, the comparison was carried on a specific FRCM fabric, but with different number of layers, and therefore having different axial stiffness. The third scenario investigated the effect of having constant axial stiffness but with different fabric type.

4.2.1.1 Effect of the FRCM fabric type on the axial stiffness

This section discusses the effect of the FRCM fabric type on the flexural behaviour of FRCM strengthened RC beams. Seven test specimens were used to investigate the effect of the fabric type, as shown in Table 4.2. Two test specimens, A2-0 and A4-0, with 2#10M and 4#10M internal reinforcement, respectively, were used as control. The strengthened beams were divided into two groups, depending on the internal steel reinforcement. Group I has two test specimens, A2-P-2L and A2-C-2L, each was reinforced with 2#10M internal steel reinforcement, strengthened with two layers of PBO and carbon-FRCM, respectively. Group II has three test specimens, A4-P-2L_{avg}, A4-C-2L and A4-G-2L_{avg}, where each was reinforced with 4#10M internal steel reinforcement and strengthened with two layers of PBO, carbon, or glass-FRCM, respectively. Table 4.2 summarizes the main test results and behaviour parameters.

Table 4.2 Test results summary on the effect of the FRCM material type

Group	Specimen ID	FRCM-Ratio $\left(\frac{EA_{frcm}}{EA_{steel}}\right)\%$	Yielding	%	Ultimate	%	PDI ratio	PCS ratio	PYS ratio
			Load (kN)	increase	Load (kN)	increase			
	A2-0	-	39.8	-	52	-	1	1	1
	A4-0	-	73.4	-	89.3	-	1	1	1
I	A2-P-2L	4.3	44.2	11	69.3	33.3	1.07	1.19	2.82
	A2-C-2L	3.1	49	23.1	52.2	0	1.07	1.30	3.42
II	A4-P-2L _{avg} ¹	2.1	87.9	19.7	115.9	29.7	1.07	1.11	0.96
	A4-C-2L	1.5	86.2	17.4	91.4	2.36	0.87	1.08	1.18
	A4-G-2L _{avg} ¹	1.1	72.6	0	91.3	2.24	1.07	0.90	1.23

¹A4-P-2L_{avg} and A2-G-2L_{avg} corresponds to the average results of two duplicate specimens

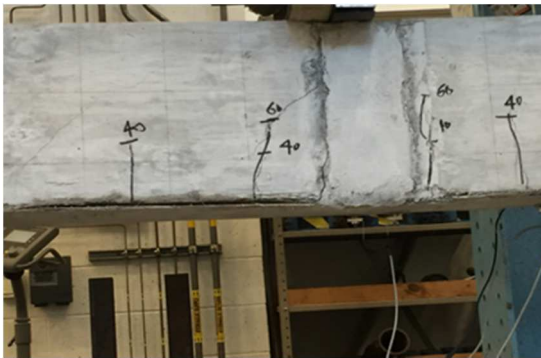
From Table, 4.2, it can be noticed that the PBO-FRCM had the most significant impact on the ultimate load capacity of the strengthened beams. Test specimens, A2-P-2L and A4-P-2L, showed 33% and 30% increase in the ultimate strength compared to A2-0 and A4-0, the control (un-strengthened) specimens. Both, A2-P-2L and A4-P-2L, showed consistent increase in the yielding load and the PCS of about 11% to 20% compared to A2-0 and A4-0. The deflection at ultimate load was always less than the control beam while the deflection at failure was almost the same. This would indicate the contribution of the FRCM in resisting the applied loads by sharing load, after yielding of the internal reinforcement. However, carbon and glass-FRCM showed insignificant increase in the ultimate load, as the increase was barely noticeable (less than 5%). The Carbon and Glass-FRCM strengthened beams showed noticeable improvement in the PDI ratio, as for A2-C-2L and A4-G-2L, the PDI ratio was equal to that of A2-P-2L. Both A2-C-2L and A4-G-2L had an increase of 7% compared to their respective control beam. Moreover, carbon-FRCM strengthened beams showed enhancement in PCS and PYS equal to or higher than that of PBO and glass, ranging from 8% to 242%.

The main reason behind the significant performance of A2-P-2L is the excellent bond performance between the PBO-FRCM and the concrete substrate. Specimen A2-P-2L suffered from a partial detachment of the FRCM from the bottom surface of the strengthened beams (type 2) before reaching the ultimate load in the zone between the load and the support as shown in Figures 4.8a and 4.8b. When the ultimate load was reached, wider cracks in the FRCM with slippage of fiber (type 1) close to the support occurred as shown in Figure 4.8c. The slippage of fiber was followed by detaching of the u-wrap under the load (type 2) as shown in failure 4.8d. This failure mode was identical for all PBO-

FRCM strengthened beams, except the ones with higher steel reinforcement on which no U-wrap detachment was observed. The observed bond behavior confirms very well with the findings of the previous studies as discussed in Chapter 2, section 2.3.



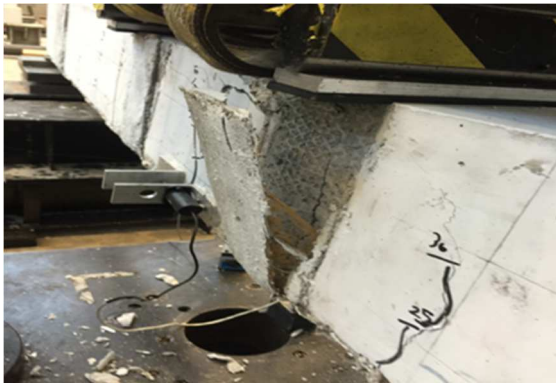
(a)



(b)



(c)



(d)



(e)

Figure 4.8 PBO-FRCM strengthened beams failure mode: (a) partial detachment of bottom side FRCM; (b) another view of FRCM partial detachment; (c) slippage of fibers close to support; (d) detachment of FRCM u-wrap strip; (e) closer photo of FRCM u-wrap strip detachment

For the carbon-FRCM strengthened beams, A2-C-2L and A4-C-2L, premature detachment of the FRCM system (type 2) occurred at mid-span slightly after the steel yielded which was quickly followed by slippage of fibers from the mortar (type 1) as shown in Figures 4.9a and 4.9b. As the load increases, an excessive slippage accompanied with an increased detachment was observed until failure as shown in Figures 4.9c and 4.9d. This premature failure compromises the strengthening effect of the carbon-FRCM compared to the PBO-FRCM as the carbon fibers slipped rather than reaching its ultimate capacity and rupturing. This failure mode was identical for all beams strengthened with carbon-FRCM.

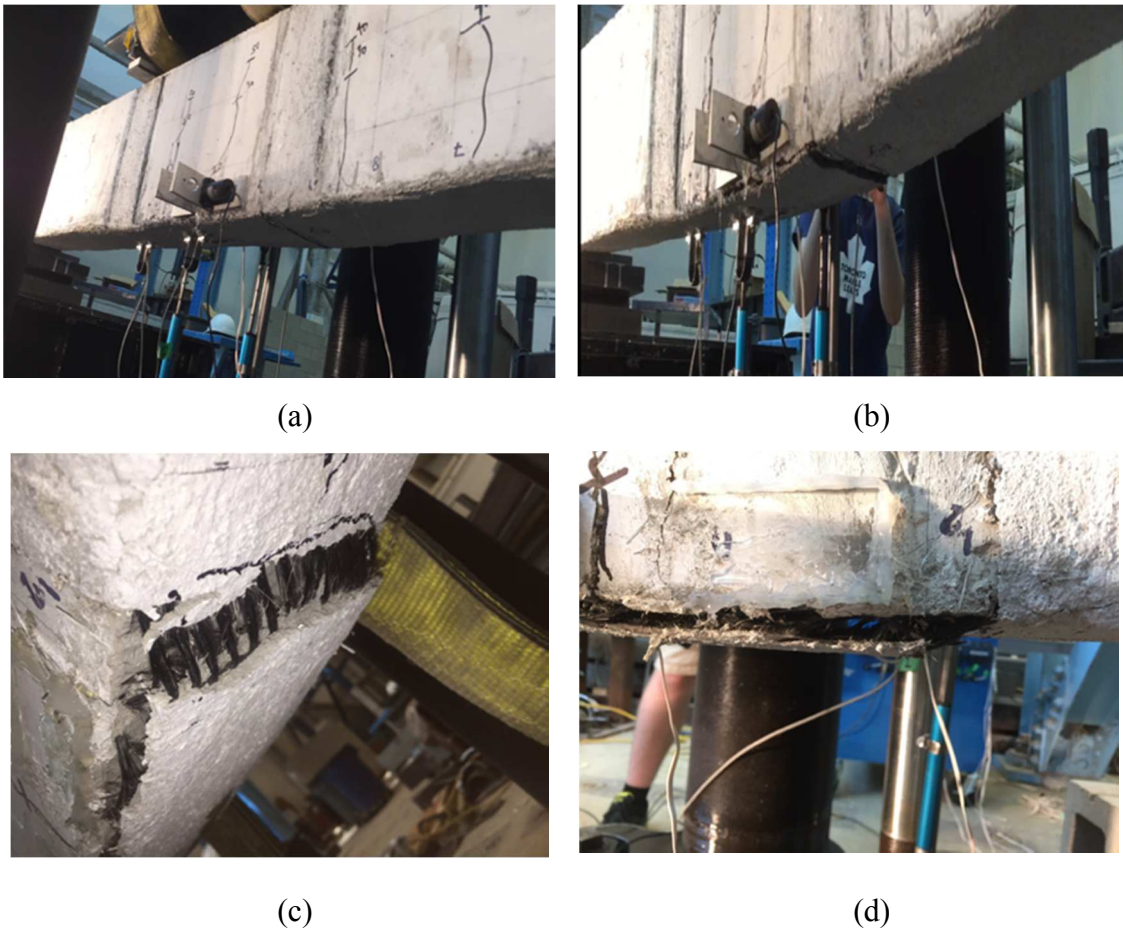


Figure 4.9 Carbon-FRCM strengthened beams failure mode: (a) detachment of FRCM; (b) slippage of FRCM; (c) increased slippage of fibers; (d) closer view of FRCM detachment

A4-G-2L, which was strengthened with only 2-layers of glass-FRCM suffered from premature bond failure between the FRCM and the concrete at early stages, after concrete cracking and before yielding which totally compromised the strengthening effect. Therefore, the behavior of A4-G-2L is almost the same as the control specimen A4-0.

The load-deflection behaviors of the tested beams in both groups I and II are shown in Figures 4.10 and 4.11. It can be noticed that in both groups, strengthening each material showed a different load-deflection behavior. Beams strengthened with PBO-FRCM showed a typical load-deflection behavior curve. They had similar behaviors as the control before cracking, however, after cracking and after yielding, they showed a significant stiffer performance than the control specimens as in Figures 4.10 and 4.11. The beams strengthened with carbon-FRCM, A2-C-2L and A4-C-2L showed a comparable behavior to the PBO in the first and second stage, however, right after yielding, the carbon strengthened beams suffered from a sharp drop in the load, losing about 6 kN. This drop is due to the premature bonding failure that occurred in the specimens strengthened with carbon-FRCM as discussed earlier. The beam strengthened with glass-FRCM, A4-G-2L, showed no change in the load-deflection behaviour compared to the control beam, A4-0.

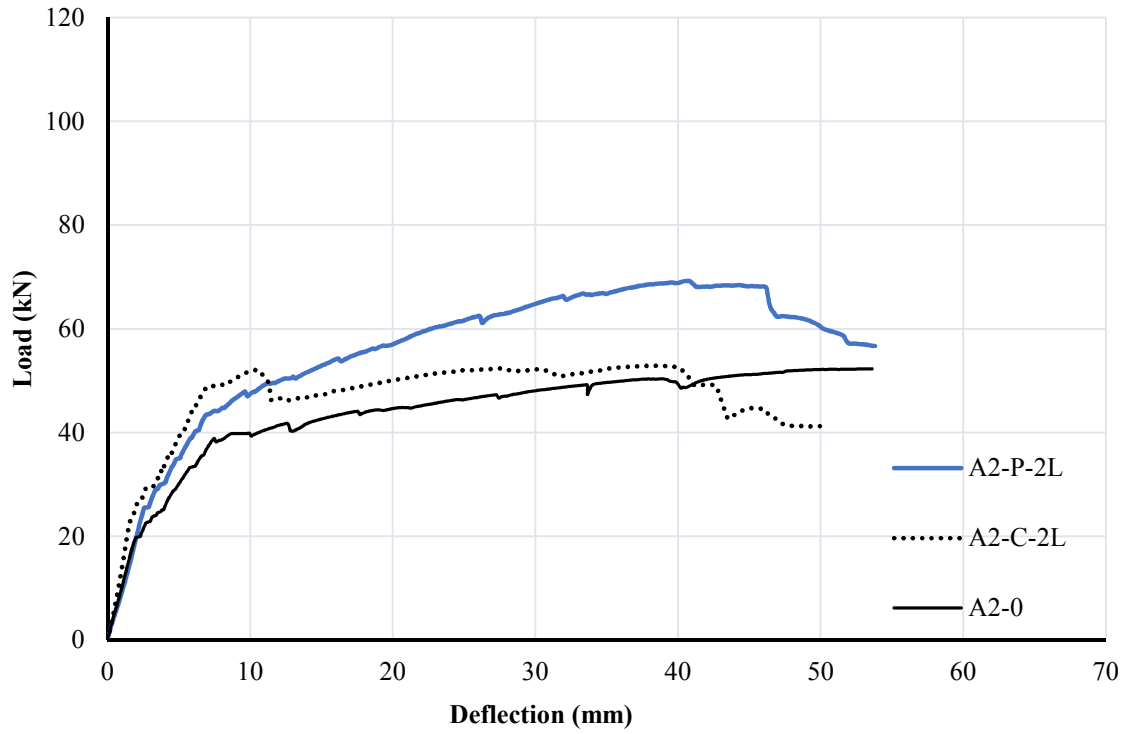


Figure 4.10 Load-deflection relationship for group I beams

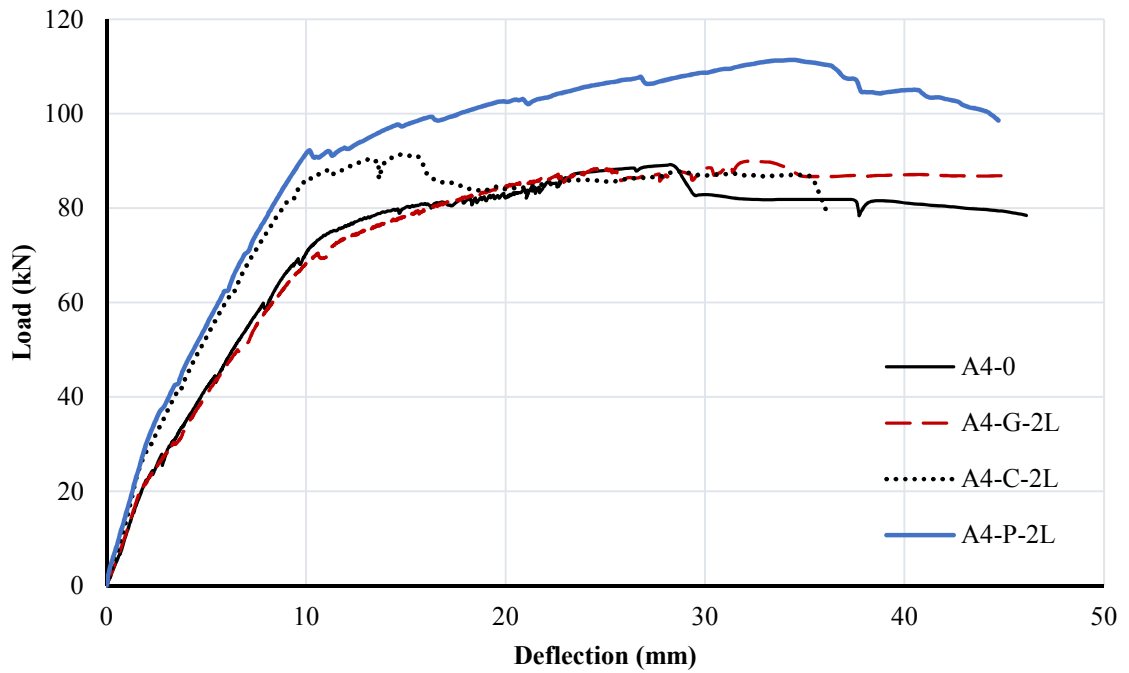


Figure 4.11 Load-deflection relationship for group II beams

A short-stroke LVDT was installed at the time first crack developed around the mid-span, region of maximum moment i.e. between the two concentrated loads. The beam is initially loaded until cracking. After cracking, the LVDT was mounted and the beam was reloaded again until failure. Figures 4.12 and 4.13 show the load and critical crack width relationships for group I and II beams. It can be noticed that, up to the yielding point, the strengthened beams had almost the same crack width as the control beams. After yielding, the strengthened beams had almost the same crack width as the control beams. After yielding, the crack width of the PBO-FRCM strengthened beams, A2-P-2L and A4-P-2L, was about 50% of the control ones. Also, the crack width in the Carbon-FRCM strengthened specimens were about 50% of the control specimens until the premature bond failure. However, glass-FRCM, seems to have no effect on the crack width.

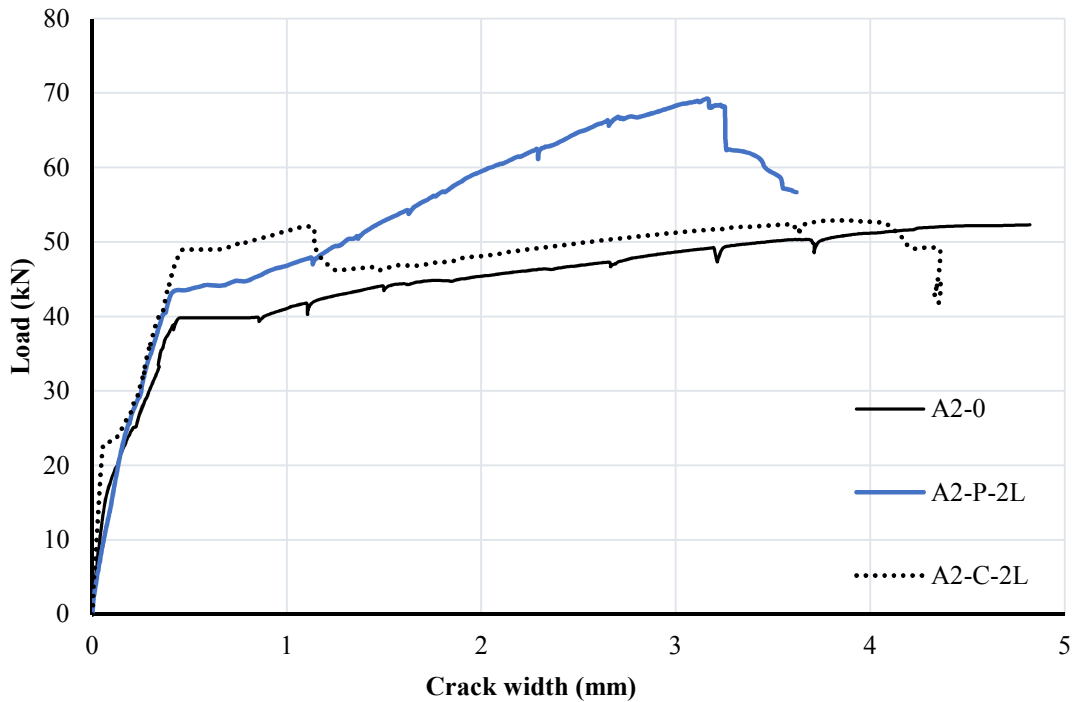


Figure 4.12 Load-critical crack width relationship for group I beams

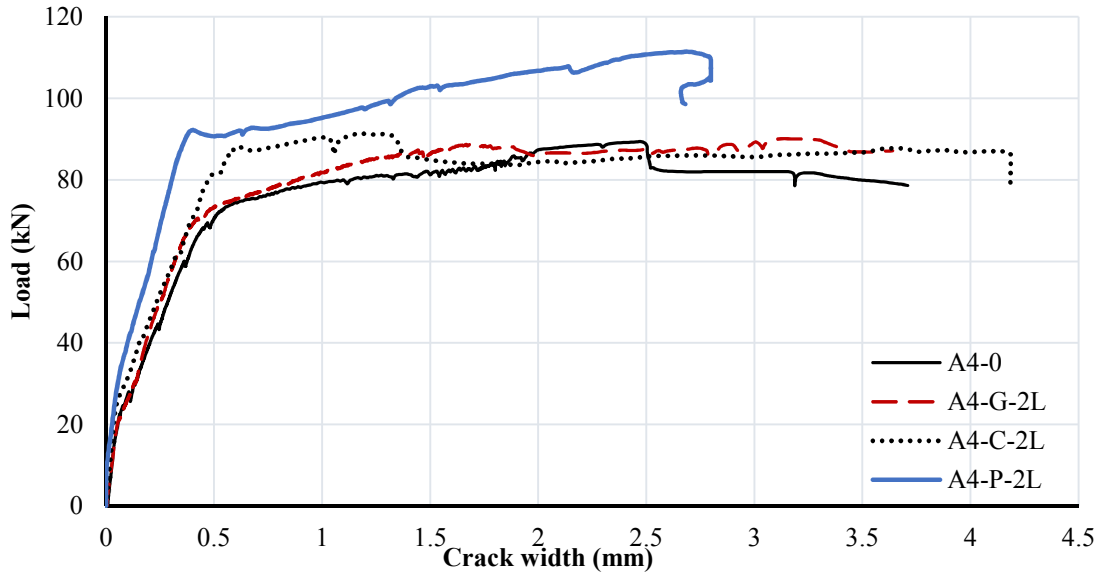


Figure 4.13 Load-critical crack width relationship for group II beams

The load and both, FRCM and concrete, strains behavior are shown in Figures 4.14 and 4.15 for groups I and II respectively. The strains are measured only at the midspan of the beam. The negative values for the strain represents the compressive strains at the top of the concrete cross-section, whereas the positive values represent the strains at the FRCM bottom surface. It can be noticed that the strain measurements in the FRCM confirms with the bond behavior noticed during testing, as were described in the previous section. Both pre-mature detaching of the FRCM and slippage of FRCM fiber nets resulted in decreasing of the strain measured in the glass and carbon-FRCM compared to the PBO-FRCM as shown in Figure 4.15. It can be noticed that the PBO-FRCM recorded the highest strain during loading. This indicated that the PBO-FRCM involved in resisting the applied load, and hence resulted in increasing the ultimate capacity. In Figure 4.15, at about 85 kN, partial detaching of the PBO-FRCM from the bottom surface of the strengthened beam, A4-P-2L, was noticed which resulted in the gradual decrease in the strain. The large horizontal plateau (sudden increase in the tensile strain) in the PBO strengthened beam in

Figure 4.15, the load-strain behavior was due to formation of wider cracks in the matrix when the load increased beyond 90 kN. The compressive strains in the concrete at failure was in the range of 3500 to 4000 microstrains in all specimens.

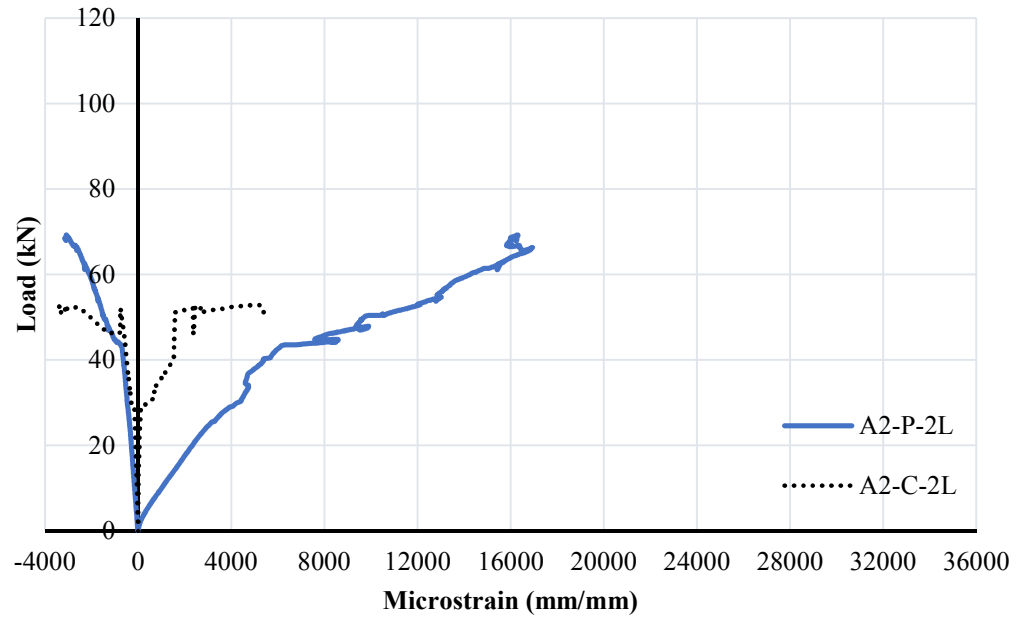


Figure 4.14 Load-concrete-FRCM strain relationship for group I

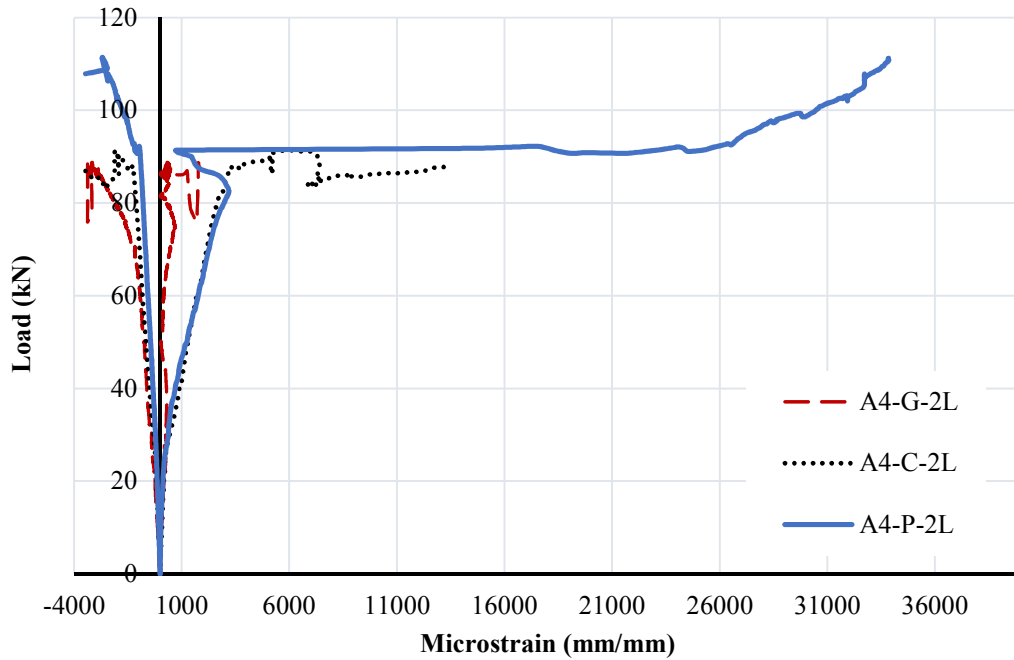


Figure 4.15 Load-concrete-FRCM strain relationship for group II

The following conclusions can be reported on the effect of the fabric type, PBO, Carbon and Glass:

- The beams strengthened with PBO showed the highest enhancement in the ultimate load capacity, as the increase ranged between 30% and 33%, compared to less than 5% for the beams strengthened with glass-FRCM and carbon-FRCM. This is mainly due to the superior bonding that the PBO-FRCM exhibited with the concrete substrate, in which no premature bonding occurred.

It should be noted the beams strengthened with glass and carbon had a much lower axial stiffness ratio, about 50% to 70% that of PBO strengthened beams, which may have contributed to their poor performance. To further investigate the effect of the FRCM material type, the next subsection investigates the effect of the axial stiffness on the behaviour of the strengthened beams.

4.2.1.2 Effect of number of FRCM layers on the axial stiffness

In this section, the effect of number of FRCM layers is studied. This study is only limited to Carbon-FRCM. In total, six beams are studied and compared. The six beams are divided into two groups. Group I has two test specimens, A2-C-2L and A2-C-3L were strengthened with two and three layers of carbon-FRCM, respectively. Group II has also two test specimens, A4-C-2L and A4-C-3L, were strengthened with two and three layers of carbon-FRCM, respectively, Table 4.3 summarizes the main results of the study.

It can be noticed from Table 4.3 that specimen, A2-C-3L, strengthened with three layers of carbon-FRCM, showed an increase of about 18%, whereas specimen A2-C-2L showed almost the same capacity as the control specimen, A2-0. Similarly, specimen A4-C-3L showed an increase of about 10%, meanwhile specimen A4-C-2L showed only an

increase of 2.4 % compared to the control specimen, A4-0. Therefore, it can be concluded that adding a third layer, increase the axial stiffness of the FRCM, significantly enhanced the ultimate load capacity of the carbon-FRCM strengthened beam. However, adding a third layer did not have a significant increase in the PDI ratio, as an increase of only 2% was obtained. Meanwhile, a remarkable increase in both, PCS and PYS, ratios was noticed. Specimens strengthened with three layers, A2-C-3L and A4-C-3L, had 19% to 28% more increase in the PCS ratio, and 11% to 72% more increase in the PYS ratio.

Table 4.3 Effect of number of layers on the axial stiffness results summary

Group	Specimen ID	FRCM	Yielding		Ultimate		PDI	PCS	PYS
		Stiffness Ratio $(\frac{EA_{frcm}}{EA_{steel}})\%$	Load (kN)	% increase	Load (kN)	% increase	ratio	ratio	ratio
	A2-0	-	39.8	-	52	-	1	1	1
	A4-0		73.4		89.3		1	1	1
I	A2-C-2L	3.1	49	23.1	52.2	0	1.07	1.30	3.42
	A2-C-3L	4.6	51.8	30.1	61.1	17.5	1.09	1.49	4.14
II	A4-C-2L	1.5	86.2	17.4	91.4	0	0.87	1.08	1.18
	A4-C-3L	2.3	89.2	21.5	98	9.7	0.89	1.36	1.29

Figures 4.16 and 4.17 shows the load-deflection relationship for groups I and II. All strengthened beams had a load-deflection pattern similar to all C-FRCM strengthened beams discussed previously. All strengthened specimens suffered from a type II failure, however, this failure happened at a later stage for specimens, A2-C-3L and A4-C-3L, that are strengthened with three layers. As expected, the beam strengthened with three layers of carbon-FRCM showed a higher increase in both, yielding and ultimate, loads compared to the two layered beam. This increase is consistent with the increase in the axial stiffness of both beams. However, the addition of a third layer did not have a noticeable effect on the critical crack width of the beams as shown in Figures 4.18 and 4.19.

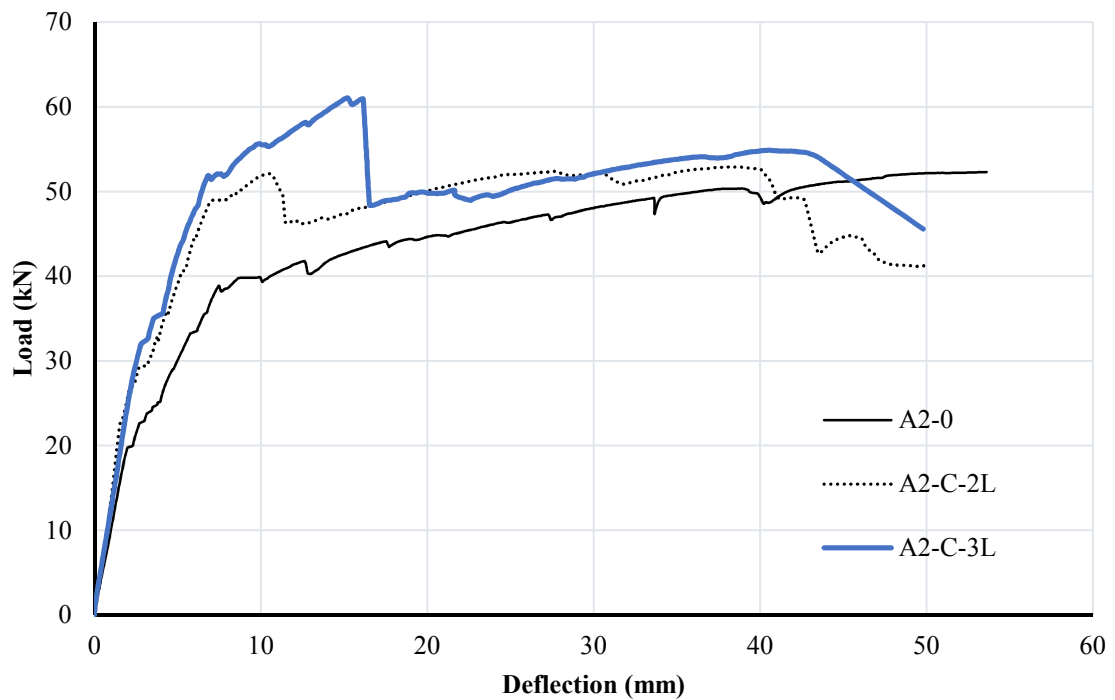


Figure 4.16 Load-deflection relationship for group I beams

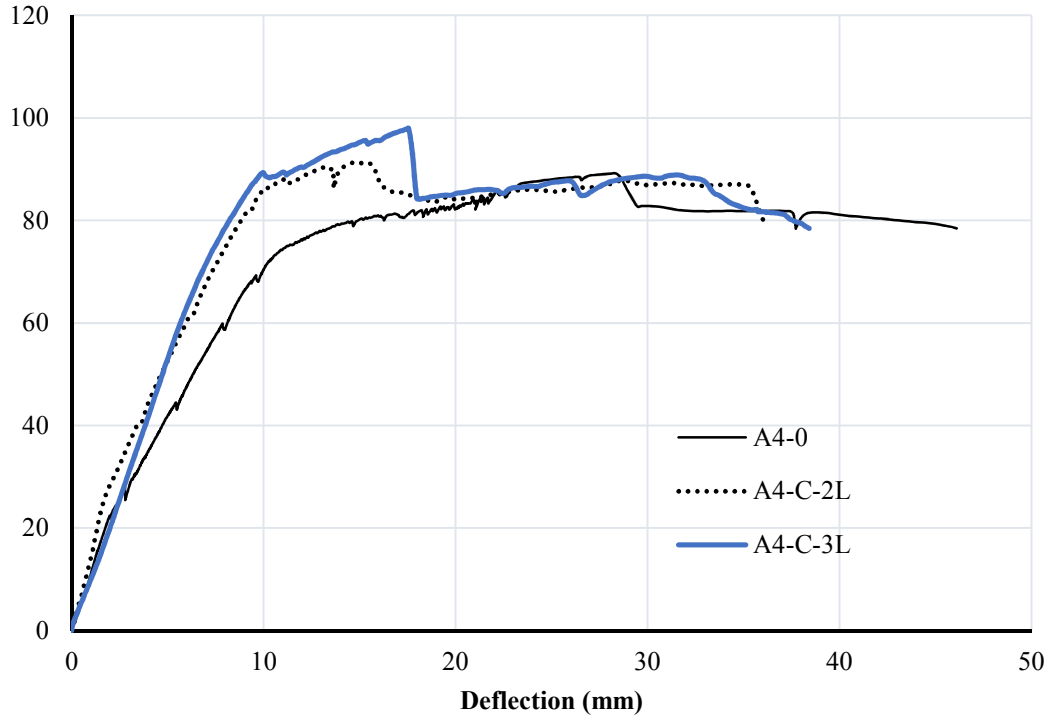


Figure 4.17 Load-deflection relationship for group II beams

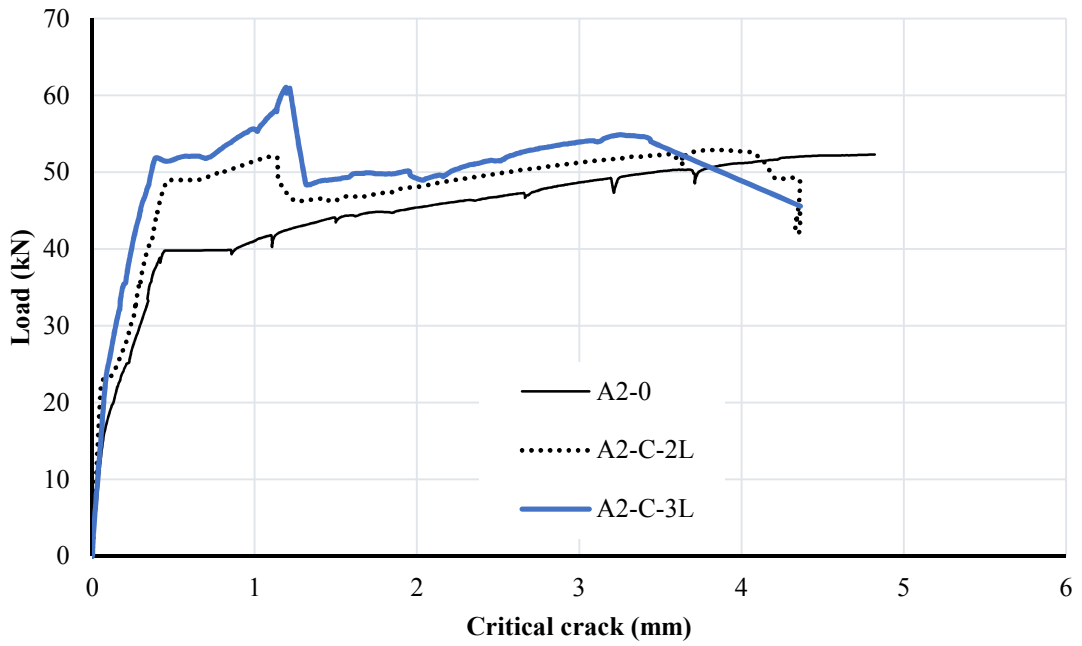


Figure 4.18 Load-critical-crack width relationship for group I beams

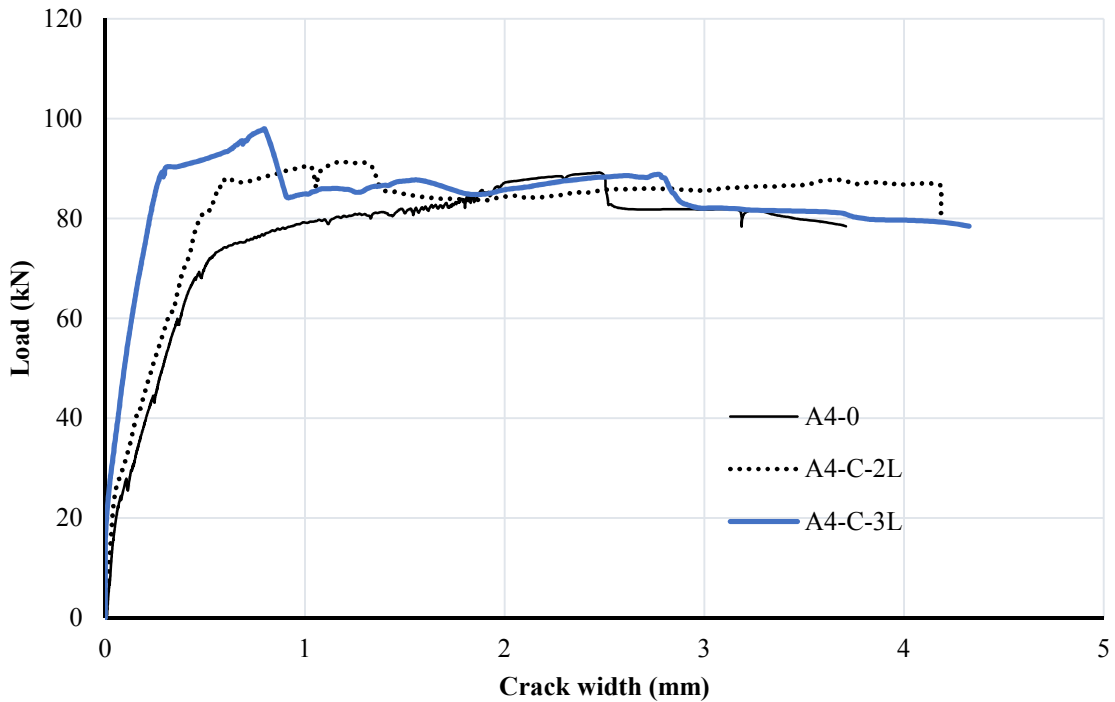


Figure 4.19 Load-critical-crack width relationship for group II beams

It can be concluded that:

- Increasing the axial stiffness of the FRCM, by adding FRCM layers, significantly enhanced the performance and load capacity carbon-FRCM strengthened beam. For group I beams, the percentage increase in ultimate load went up from 0% to 17.5%. Similarly, for group II beams, ultimate load increase went up from 0% to 9.7%.
- Increasing the axial stiffness of the FRCM, by increasing the number of layers, did not have a noticeable increase in the PDI ratio, as an increase of only 2% was obtained. Meanwhile, a remarkable increase ranging from 11 to 72% was obtained in both, PCS and PYS, ratios.

4.2.1.3 Effect of the fabric type on constant Axial Stiffness

In this section, the effect of the FRCM fabric type with constant axial stiffness on the flexural behaviour of FRCM strengthened RC beams is investigated. Six beams were used in the comparison as shown in table 4.4. Two test specimens, A2-0 and A4-0, were used as control beams, and the remaining beams were divided onto two groups. Group I has two test specimens, A2-P-2L, and A2-G-4L and group II has two test specimens, A4-P-2L and A4-C-3L. The test specimens in each group were strengthened with different FRCM fabric type and number of layers. To investigate the effect of the constant axial stiffness, the number of layers for each beam were selected so that all beams have almost the same axial stiffness. Table 4.4 summarizes the main test results.

Although all the specimens had comparable axial stiffness ratio, it can be noted that the PBO-FRCM strengthened beams, A2-P-2L and A4-P-2L, have the best performance in terms of enhancement in the ultimate load capacity. The PBO-FRCM strengthened beam, A2-P-2L, showed an increase of about 33% in the ultimate load capacity, compared to 4% for the glass-FRCM strengthened beam (A2-G-4L). In terms of PDI ratio, the glass-FRCM strengthened beam, A2-G-4L, showed the best performance, as it had an increase of about 28% compared to 7% and for PBO-FRCM strengthened beam. Carbon-FRCM strengthened beam, A4-C-3L, had the highest increase in the yielding load, PCS and PYS. Moreover, A2-G-4L, strengthened with 4-layers of glass-FRCM, had high PCS and PYS ratios, however, slightly lower than the PBO-FRCM

Table 4.4 Test results summary for the effect of the FRCM system type

Group	Specimen ID	EA_{frcm} (kN)	FRCM-Ratio $\left(\frac{EA_{frcm}}{EA_{steel}}\right)\%$	Yielding	%	Ultimate	%	PDI	PCS	PYS
				Load (kN)	increase	Load (kN)	increase	ratio	ratio	ratio
	A2-0		-	39.8	-	52	-	1	1	1
	A4-0		-	73.4	-	89.3	-	1	1	1
I	A2-P-2L	1710	4.3	44.2	11	69.3	33.3	1.07	1.19	2.82
	A2-G-4L	1700	4.2	46.1	15.8	54.2	4.2	1.28	1.14	2.5
II	A4-P-2L _{avg} ¹	1710	2.1	87.9	19.7	115.9	29.7	1.07	1.11	0.96
	A4-C-3L	1850	2.3	89.2	21.5	98	9.7	0.89	1.36	1.29

¹A4-P-2L_{avg} corresponds to the average results of two duplicate specimens.

The specimen strengthened with three layer of carbon-FRCM, A4-C-3L, failed in a similar manner as the specimen strengthened with two layers, A4-C-2L, which was discussed in the previous subsection. However, the premature failure in A4-C-3L happened at a later stage. A2-G-4L, the specimen strengthened with 4-layers of glass-FRCM, had a premature bond failure in the form of detaching of FRCM (type 2) occurred at mid-span and propagating through the entire area between the concentrated loads after yielding of the internal reinforcement as shown in Figure 4.20. This was followed by slippage of fibers (type 1) and complete detachment with rupture of the glass-FRCM at failure as shown in Figure 4.20.



Figure 4.20 Glass-FRCM strengthened beam, A4-G-4L, failure mode

The pre-cracking load-deflection behavior for all beams was identical as shown in Figure 4.21, however after cracking, the strengthened beams showed a steeper slope, stiffer behavior, in comparison to the control beam. At the region extending up to the yielding load, the strengthened beams had a higher load capacity of at least 11%. It can be observed that shortly after the beams reached their yielding point, the premature bond failure in specimen, A2-G-4L, played a very important role in compromising the strengthening

effect. This premature is represented by the sharp drop in the load that occurred at around 60 kN for specimen, A2-G-4L.

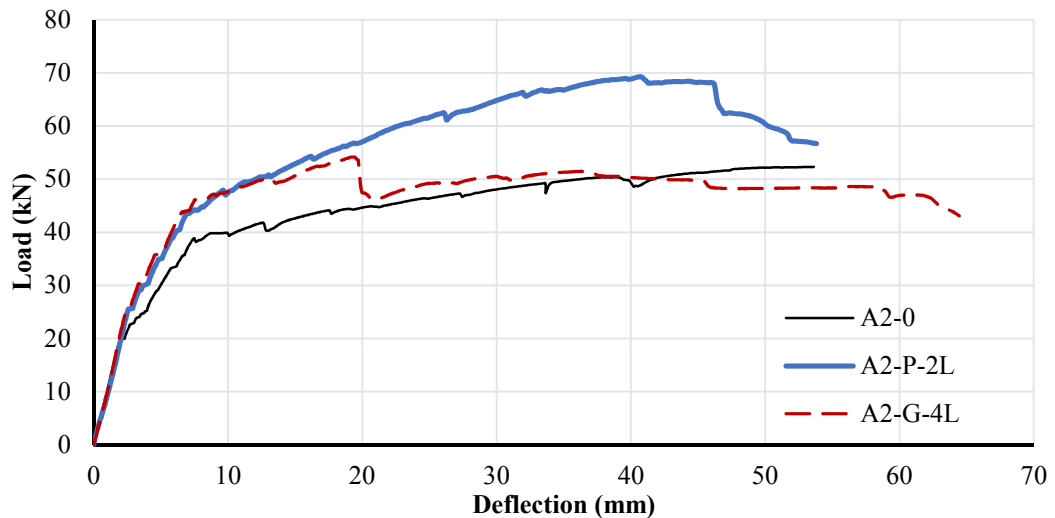


Figure 4.21 Load-deflection relationship for group I beams

The load-critical crack behavior is shown in Figure 4.22. It can be noted that a significant increase in the crack width after yielding of the steel reinforcement was observed in all specimens. However, the carbon-FRCM (before bond failure) and PBO strengthening decreased the crack width growth after yielding to about 50% of the control specimen. Due to the excellent observed bond between PBO-FRCM and the concrete substrate, the PBO strengthened beams, A2-P-2L and A4-P-2L, had the least crack width, compared to all the other specimens.

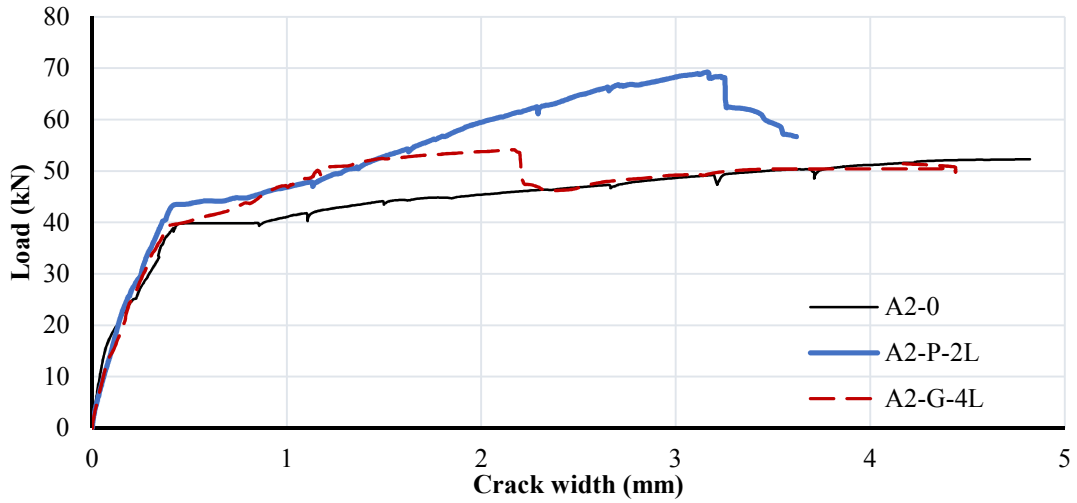


Figure 4.22 Load-critical crack width relationship for group I beams.

Figure 4.23 shows the load vs concrete and FRCM strain behaviours for group I beams. The PBO-FRCM strengthened beam, A2-P-2L, had the highest FRCM tensile strain. This is due to excellent bond observed between the PBO-FRCM and the concrete substrate.

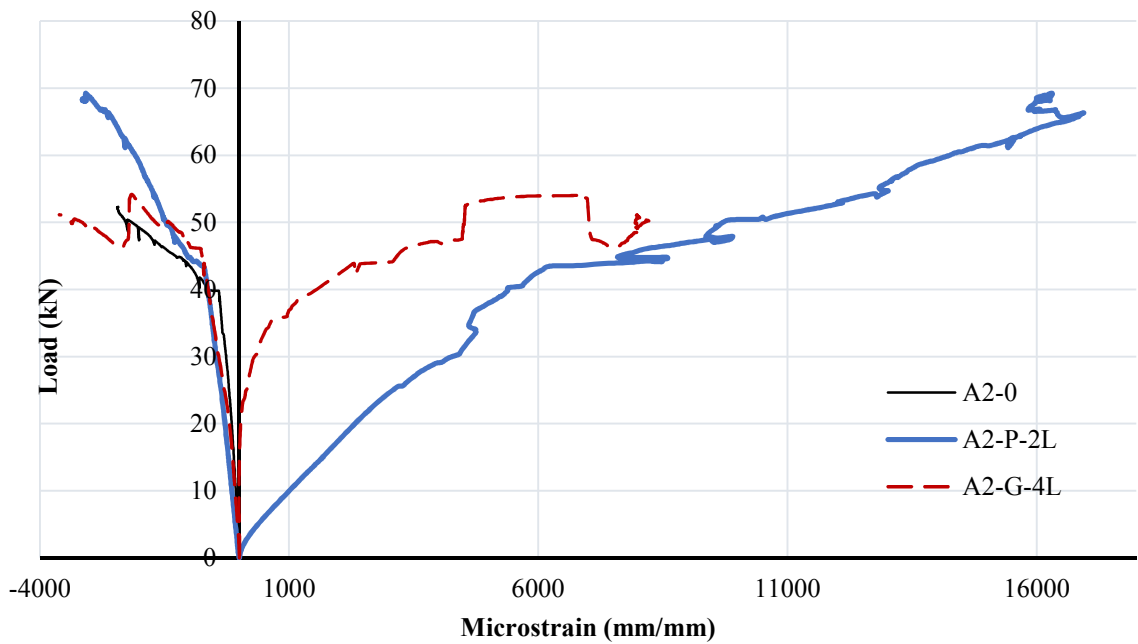


Figure 4.23 Load-concrete-FRCM strain relationship for group I beams

Referring to the effect of the axial stiffness, it can be concluded that:

- Although the specimens studied had very comparable axial stiffness ratio, PBO-FRCM still showed the greatest enhancement on the ultimate capacity of the strengthened beams. An increase of 33% and 4% was obtained in comparison with the control (unstrengthened beam) for group I specimens.
- The premature failure that occurred in specimens strengthened with carbon-FRCM and glass-FRCM compromised the strengthening effect, which caused them to have lower increase in the ultimate load capacity compared to the specimens strengthened with PBO-FRCM.
- The excellent bond observed between PBO-FRCM and concrete was the main reason behind its superior performance and great strength enhancement.
- The glass-FRCM strengthened beam, A2-G-4L, showed the best ductile performance, as it had an increase in the PDI ratio of about 28% compared to 7% for PBO strengthened beam.

4.2.2 Effect of the internal steel reinforcement ratio

In this subsection, detailed analysis is carried to study the effect of the internal steel reinforcement ratio on the strengthening of RC beams using FRCM. Two internal steel reinforcements, 2#10M (low steel reinforcement, LSR) and 4#10M (moderate steel reinforcement, MSR) were studied. Two beams, A2-0 and A4-0, having LSR and MSR, were used as control specimens. The remaining beams were divided into three groups, each group having two test specimens. Group I consists of two beams, A2-P-2L and A4-P-2L_{avg}, both strengthened with two layers of PBO-FRCM. Similarly, group II consists of two beams, A2-C-2L and A4-C-2L, both strengthened with two layers of carbon-FRCM. Group III consists of two beams, A2-C-3L and A4-C-3L, both strengthened with three

layers of carbon-FRCM. Table 4.5 summarizes the main test results.

The comparison is carried out between the two specimens within each group. For example, specimen A2-C-3L is compared with A4-C-3L, and specimen A2-P-2L is compared with A4-P-2L_{avg}. In other words, all the parameters are kept constant except the reinforcement ratio and both beams are compared with their respective control unstrengthened beams. Figure 4.24 shows the comparison of the increase in ultimate load capacity for the MSR and LSR strengthened specimens.

Table 4.5 Effect of steel reinforcement ratio test results

Group	Specimen ID	FRCM-ratio ($\frac{EA_{frcm}}{EA_{steel}}$)%	Yielding Load (kN)	% increase	Ultimate Load (kN)	% increase	PDI ratio	PCS ratio	PYS ratio
-	A2-0	-	39.8	-	52	-	1	1	1
-	A4-0	-	73.4	-	89.3	-	1	1	1
I	A2-P-2L	4.8	44.2	11	69.3	33.3	1.07	1.19	2.82
	A4-P-2L _{avg} ¹	2.4	87.9	19.7	115.9	29.7	1.07	1.11	0.96
II	A2-C-2L	3.1	49	23.1	52.2	0	1.07	1.30	3.42
	A4-C-2L	1.5	86.2	17.4	91.4	0	0.87	1.08	1.18
III	A2-C-3L	4.6	51.8	30.1	61.1	17.5	1.09	1.49	4.14
	A4-C-3L	2.3	89.2	21.5	98	9.7	0.89	1.36	1.29

¹A4-P-2L_{avg} is the average results of the two specimens, A4-P-2L and A2-P*-2L

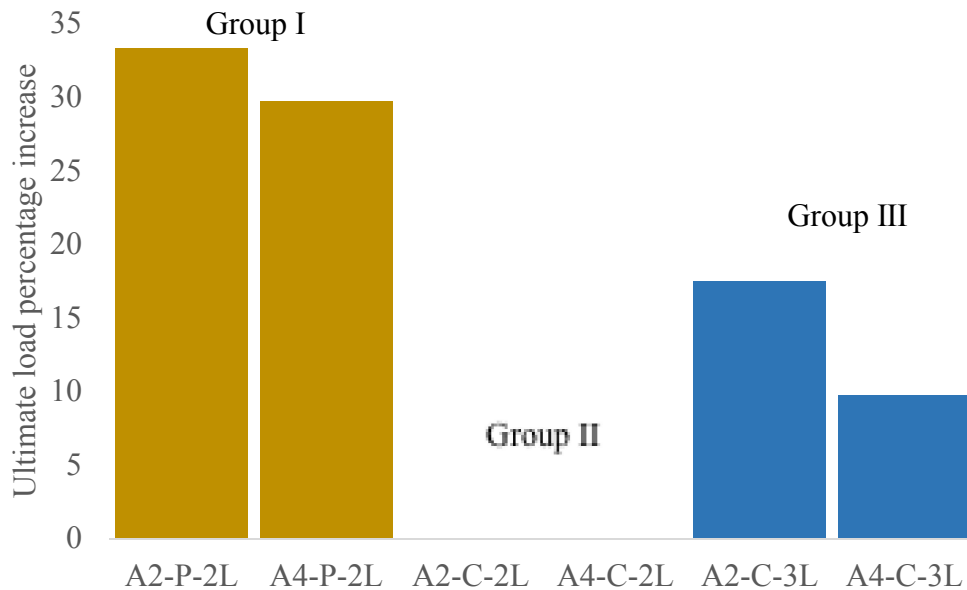


Figure 4.24 Percentage increase in load capacity on the effect of steel reinforcement ratio

Specimen A2-P-2L showed an increase of about 33% in the ultimate load capacity, whereas, specimen A4-P-2L_{avg} showed an increase of about 30% compared to their respective control specimens, A2-0 and A4-0 as shown in table 4.5. Similarly, specimen A2-C-3L showed an increase of about 17 % in ultimate load capacity, whereas specimen A4-C-3L showed an increase of about 10 % compared to the control ones. Accordingly, increasing the steel reinforcement by 100%, decreases the gain in ultimate strength by 10% and 45% for PBO-FRCM and carbon-FRCM, respectively. Therefore, it can be concluded that the increase in steel reinforcement, decreases the FRCM strengthening effect on the ultimate load capacity. In terms of PDI ratio, no change was noticed with the specimen strengthened with PBO-FRCM when internal steel reinforcement was increased. However, the MSR beams strengthened with carbon-FRCM, showed a decrease of about 20% in the PDI ratio compared to LSR strengthened beams. Moreover, MSR strengthened beams showed about 8% to 22% decrease in PCS compared to LSR strengthened beams. In

addition, MSR strengthened beams showed about 186% to 285% decrease in PCS compared to LSR strengthened beams. Based on the above analysis, it can be concluded that regardless of the internal steel reinforcement, the FRCM systems enhanced the PCS and PYS, however, this enhancement becomes less significant as the internal steel reinforcement increases.

Based on the load-deflection curve for group I shown in Figure 4.25, it can be noticed that the two PBO-FRCM strengthened beams had a very similar flexural behaviour although they had different internal steel reinforcements. After cracking, the PBO-FRCM strengthened beams starts to have higher slopes (higher stiffness) compared with the unstrengthened ones. Specimen A4-P-2L had a larger increase in the yielding load compared to specimen A2-P-2L. Bond failure (type I) for specimen A4-P-2L happened right after the beam reached its ultimate capacity at around 88% of its failure deflection, which is noted by the drop in load in Figure 4.25. Similarly, specimen A2-P-2L had a bond failure (type I) happened right after the specimen reached its ultimate capacity at around 85% of its failure deflection.

For group II and III specimens, the load-deflection relationship is shown in Figure 4.26. For both sets of specimens, it can be noticed, as in group I, after cracking, LSR strengthened beams, A2-C-2L and A2-C-3L, had a much steeper slope in comparison with the control, whereas MSR strengthened beams, A4-C-2L and A4-C-3L, had less increase in the steepness of the slope. This implies that, A2-C-2L and A4-C-3L, had higher PCS ratio. Moreover, group I strengthened beams, A2-C-2L and A4-C-3L, reached their ultimate load capacity at about only 20% to 40% of their failure deflection. After reaching the ultimate capacity there was a sudden drop in the load due to the bond failure (type II) for

all group II and III beams. However, for group I, the strengthened beams continued sustaining the load until at larger deflection fibers started to slip which can be characterized as type I bond failure as shown by the second drop in load that occurred very close to the failure of the beam as shown in Figure 4.27

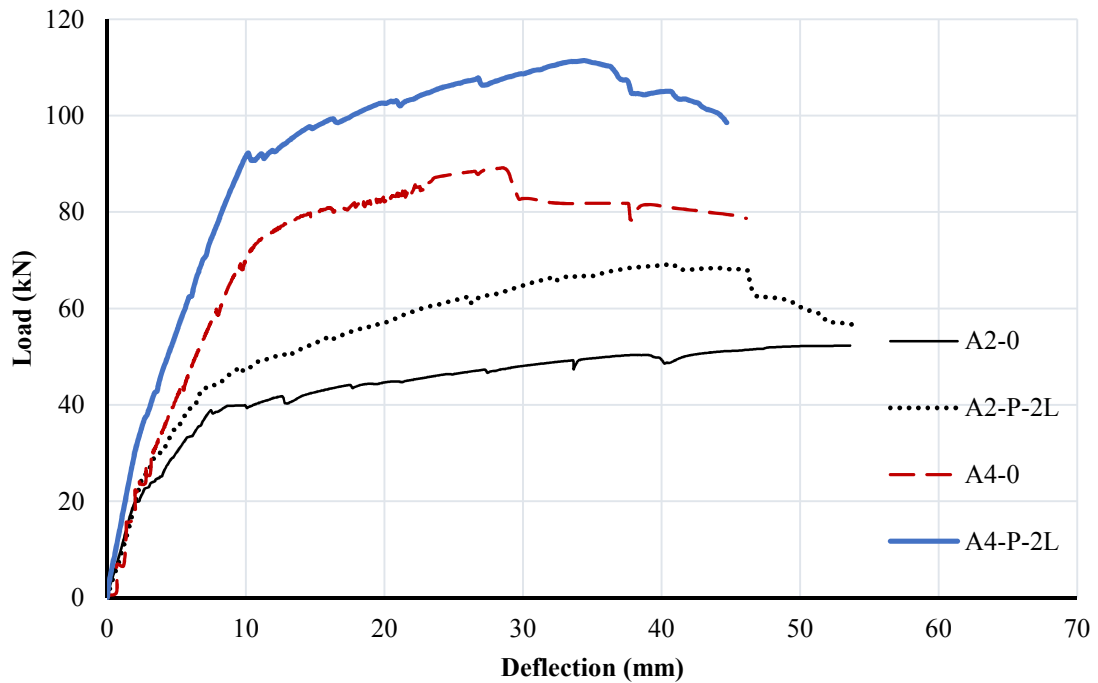


Figure 4.25 Load-deflection relationship for group I beams

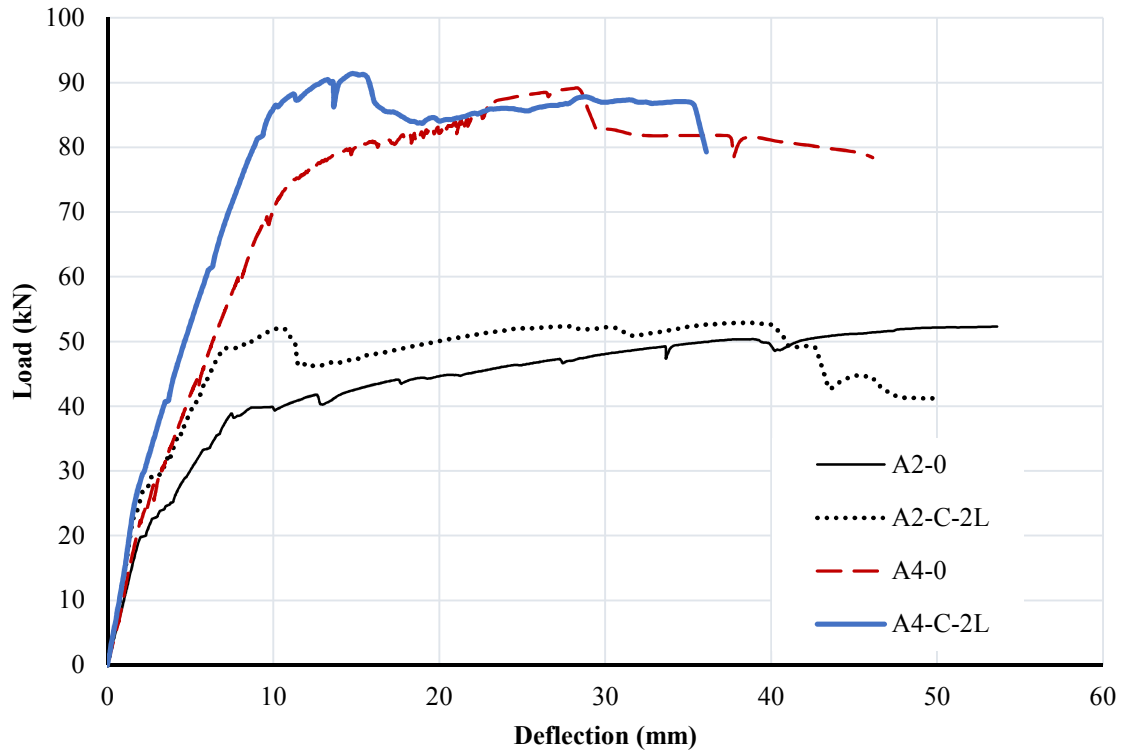


Figure 4.26 Load-deflection relationship for group II beams

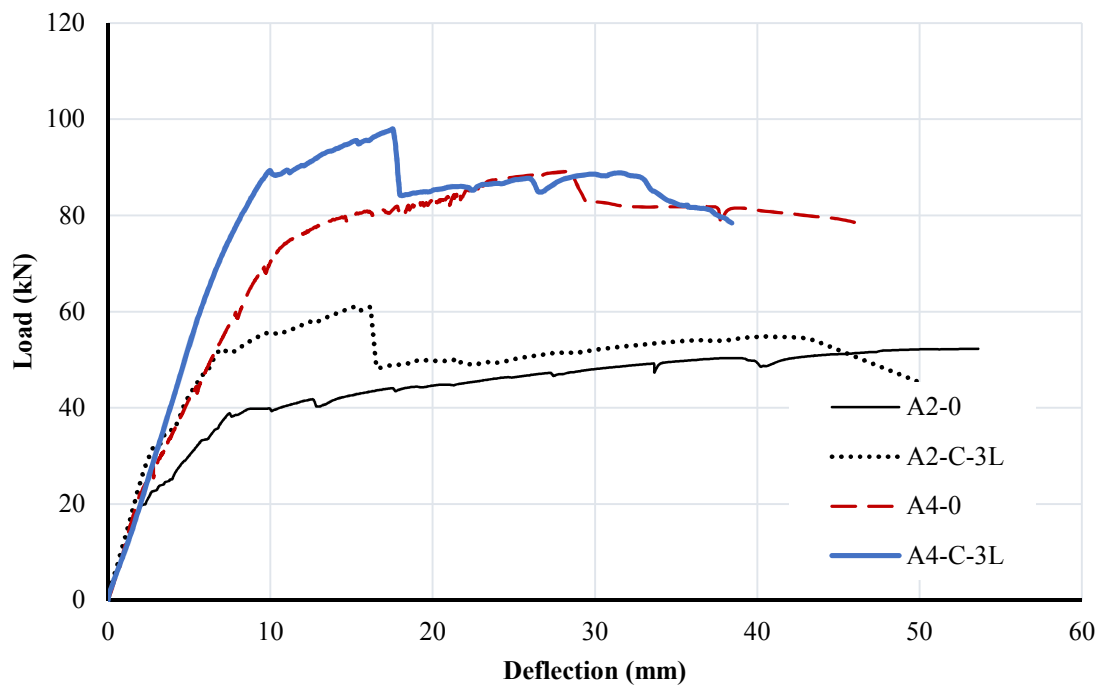


Figure 4.27 Load-deflection at midspan relationship for group III beams

It was noticed that group I beams strengthened with PBO-FRCM systems had less critical crack width in comparison with their respective unstrengthened beams as shown in Figure 4.28. The LSR strengthened beam had a critical crack width of about 75% of the control, whereas the MSR strengthened beam had a critical crack width of about 44% of the unstrengthened beam.

Figures 4.29 and 4.30 shows the load and critical crack width for group II and III beams. It can be reported that up to yielding load, no change in the crack width is noticed. However, LSR strengthened beams, A2-C-2L and A2-C-3L, had a critical width that is 90% of their control beams, whereas MSR strengthened beams, A4-C-2L and A4-C-3L had a critical crack width that is 110% to 130% of their respective control beams. It can be concluded that increasing the steel reinforcement, increases the crack width of the strengthened beam compared to the control beam.

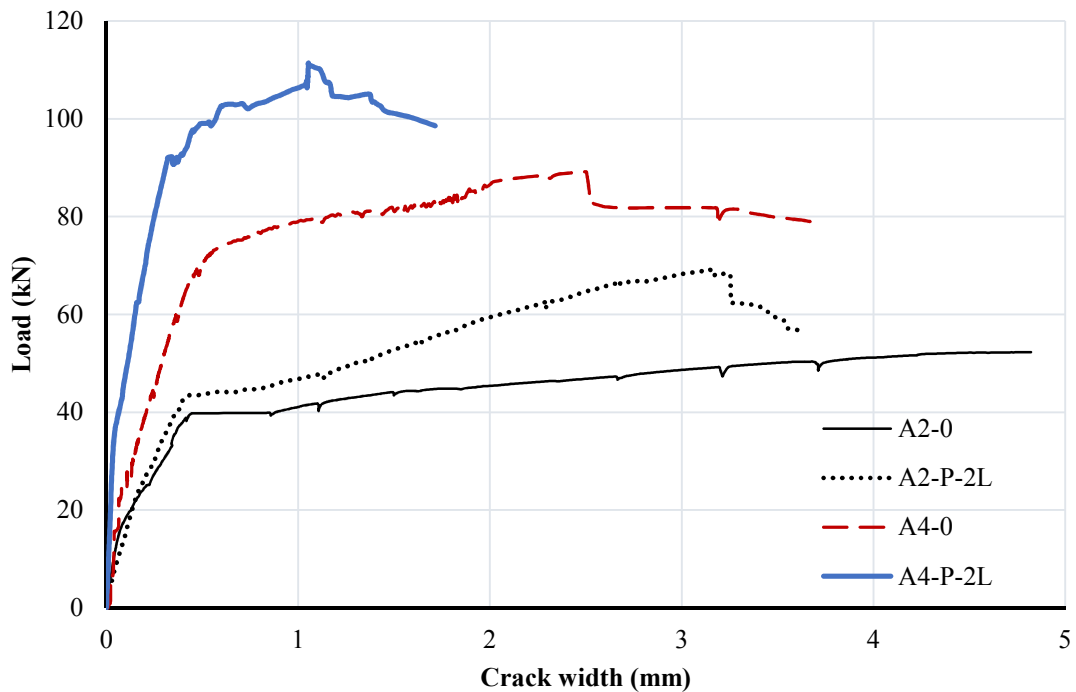


Figure 4.28 Load-critical crack width relationship for group I beams

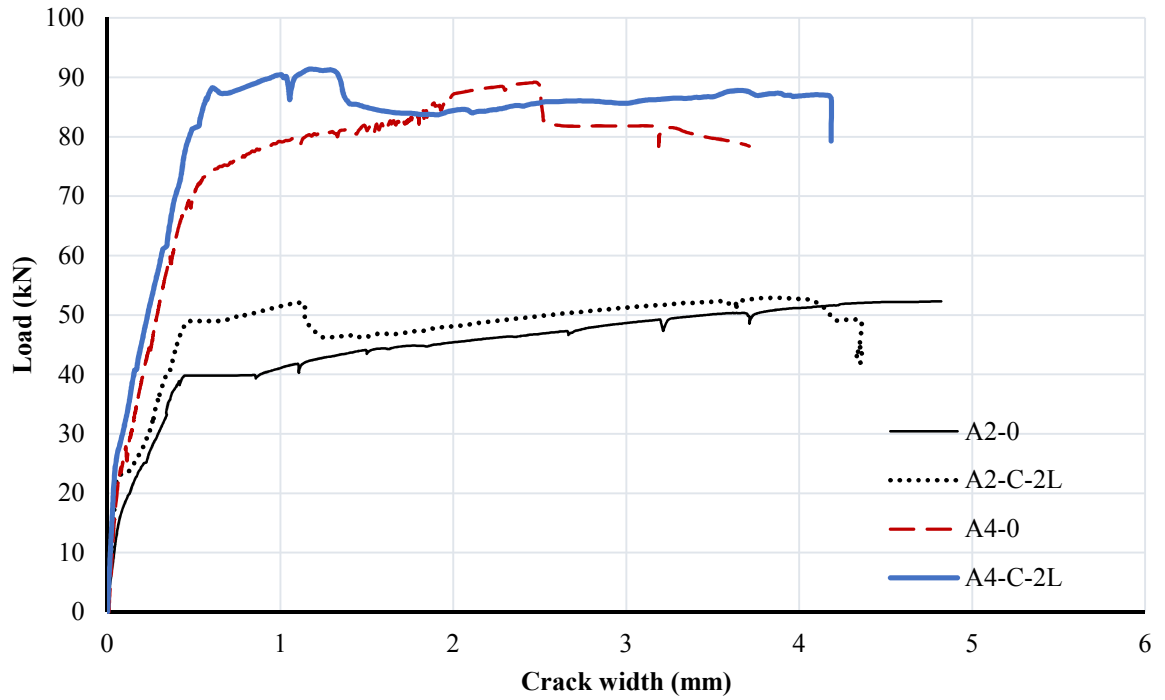


Figure 4.29 Load-critical crack width relationship for group II beams

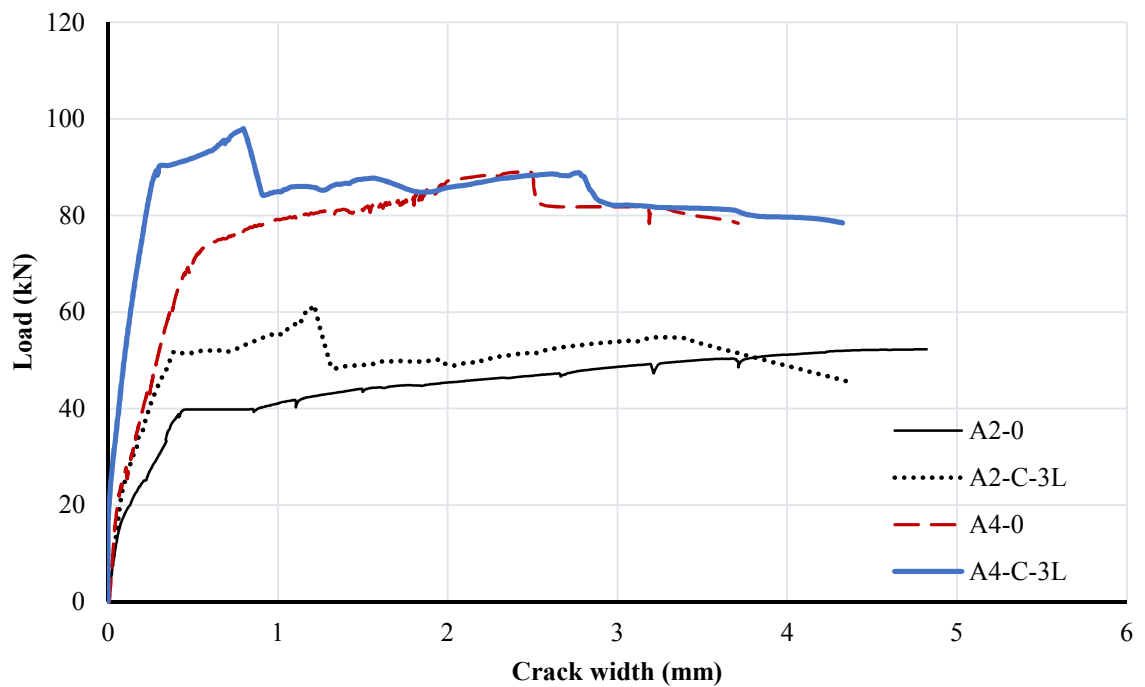


Figure 4.30 Load-critical crack width relationship for group III beams

Figure 4.31 shows the load and both, concrete and FRCM, strain behaviours for the PBO strengthened MSR and LSR beams. The MSR strengthened beams reached relatively higher FRCM strains compared to LSR strengthened beams. However, the compressive strains in the concrete at failure were in the range of 3000 to 3500 microstrain for both MSR and LSR strengthened beams.

Figure 4.32 and 33 shows the load and concrete and FRCM strain relationship. It should be noted that the FRCM strain reading for specimen A2-C-3L, (in Figure 4.33), was lost at around 51 kN. Comparing the compressive strains of both strengthened beams, it can be observed that the increase in the both compressive and tensile strains in the strengthened specimens are identical. After the internal steel reinforcement yields, the tensile strain of the strengthened specimens increases at a very higher rate which can be observed by the horizontal plateau in Figures 4.32 and 4.33.

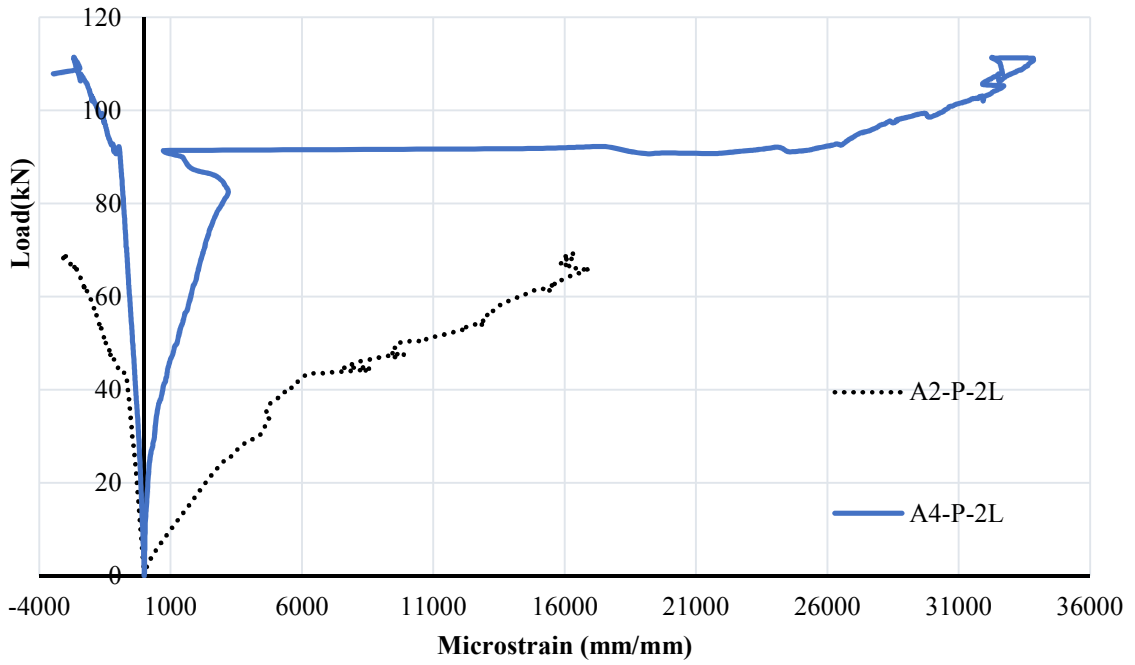


Figure 4.31 Load-concrete-FRCM strain relationship for group I beams

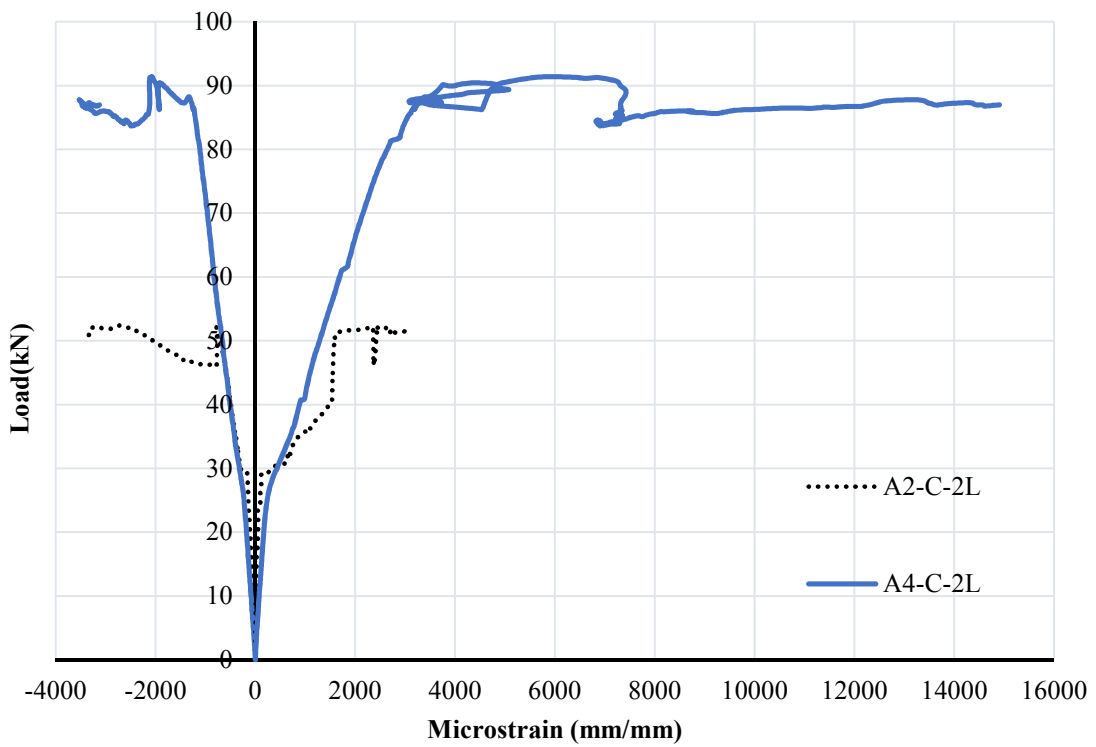


Figure 4.32 Load-concrete-FRCM strain relationship for group II beams

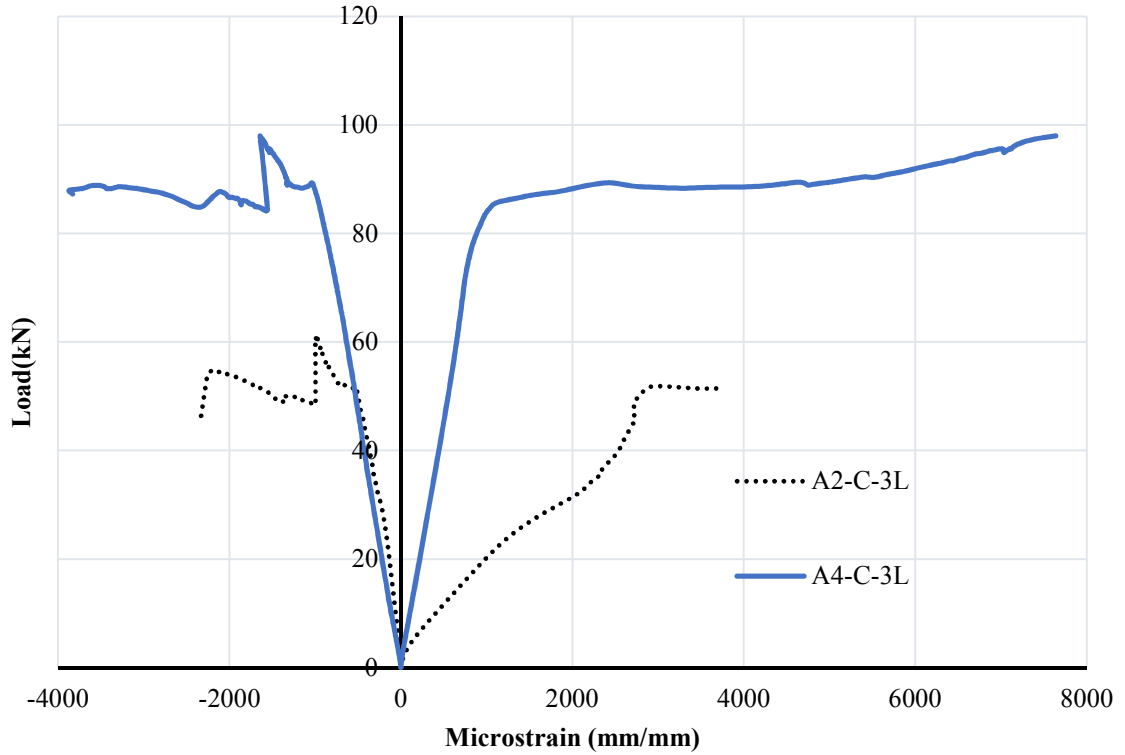


Figure 4.33 Load-concrete-FRCM strain relationship for group III beams

It can be concluded that:

- The increase in steel reinforcement, decreases the FRCM strengthening effect on the ultimate load. LSR strengthened beams with PBO and carbon had an increase of 33% and 17.5%, respectively, compared to 30% and 10% for MSR strengthened beams with PBO and carbon, respectively.
- LSR strengthened beams showed higher PCS and PYS ratios compared to MSR strengthened beams. In other words, as the steel reinforcement of the beam decreases, the post-cracking and post-yielding stiffness's increases.

4.2.3 Effect of Concrete Compressive Strength

In this section, the effect of the concrete compressive strength on FRCM strengthened RC beams is investigated. Two concrete mixes, A and B, of 33 MPa (Normal Strength Concrete, NSC) and 48 MPa (High Strength Concrete, HSC), respectively, were studied. Two test specimens, A2-0 and B2-0, with 2#10M internal steel reinforcement were used as control specimens. Group I has two test specimens, A2-P-2L and B2-P-2L, each was strengthened using two layers of PBO-FRCM. Group II has the other two test specimens, A2-C-3L and B2-C-3L, where each was strengthened with two layers of Carbon FRCM. Figures 4.34 and 4.35 show comparisons of the load-deflection behaviours of the six test specimens while table 4.6 summarizes the main test results and behaviour parameters.

Table 4.6 Effect of concrete compressive strength test results

Group	Specimen ID	Concrete Strength (MPa)	FRCM-Ratio $(\frac{EA_{frcm}}{EA_{steel}})\%$	Yielding	%	Ultimate	%	PDI ratio	PCS ratio	PYS ratio
				Load (kN)	increase	Load (kN)	increase			
	A2-0	33	-	39.8	-	52	-	1	1	1
	B2-0	48		42	-	55.5	-	1	1	1
I	A2-P-2L	33	4.3	44.2	11	69.3	33.3	1.07	1.19	2.82
	B2-P-2L	48	4.3	45.5	8.3	69.9	26.0	1.55	1.42	1.97
II	A2-C-3L	33	4.6	51.8	30.1	61.1	17.5	1.09	1.49	4.14
	B2-C-3L	48	4.6	50.2	19.5	61.2	10.3	1.26	1.31	3.24

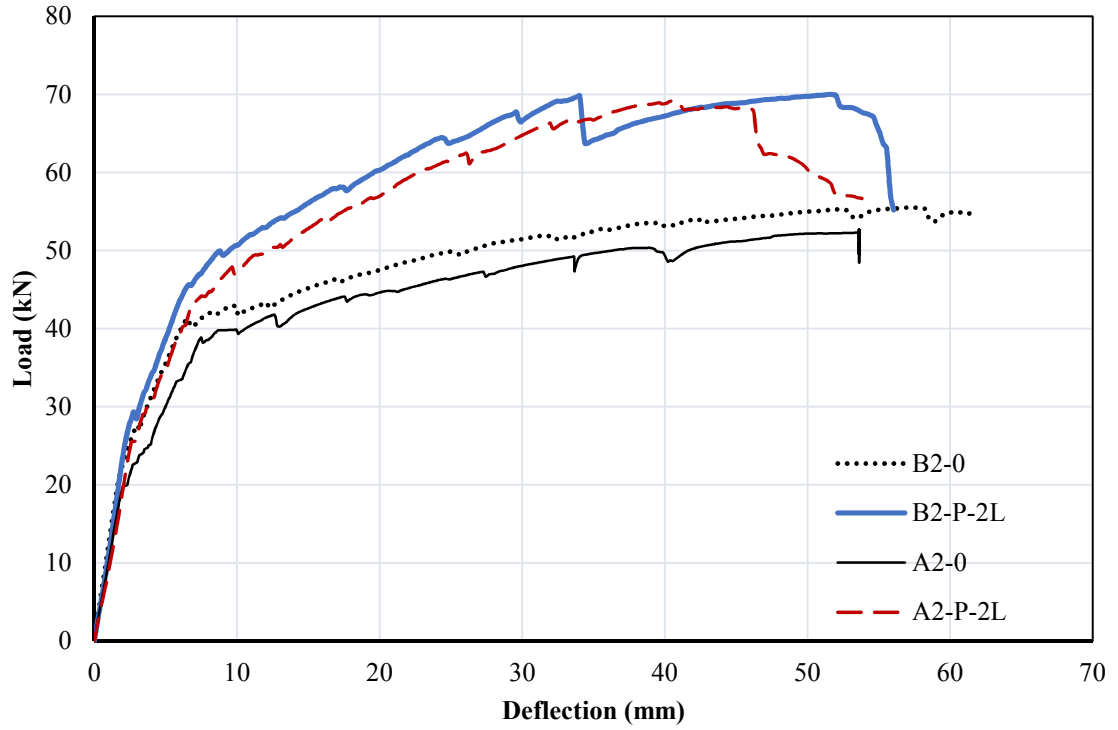


Figure 4.34 Load-deflection relationship for group I beams

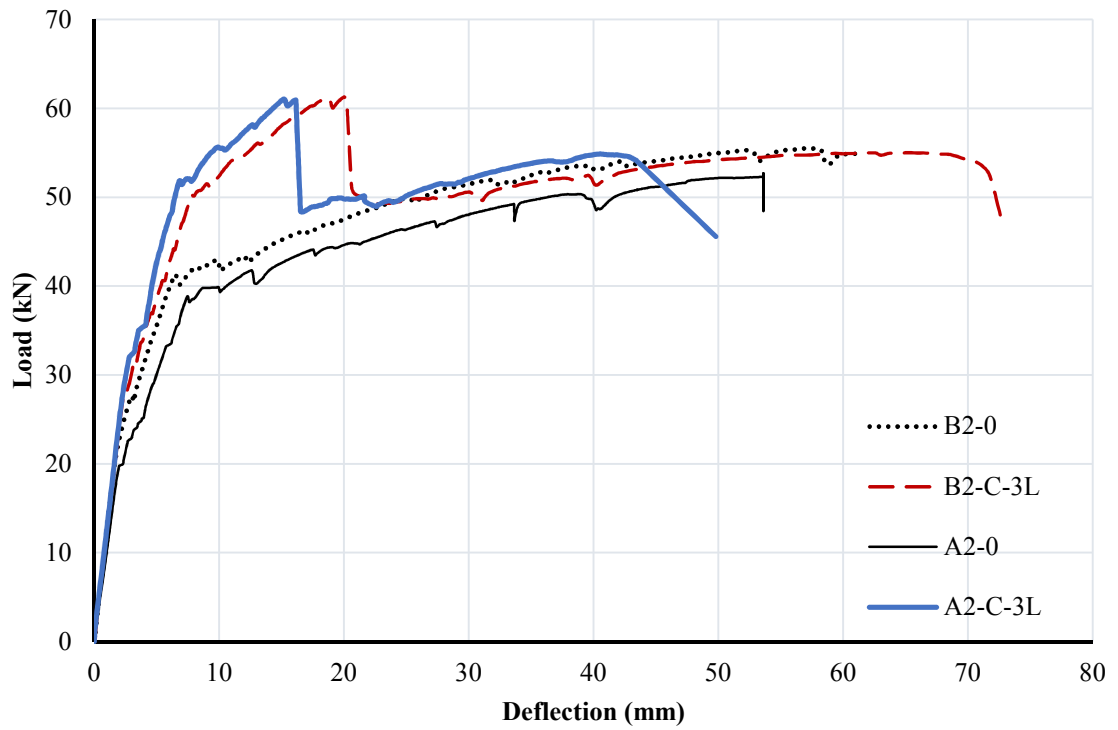


Figure 4.35 Load-deflection relationship for group II beams

Specimen A2-P-2L showed an increase of about 33 % in ultimate load capacity, whereas specimen B2-P-2L showed an increase of about 26.0% compared to their control specimens, A2-0 and B2-0. Similarly, specimen A2-C-3L showed an increase of about 17 % in ultimate load capacity, whereas specimen B2-C-3L showed an increase of about 10 % compared to the control ones. Accordingly, increasing the concrete strength by about 45% (from 33 to 48 MPa), decreases the gain in the ultimate strength by about 20 to 40% for PBO and carbon FRCM strengthening. Therefore, it can be concluded that the increase in the concrete compressive strength decreases the FRCM strengthening effect on the ultimate load. However, the PBO and carbon FRCM strengthened HSC specimens showed between 17 to 48% more increase in the PDI, in comparison with the NSC strengthened ones. Furthermore, the HSC specimen showed about 23% increase in PCS when strengthened with PBO-FRCM, and 18 % decrease in PCS for the ones strengthened with carbon-FRCM compared to the NSC ones. Meanwhile, the FRCM strengthened HSC specimens showed about 90% less increase in PYS compared to FRCM strengthened NSC ones.

The strengthened HSC and NSC specimens showed similar behaviours until the yielding of steel. After yielding, specimen B2-P-2L had a type II failure which can be observed by the sharp drop in load at 70 kN load and 34 mm deflection at midspan. Then the specimen continued to sustain an increasing load up to 70 kN with rapid increase in the deflection until it had a type I failure mode at 54 mm deflection. Type I failure, excessive slippage of fibers within the matrix, occurred very close to the support as shown in Figure 4.8c. Failure was also accompanied by detaching of the U-wraps at mid-span as shown in Figure 4.8e. Specimen A2-P-2L developed the same ultimate load of 70 kN but at larger

deflection of 42 mm before it started to fail gradually under type II bond failure, which was quickly followed by type I failure close to the support with detachment of one of the u-wraps under the concentrated load as well. Both the carbon strengthened HSC and NSC failed suddenly due to premature detachment of the FRCM

Figures 4.36 and 4.37 show the load-crack-width relationships for the HSC and NSC strengthened and control specimens. It can be concluded that, up to yielding, there is very little change in the crack width. However, after yielding of the internal steel reinforcement, the crack width increased at much lower rate, indicating stiffer performance, than the strengthened specimens. The PBO strengthened NSC and HSC had crack widths which were 4 to 5 times less than the control ones. The significant delay in the yielding load in case of the carbon strengthened specimens results in significant reduction in the crack width of both the NSC and HSC.

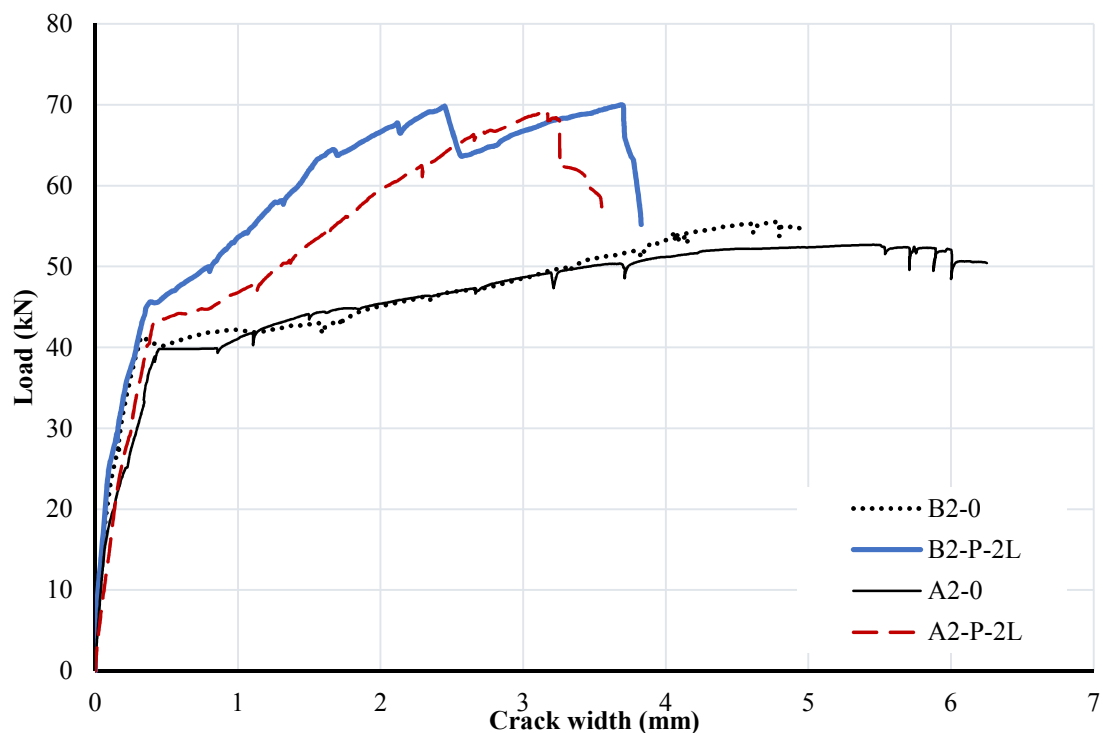


Figure 4.36 Load-critical crack width relationship for group I beams

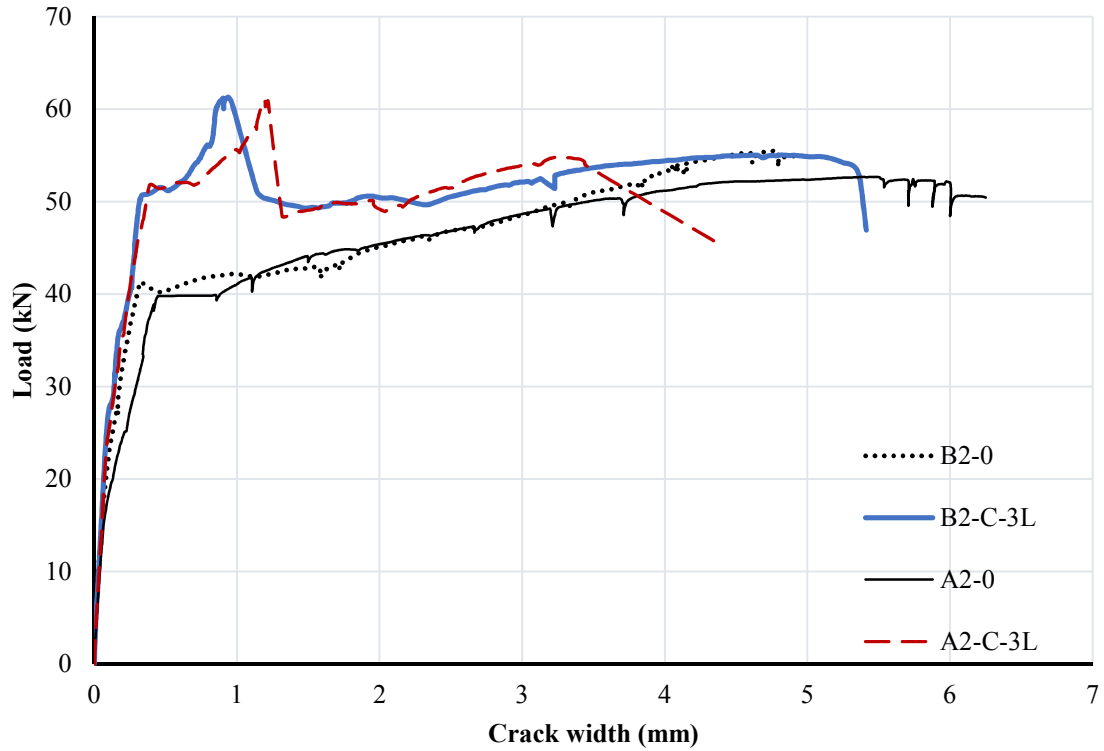


Figure 4.37 Load-critical crack width relationship for group II beams

Figure 4.38 shows the load-concrete-FRCM strain behaviour for the PBO strengthened HSC and NSC beams. It can be concluded that the HSC strengthened beam reduced the compressive and tensile strain compared to the NSC. Both, tensile strain measured at the FRCM outer layer, and compressive strain at the top of the concrete, of NSC strengthened beam, increased at higher rate up to failure. This confirms with the observations made from the load and deflection relationship in Figure 4.34, and load and critical crack width relationship in Figure 4.36, as in both behaviours the NSC strengthened beam showed a higher increase rate. The compressive strain for the NSC strengthened beam was slightly above 3000 microstrain compared to 2500 microstrain for the HSC strengthened beam.

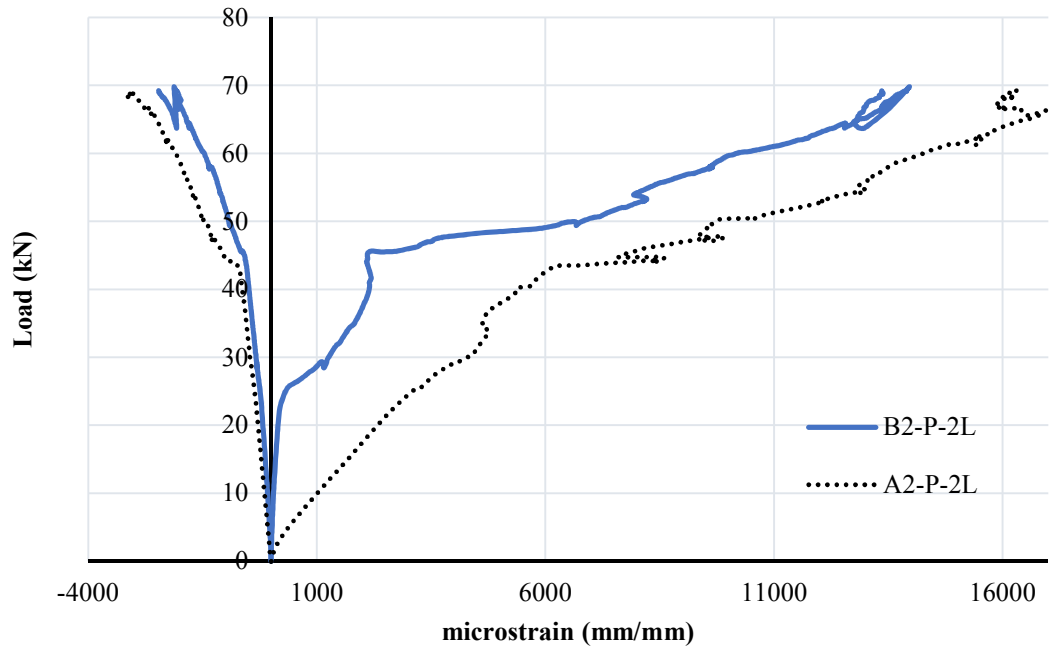


Figure 4.38 Load vs concrete-FRCM strain relationship for group I beams.

It can be concluded that:

- The increase in the concrete compressive strength decreases the FRCM strengthening effect on the ultimate load.
- The increase in the concrete compressive strength results in higher increase in the PDI, and lower increase in the PYS.

4.2.4 Effect of Mortar type

In this section, a brief comparison is carried out between two types of mortars, M750 and M25, as described in section 3.1.2. Three beams are studied, one control beam and two strengthened beams with carbon-FRCM using two different matrices M25 and M750. Specimen A2-C-2L is strengthened using M25 mortar, whereas specimen A2-C*-2L is strengthened using the M750. It must be noted that all the PBO-FRCM were installed using the M750 mortar where all the carbon-FRCM were installed using the M25 mortar, except for A2-C*-2L where M750 was used. Table 4.7 summarizes the main results of this study.

Specimen A2-C*-2L, strengthened with carbon-FRCM using M750, showed about 7.3% increase in the ultimate load, whereas, specimen A2-C-2L, strengthened with carbon-FRCM using M25, showed almost the same capacity as the control specimen. Also, specimen A2-C*-2L showed 23% more increase in the PDI ratio compared to A2-C-2L. Both specimens showed a very comparable PCS ratio. However, A2-C-2L showed 275% more increase in the PYS ratio compared to A2-C*-2L.

Table 4.7 Effect of mortar type (summary of results)

Specimen ID	Matrix type	FRCM-ratio $\left(\frac{EA_{frcm}}{EA_{steel}}\right)\%$	Yielding	%	Ultimate	%	PDI ratio	PCS ratio	PYS ratio
			Load (kN)	increase	Load (kN)	increase			
A2-0		-	39.8	-	52	-	1	1	1
A2-C-2L	M25	3.1	49	23.1	52.2	0	1.07	1.30	3.42
A2-C*-2L	M750	3.1	48.8	22.6	55.8	7.3	1.30	1.27	0.67

Both strengthened specimens showed no noticeable difference in the load-deflection behaviour up to yielding of steel as shown in Figure 4.39. However, after steel yielding, specimen A2-C*-2L showed better ductility in comparison with specimen A2-C-2L. Specimen A2-C*-2L failed after reaching about 62 mm deflection at midspan, whereas specimen A2-C-2L failed at about 50 mm deflection at midspan. The increase in ductility is mainly due to the bond failure mode that happened. Both specimens had a type II failure, detaching from the concrete, quickly after the yielding of steel, which can be observed in the load-deflection diagram by the drop in the load after reaching about 52 kN. However, specimen A2-C-2L suffered from an early excessive crack that propagates through the FRCM and then type I bond failure occurs in which slippage of fibers was observed. Meanwhile, specimen A2-C*-2L, also suffered from type I bond failure, however, it happened at a later stage.

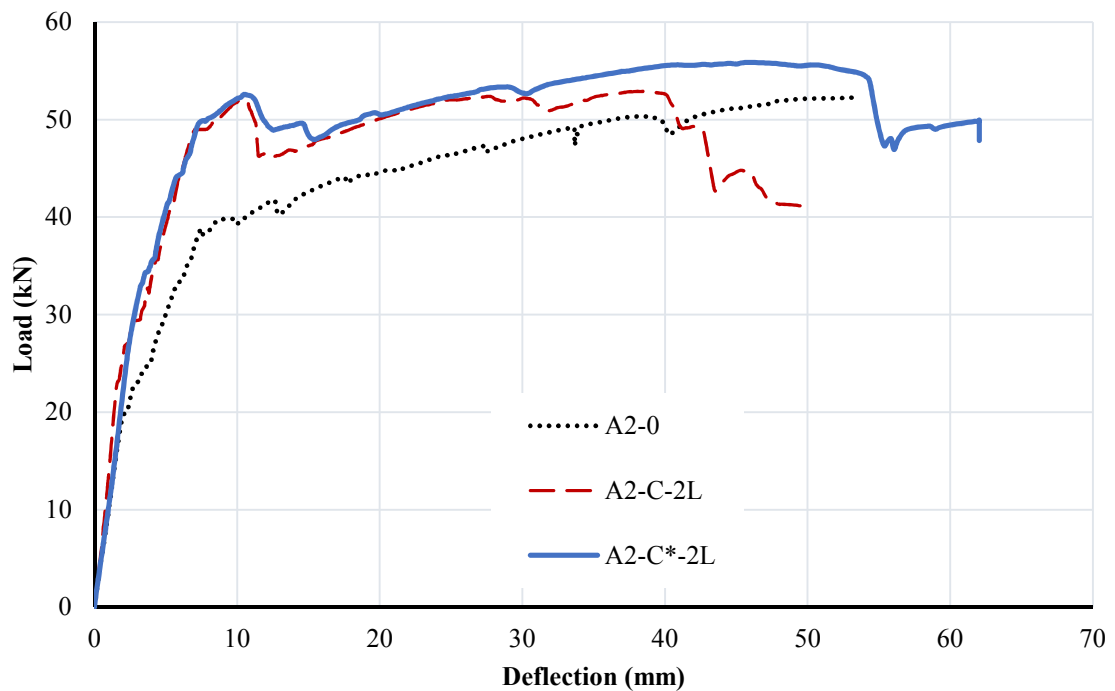


Figure 4.39 Load-deflection relationship for A2-C*-2L and A2-C-2L

It can be concluded that:

- The beam strengthened with C-FRCM having M750 mortar showed a marginal improvement in the load capacity as it showed about 7.3% increase in the ultimate load, compared to almost no increase for the specimen having M25 mortar.
- In terms of Pseudo-ductility, a significant increase is noted with the use of M750 mortar, as specimen A2-C*-2L showed 23% more increase in the PDI ratio compared to A2-C*-2L.

In general, the FRCM strengthening showed insignificant effect on the cracking load and pre-cracking flexural stiffness. However, after cracking of the concrete and the cement matrix of the FRCM, the FRCM strengthening showed significant effect to increase the post-cracking stiffness and the yielding load depending on the fiber net type. To put all the tested specimens together, table 4.8 was constructed. Table 4.8 shows the summary of the test results for all the tested specimens.

Table 4.8 Test results for all specimens

Specimen ID	Tested f'_c (MPa)	Experimental Load			Ultimate Load Experimental/Theoretical ratio	Experimental Deflection				Failure Mode ^c
		Cracking Load (kN)	Yielding Load (kN)	Ultimate Load (kN)		Deflection @ cracking (mm)	Deflection @ yielding (mm)	Deflection @ ultimate ^a (mm)	Deflection @ failure ^b (mm)	
A2-0	33	14.2	39.8	52	1.1	1.19	8	53.6	53.6	C
A2-P-2L		17.6	44.2	69.3	1.17	1.57	7.5	40.8	53.8	DB-C
A2-C-2L		20.2	49	52.2	1.00	1.12	7	10.5	50	DB-C
A2-C-3L		24.6	51.8	61.1	1.10	1.93	6.8	15.2	49.8	DB-C
A2-C*-2L		22.8	48.8	55.8	1.07	1.66	7.1	46.1	62	DB-C
A2-G-4L		20.7	46.1	54.2	0.98	1.59	7.5	19.4	64.5	DB-R-C
A4-0		18.6	73.4	89.3	1.01	2.59	10.6	28.3	46.1	C
A4-P-2L		27.2	92.1	111.4	1.14	1.94	10.1	34.3	44.7	DB-C
A4-P*-2L		20.2	83.7	120.3	1.23	1.62	10.3	49.4	50.9	DB-C
A4-C-2L		24.5	86.2	91.4	0.97	1.67	10	14.9	37.8	DB-C
A4-C-3L		24.1	89.2	98	1.01	2.88	9.9	17.5	38.4	DB-C
A4-G-2L		20.2	74.6	92.5	0.99	2.46	11	24.6	45.1	DB-C
A4-G-2L	20.2	70.5	90.1	0.97	2.05	10.6	32.7	54.8	DB-R-C	
B2-0	48	17.1	42	55.5	1.16	1.59	8.4	57.3	61.4	C
B2-P-2L		20.8	45.5	69.9	1.16	1.93	6.7	51.5	76.1	DB-C
B2-C-3L		21	50.2	61.2	1.08	1.72	7.8	20.1	71.4	DB-C

^aDeflection @ ultimate is considered the maximum load capacity the beam reaches.

^b Deflection @ failure is taken as the deflection after 20% drop in the ultimate load.

^c Failure mode designated by C indicates concrete compression failure, and DB-C indicates debonding or delamination of the FRCM system followed by concrete compression failure, DB-R-C indicates that the FRCM system debonded followed by fiber rupture and then followed by concrete compression failure

CHAPTER 5

CONCLUSION

5.1 Overview

This experimental study was carried out mainly in two phases. The first phase focused on the tensile characterization testing to obtain the mechanical properties of FRCM systems. Three systems were studied, glass-FRCM, carbon-FRCM and PBO-FRCM. The second phase included constructing and testing 16 large-scale beams, strengthened in flexure with various FRCM systems to study several parameters. The studied parameters are as follows:

1. Axial Stiffness of the FRCM system
2. Steel reinforcement ratio ($0.18 \rho_b$ and $0.36 \rho_b$)
3. Concrete Strength (30 and 50 MPa)
4. Bonding material (M25 vs M750 mortar)

5.2 Conclusions

Based on the results obtained in this study, it can be concluded that:

- When comparing the FRCM type to study the effect of axial stiffness, beams strengthened with PBO showed the highest enhancement in the ultimate load capacity, as the increase ranged between 30% and 33%, compared to less than 5% for the beams strengthened with glass-FRCM and carbon-FRCM. This is mainly due to the superior bonding that the PBO-FRCM exhibited with the concrete substrate, in which no premature bonding occurred.
- Increasing the axial stiffness of the FRCM, by adding FRCM layers, significantly

enhanced the performance and load capacity of carbon-FRCM strengthened beams. The percentage increase in ultimate load went up from 0% to 17.5 and 0% to 9.7% for carbon-FRCM strengthened beams.

- Increasing the axial stiffness of the FRCM, by adding FRCM layers, did not have a noticeable increase in the PDI (pseudo-ductility index) ratio, as an increase of only 2% was obtained. Meanwhile, a remarkable increase ranging from 11 to 72% was obtained in both, PCS (post-cracking stiffness) and PYS (post-yielding stiffness), ratios.
- Even when having the very comparable axial stiffness ratio, PBO-FRCM still showed the greatest enhancement on the ultimate capacity of the strengthened beams. An increase of 33% and 4% was obtained in comparison with the control (unstrengthened beam) for specimens strengthened with PBO and glass, respectively.
- The increase of the steel reinforcement, decreases the FRCM strengthening effect on the ultimate load. LSR (low steel reinforcement) strengthened beams with PBO and carbon had an increase of 33% and 17.5%, respectively, compared to 30% and 10% for MSR (moderate steel reinforcement) strengthened beams with PBO and carbon, respectively.
- LSR strengthened beams showed higher PCS and PYS ratios compared to MSR strengthened beams. In other words, as the steel reinforcement of the beam decreases, the post-cracking and post-yielding stiffness's increases.
- The increase in the concrete compressive strength decreases the FRCM strengthening effect on the ultimate load.

- The increase in the concrete compressive strength results in higher increase in the PDI, and lower increase in the PYS.
- The beam strengthened with C-FRCM having M750 mortar showed a marginal improvement in the load capacity as it showed about 7.3% increase in the ultimate load, compared to almost no increase for the specimen having M25 mortar.
- In terms of Pseudo-ductility, a significant increase is noted with the use of M750 mortar, as specimen A2-C*-2L showed 23% more increase in the PDI ratio compared to A2-C*-2L.
- Comparing the theoretical and experimental ultimate load capacity, it can be observed that the ACI prediction produces an overall good estimation of the ultimate load capacity. For the PBO-FRCM strengthened beams, the ACI prediction gave a conservative underestimation of the capacity. However, for the C-FRCM and G-FRCM it gave an overestimation due to the premature debonding failure that happened in those specimens that is not considered by the ACI prediction.

5.3 Recommendation for Future Work

Based on the test results and discussions, the following recommendations for future work are suggested:

- Study the tensile behaviour of FRCM using different tab lengths at the boundaries of the coupon specimen.
- Investigate the effect of matrix M750 and other matrix on beams strengthened with three and more layers of Carbon-FRCM.
- Study the effect of different strengthening schemes on the flexural performance of Glass and Carbon-FRCM with high number of layers.

REFERENCES

- ACI 549.4R-13. (2013) "Design and construction guide of externally bonded FRCC systems for concrete and masonry repair and strengthening.", American Concrete Institute, Farmington Hills, MI
- AC434. (2013) "Acceptance criteria for masonry and concrete strengthening using fiber-reinforced cementitious matrix (FRCC) composite systems." ICC-Evaluation Service, Whittier, CA.
- Al-Salloum, Y. A., Elsanadedy, H. M., Alsayed, S. H., and Iqbal, R. A. (2012). "Experimental and numerical study for the shear strengthening of reinforced concrete beams using textile-reinforced mortar." *ASCE J. Compos. Constr.*, 16(1), 74–90.
- Architects, H. (2014). Retrieved July 20, 2016, from <http://www.constructionspecifier.com/dont-seal-your-fate-considerations-for-parking-garage-surface-treatments/>
- Arboleda, D. (2014). "Fabric reinforced cementitious matrix (FRCC) composites for infrastructure strengthening and rehabilitation: characterization methods." Ph.D. Univ. of Miami, Miami, FL, USA
- Arboleda, D., Carozzi, F., Nanni, A., and Poggi, C. (2015). "Testing Procedures for the Uniaxial Tensile Characterization of Fabric-Reinforced Cementitious Matrix Composites." *ASCE Journal for Composites for Construction*, 20(3), 04015063
- Babaeidarabad, S., Loreto, G., and Nanni, A. (2014). "Flexural Strengthening of RC Beams with an Externally Bonded Fabric-Reinforced Cementitious Matrix." *J. Compos. Constr.*, 10.1061/(ASCE)CC.1943-5614.0000473, 04014009.

- Bisby, L.A. and Briglio, M.B. (2004). "ISIS Canada Educational Module No. 5: An Introduction to Structural Health Monitoring." ISIS Canada, Page 3.
- Bisby, L., Stratford, T., Smith, J. & Halpin, S. (2010), "Comparative performance of Fibre Reinforced Polymer and Fibre Reinforced Cementitious Mortar Strengthening Systems in Elevated Temperature Service Environments in Structural Faults and Repair 2010." Engineering Technics Press, Edinburgh, Structural Faults and Repair 2010, Edingburgh, United Kingdom, 15-17 June.
- Bisby, L.A., Stratford, T.J., Smith, J. & Halpin, S. (2011). "FRP versus Fibre Reinforced Cementitious Mortar Strengthening Systems at Elevated Temperature." ACI SP-279 CD-ROM: 10th International Symposium on Fiber Reinforced Polymer Reinforcement for Reinforced Concrete Structures, American Concrete Institute, pp. 49.1-49.20.
- Cement Organization (2012). "Types and Causes of Concrete Deterioration". Retrieved August 4, 2016, from <http://www.cement.org/>
- Chemosystems photo titled steel plate bonding, Retrieved on November 12, 2016, from http://www.chemcosystems.com/tech_platebond.html
- Corrosion Central NACE, Retrieved on August 04, 2016, from <https://www.nace.org/Corrosion-Central/Industries/Highways-and-Bridges/>
- D'Ambrisi, A., and Focacci, F. (2011). "Flexural strengthening of RC beams with cement based composites." *Journal for Composites for Construction*, 15(5), 707-720

- D'Ambrisi, A., Feo, L., Focacci, F. (2012). "Bond-slip relations for PBO-FRCM materials externally bonded to concrete." *Composites Part B: Engineering*, 43(8), 2938-2949, doi: 10.1016/j.compositesb.2012.06.002.
- D'Ambrisi, A., Feo, L., Focacci, F. (2013). "Experimental analysis on bond between PBO-FRCM strengthening materials and concrete." *Composites Part B: Engineering*, 44(1), 524-532, doi: 10.1016/j.compositesb.2012.03.011.
- D'Antino T, Carloni C, Sneed LH, Pellegrino C. (2014) "Matrix-fiber bond behavior in PBO FRCM composites: A Fracture Mechanics Approach." *Eng Fract Mech* 2014;117;94-111.
- Exclutec, photo titled carbon fiber sheets, Retrieved on August 04, 2016, from <http://exclutec.com/de/was-ist-carbon.html>
- ESR-3265 (2016) "Ruredil X Mesh C10 and Ruredil X Mesh Gold Fabric-Reinforced Cementitious Matrix (FRCM) Composite Systems", ICC-Evaluation Service Report.
- G.H. Koch, M.P.H. Brongers, N.G. Thompson, Y.P. Virmani, J.H. Payer, (2002) "Corrosion Costs and Preventive Strategies in the United States," Publication No. FHRD-01-156 (Washington, D.C.: FHWA, 2002).
- Jabr, A. Elragaby, A. Ghrib F. (2016). "Flexural Strengthening of RC Beams Using Glass-FRCM." *Proceedings of the 5th International Structural Specialty Conference, CSCE 2016, LONDON.*
- Jabr, A. Elragaby, A., Ghrib, F. (2017). "Effect of the Fiber Type and Axial Stiffness of FRCM on the Flexural Strengthening of RC Beams" *MDPI Fibers* **2017**, 5(1), 2.

- Jung, K., Hong, K., Han, S., Park, P., and Kim, J. (2015) "Prediction of Flexural Capacity of RC Beams Strengthened in Flexure with FRP Fabric and Cementitious Matrix," *International Journal of Polymer Science*, vol. 2015, Article ID 868541, 11 pages, 2015. doi:10.1155/2015/868541
- Loreto, G., Leardini, L., Arboleda, D., and Nanni, A. (2013). "Performance of RC slab-type elements strengthened with fabric-reinforced cementitious-matrix (FRCM) composites." *Journal for Composites for Construction*, 18(3), A4013003
- Mahoney, M. (2006). "The Future of Fiber-Reinforced Concrete. ASCC Webinar Series." American Society of Concrete Contractors. Web Conference, 11 Sept. 2013. Speech.
- Media Buildings Photo titled application of Externally Bonded FRP retrieved on June 20, 2016 from
<http://media.buildingsmedia.com/images/B_0408_Eyesore4.jpg>
- Mobasher, B., Peled, A., and Pahilajani, J. (2012). "Distributed cracking and X stiffness degradation in fabric-cement composites." *Material Structures*. 39(3), 317–331.
- Newhook, J., Svecova, D., (2007). "Reinforcing Concrete Structures with Fibre-Reinforced Polymers", Design Manual No. 3, Version 2, ISIS Canada
- Ombres, L. (2011). "Structural performance of PBO FRCM-strengthened RC beams." *Proceedings Institution of Civil Engineers Structures and Buildings*. 164(4), 265–272.

- Ombres, L. (2012). Debonding analysis of reinforced concrete beams strengthened with fiber reinforced cementitious mortar. *Engineering Fracture Mechanics*. 81(1), 94–109.
- Ombres, L. (2015) “Analysis of the bond between fabric reinforced cementitious mortar (FRCM) strengthening systems and concrete,” *Composites Part B: Engineering*, vol. 69, pp. 418–426, 2015.
- Ruredil, photo titled FRCM application, retrieved on June 20, 2016 from <http://www.ruredil.it/prodotti/foto/ruregold_xr_muratura>
- Ruredil X Mesh Gold. retrieved on November, 2nd, 2016 from http://english.ruredil.it/SchedeProdottoENG/RuredilXMeshGOLD_ing_1.pdf
- Sika®-Monotop 623. retrieved on November, 2nd, 2016 from https://can.sika.com/dms/getdocument.get/91bef53e-75e5-3a27-b78c-2e8e67b244b8/SikaMonoTop623_pds.pdf
- SikaWrap®-350 G Grid. Retrieved on August 7, 2016, from http://grc.sika.com/dms/getdocument.get/1d5e3ced-4748-3bf2-9f66-3b5cb8e403d5/010206020040000001_SikaWrap_350_G_gr.pdf
- Teng, J. G., Smith, S.T., Yao, J. and Chen, J.F. (2003) “Intermediate crack-induced debonding in RC beams and slabs,” *Journal of Construction and Building Materials*, vol. 17, no. 6-7, pp. 447–462, 2003.
- Tumialan, G., and De Luca, Antonio. (2014). “FRCM Systems.” *STRUCTURE Magazine*. National Council of Structural Engineers Association.
- Turk, A., (2013). “Seismic Response Analysis of Masonry Minaret and Possible Strengthening by Fiber Reinforced Cementitious Matrix (FRCM)

Materials,” *Advances in Materials Science and Engineering*, vol. 2013, Article
ID 952497, doi:10.1155/2013/952497

VITA AUCTORIS

NAME: Abdulla Jabr
PLACE OF BIRTH: Sana'a, Yemen
YEAR OF BIRTH: 1991
EDUCATION: MGIS H.S., Aden, Yemen

University of Windsor, Windsor, Ontario
2010-2014 B.A.Sc.

University of Windsor, Windsor, Ontario
2014-2016 M.A.Sc.